January 2019

Nonadiabatic Dynamics: A Semiclassical Approach

Ruixi Wang
Wayne State University

NONADIABATIC DYNAMICS: A SEMICLASSICAL APPROACH

by

RUIXI WANG

DISSERTATION

Submitted to the Graduate School

of Wayne State University,

Detroit, Michigan

in partial fulfillment of the requirements

for the degree of

DOCTOR OF PHILOSOPHY

2019

MAJOR: CHEMISTRY (Physical)

Approved by:

_____

Advisor Date

_____

_____

_____

_____

DEDICATION

This dissertation is dedicated to my wife Jin Wen, my mother Mei Wang, and my father Yinyong Wang.

ACKNOWLEDGMENTS

First, I would like to thank my advisor Dr. Vladimir Y. Chernyak. Vladmir is a brilliant scientist with very deep understanding of the mathematics behind physics and chemistry. Discussions with Vladimir have always been helpful and insightful which guided my way towards my Ph.D. degree. His wisdom extends beyond science as his lectures are informative and humorous with various interesting knowledge.

Many thanks to my friends and colleagues Dr. Michael Catanzaro, Dr. Kangmin Liu, Dr. Tian Shi, and Austin Walsh. Thank you for all the time these years we spent working together and talking with each other.

I appreciate the collaboration with Dr. Sergei Tretiak, Dr. Dmitry Mozyrsky, and Dr. Alexander J. White from Los Alamos National Lab. The work at Los Alamos National Lab has been an invaluable part of my Ph.D. life and constituted an important part of my Ph.D. study.

I would like to thank my committee members, Dr. Groysman, Dr. Klein, Dr. Li, and previous committee member Dr. Cisneros. Thank you for your valuable and inspirational comments, questions, and suggestions.

I am grateful for working as a teaching assistant for Dr. Barber, Dr. Chernyak, and Dr. Li, especially to Dr. Barber for generously providing food for the TA's grading the exams.

My appreciation extends to Department of Chemistry staff members, especially Ms. Melissa Rochon and Ms. Jacqueline Baldyga, for helping with various things during my Ph.D. study.

At last, I would like to give most of my appreciation to my wife Jin Wen, my mother Mei Wang, and father Yinyong Wang, for all the understanding, help, and support throughout my life.

TABLE OF CONTENTS

LIST OF FIGURES

CHAPTER 1 INTRODUCTION

It has been decades since people started investigating nonadiabatic dynamics [1, 2]. In the 1930's, following the first potential energy surface (PES) diagram made by Eyring and Polanyi in their historic paper "Über einfache gasreaktionen" (On Simple Gas Reactions) in 1931 [3], Landau and Zener separatedly discovered the Landau-Zener formula as an approximate solution to a two-PES-level quantum dynamics problem in 1932 [4, 5].

Nonadiabatic effects play a crucial role in photoinduced molecular dynamics in condensed, as well as gas phase, in small and large molecules, showing up in various kinds of photoinduced reactions [1, 6, 7], including photo-dissociation [8, 9] and photo-isomerization [10, 11]. Conical Intersections (CIs) [12–14] play an extremely important role in all areas that involve nonadiabatic transitions for a variety of reasons. First of all they are unavoidable in a sense that once you have a single CI point, by the implicit function theorem [15], you immediately get a codimension 2, i.e., $(d-2)$-dimensional Conical Seam (CS). In fact it is natural to interpret an avoided crossing, i.e., two adiabatic Potential Energy Surface (PES) coming close, as the system just being close to an unidentified CS(e.g., due to considering a reduced configuration space). Secondly, CIs have been found computationally in a variety of molecules [16–18], by using clever identifying algorithms [19,20], as well as multi-reference electronic structure methods [18,21,22] capable of handling the symmetries, associated with electronic state degeneracy. Thirdly, CI are usually responsible for ultrafast nonadiabatic transitions in gas phase [23–25], as well as ultrafast photo-relaxation [26, 27] and photo-isomerization [28, 29] in biological molecules, including such super-important examples as photo-isomerization of rhodopsin [30–32].

CIs have been under theoretical/computational studies in terms of their electronic structure [17, 33, 34], as well as wavepacket dynamics in both closed [35–37] and open (a molecule coupled to environment/heat bath) [38–40] cases. The dynamical problem, however, is complex for a full quantum treatment, even assuming one has perfect knowledge on PES and nonadiabatic couplings, due to high dimensionality of the configuration space, even in the closed dynamics case. Even sophisticated computational schemes, capable of performing quantum mechanical simulations [41–43], including such clever approaches as spawning [44, 45], scale unfavorably with the number of

atoms, so that much more cost-efficient semiclassical or/and mixed quantum-classical methods are highly desired.

There is, however, an intrinsic issue on the way of developing semiclassical approaches capable of handling nonadiabatic transitions in a proper way. As far as adiabatic dynamics is concerned, there is an excellent understanding of the semiclassical limit, which is asymptotically exact, in terms of the semiclassical Van-Vleck [46,47], or more sophisticated Herman-Kluk [48,49], providing an intuitive picture for the case when semiclassical propagation is no longer quantitatively precise. Such intuition is still to merge for the case of nonadiabatic transitions, despite several decades of activity in the aforementioned field. There is a reason behind that. Although apparently not truly appreciated in modern literature on nonadiabatic transitions, it is known since the 1950s [50] that in the absence of level crossing, in the truly semiclassical $\hbar \to 0$ limit, the nonadiabatic effects vanish in a non-analytical exponential $\sim \exp(-1/\hbar)$ way; therefore applying semiclassical approximations that involve hopping far from true intersections, in a situation when the semiclassical parameter is not small faces serious difficulties.

The surface hopping algorithms originally formulated by Tully [51,52] and further developed by other authors [53,54], scale favorably with the system size, and provide an efficient tool for studying nonadiabatic effects in molecular dynamics [6, 53, 55], especially in condensed phase [56, 57]. The aforementioned algorithms generally address the problem of branching ratios and demonstrate an ability to predict/interpret the latter with decent accuracy. However, due to the extremely intuitive nature of these algorithms (namely the associated Monte Carlo procedure does not converge to the solutions of the Schrödinger equation), as well as not accounting for the wavefunction phase, associated with the classical trajectories in between the hopping events, makes their capability to predict the wavepacket shapes a big question. More sophisticated algorithms, see e.g., [58,59], that represent an attempt to solve the Schrödinger equation using a valid Monte Carlo scheme, face a problem of making a choice of which integrations in a path-integral representation should be done in the saddle-point, and which should be performed numerically exactly using a Monte Carlo procedure. The problem is usually referred to as the choice of initial conditions for the classical trajectory after hopping [60,61], with the numerical results being choice dependent, which demonstrates inconsistency of the scheme itself. Also the method apparently has not shown capability of describing nonadiabatic dynamics near CSs.

Advances in theoretical methods as well as in computational power have positioned quantum chemistry as a powerful tool in studying various properties of multi-atomic molecules and molecular complexes. [62, 63] Accurate, but numerically expensive, wavefunction based approaches enable detailed description of electronic properties in relatively small molecules. In contrast, efficient Density functional theory (DFT) methods in combination with molecular dynamics (MD) allow one to deduce valuable information on ground state properties for molecules with hundreds of atoms in size. [64] Further advances in time-dependent density functional theory (TDDFT) have made it possible to carry our efficient calculations for exited states in these systems and thus predict their susceptibilities, absorption and emission spectra, etc. [65]

At present quantum chemistry faces a new frontier: Now it aims not only at computations of the equilibrium (static) molecular properties, but also at modeling dynamics of photophysical processes and (photo)chemical reactions in molecular systems [6, 66]. The latter are characterized by different reaction pathways that lead to different reaction products. For example, upon absorbing a photon, a molecule may undergo radiative relaxation processes [67], such as fluorescence [68] and phosphorescence; non-radiative relaxation processes, such as photodissociation [9, 69, 70] or photoisomerization; [71–74] charge [75–78] and energy transfer; [79–81] or intersystem crossing [82–84]. Such dynamics are obviously accompanied by electronic transitions, involving complex electron-phonon interaction [85, 86] and possibly many electronic states, and therefore can not be described within the standard adiabatic or Born-Oppenheimer approximation. That is, while in the traditional adiabatic approximation the nuclei move along a given potential energy surface (PES) of a molecule, description of photophysical or photochemical processes requires accounting for the transitions between different PESs. Such transitions typically occur in the relatively small regions of the phase space where the PESs closely approach or cross each other, so that the the energy separation between relevant PESs becomes comparable with inverse time scales of the nuclear motion (in units of $\hbar$), i.e., phonon frequencies. Thus the assumption of separation between electronic and nuclear timescales breaks down in the vicinity of electronic PES crossings and dynamics becomes nonadiabatic.

Several approaches exist in the literature to treat the nonadiabatic dynamics within the framework of quantum chemistry [2, 44, 87–93]. The most well known of these are mixed quantum classical treatments, the Ehrenfest and surface hopping methods. The Ehrenfest method is easy

to implement. It requires one to run a single trajectory of the nuclei, on an average PES, with electronic populations being evaluated on the fly [94]. The simplicity of the implementation of the method is flawed by its poor accuracy, related to its mean field nature. Usually different electronic configurations are associated ("entangled") with different paths of the nuclei and so the mean field approach becomes inadequate when these paths are very dissimilar. In order to fix this problem, Tully introduced a surface hopping approach, which accounts for the trajectory branching by running multiple trajectories that can hop between PESs [52]. Fewest switches surface hopping (FSSH) has become the most popular approach for problems at various scales, from molecules to nanoclusters [55, 95–100]. However, the method is built on *ad-hoc* assumptions and, as a result, frequently fails to properly describe correlations between the trajectories of nuclei and electronic states. In particularly, it does not take into account *decoherence* arising due to spacial separation between the components of the nuclear wavefunctions corresponding to different electronic states (PES) and, as a results, does not properly accounts for the intereference effects, etc. [101–103] Many approaches exist in the literature for overcoming this decoherence problem. Some attempt to add decoherence into Tully's surface hopping procedure [102, 104–116], while others involve rigorous treatments at the density matrix level, *e.g.* quantum classical Liouville equation (QCLE) [117–123] and the Meyer-Miller-Stock-Thoss [93, 124, 125] formalism. While these approaches all improve upon the FSSH algorithm, they are often either too costly, lead to complicated algorithms, or may not be accurate in certain scenarios.

The work presented here introduces a systematic way of studying nonadiabatic dynamics in the semiclassical regime, and is based on the semiclassical nonadiabatic scattering theory first developed by Piryatinski et al. [126]. in 2005. It is outlined in the following way: In Chapters 2 and 3, new theories are developed based on the aforementioned previous work. In Chapter 2, an improved theory with a discussion about nonadiabatic scattering region is given. In Chapter 3 an improved theory including time reversal symmetry in given. In Chapter 4, the Semiclassical Monte-Carlo algorithm is presented, which was first developed by Gorshkov et al. [58] in 2013, then presented in details by White et al. [59].

CHAPTER 2 PROPERTY OF SCATTERING REGION IN NONADIABATIC DYNAMICS

2.1 Overview

In this chapter, we investigate the property of the scattering region of an even-number-electron system. In the previous work by Piryatinski et. al. in 2005 [126], the semiclassical scattering at conical intersection was studied, in which they used a two-level system with two nuclear degrees of freedom. They proposed that, in the vicinity of the conical intersection, there exists a scattering region. They argued that, in the semiclassical limit, the quantum fluctuation near the conical intersection is neglectable, and the propagation of a nuclear wavepacket in this scattering region is ballistic, i.e. propagates in a straight line with constant velocity. The Schrödinger equation was solved in the semiclassical limit which gave a scattering matrix governing the scattering process. Numerical calculation has been done in their study and shown better agreement with quantum exact solution can be reached when the semiclassical scaling parameter is smaller, hence closer to quantum situation. In our study, a two-level model of linear electronic potentials is used to further study the property of scattering region near conical intersection. For a propagating wavepacket, we suggest that in the vicinity of conical point, it will go ballistically and avoid going through the conical point. Upon taking the semiclassical limit $\hbar \to 0$, we have proven that within a certain small range of the conical point, the exact starting and ending point of the ballistic path does not matter. The calculated result of propagation is governed by a classical propagator along the reference path which connects the initial and final points, and an integration over the impact parameter, which should be calculated numerically.

2.2 Theory

The fundamental quantity of quantum dynamics is the Schrödinger equation of a system

$$\hat{\mathcal{H}}\Psi(\boldsymbol{r}, \boldsymbol{r}_{\mathrm{e}}) = E\Psi(\boldsymbol{r}, \boldsymbol{r}_{\mathrm{e}}), \tag{2.1}$$

where we introduce the electronic coordinates $\boldsymbol{r}_{\mathrm{e}}$, of dimension $3n$, for an n-electron system; and the nuclear coordinates $\boldsymbol{r}$, of dimension k, for an arbitrary system with k degrees of freedom.

In a 3-dimensional world of N particles without constraint then $k = 3N$. The Hamiltonian $\hat{\mathcal{H}}$ operator of the system consists of the nuclear kinetic $\hat{T}_{\rm n}$ and the electronic Hamiltonian operator $\hat{\mathcal{H}}_{\rm e}$. Solving the Schrödinger equation of $\hat{\mathcal{H}}_{\rm e}$ gives a set of electronic eigenfunctions $\{\psi^l(\boldsymbol{r}, \boldsymbol{r}_{\rm e})\}$, which is infinite dimensional as for a real physical system there should be infinitely many states. This set of electronic eigenfunctions can be used as the basis set to expand the system wavefunction $\Psi(\boldsymbol{r}, \boldsymbol{r}_{\rm e})$, which is the well-known Born-Oppenheimer expansion [12, 127]

$$\Psi(\boldsymbol{r}, \boldsymbol{r}_{\rm e}) = \chi_\mu(\boldsymbol{r})\psi^\mu(\boldsymbol{r}, \boldsymbol{r}_{\rm e}), \tag{2.2}$$

where Einstein notation is used; the vector $\boldsymbol{\chi}(\boldsymbol{r})$ has elements as expansion coefficients and is of the same dimension as electronic eigenfunction basis set, so Eq. (2.2) is just the inner product between $\boldsymbol{\chi}(\boldsymbol{r})$ and $\boldsymbol{\psi}(\boldsymbol{r}, \boldsymbol{r}_{\rm e})$. The choice of basis set $\{\psi^l(\boldsymbol{r}, \boldsymbol{r}_{\rm e})\}$ determines the matrix $\mathbf{V}(\boldsymbol{r})$ of eigenvalues for the Schrödinger equation of $\hat{\mathcal{H}}_{\rm e}$. The often chosen orthonormal basis set diagonalizes $\mathbf{V}(\boldsymbol{r})$ and is referred to as the *adiabatic basis set*. Since the nuclear kinetic operator $\hat{T}_{\rm n}$ is defined as $\hat{T}_{\rm n} = -\sum_{j=1}^{k}(\hbar^2/2m_j)\partial^2/\partial {\rm R}_j{}^2$, and for the simplicity of formulas we let $m_j = m$ for all j's, then we can define the nonadiabatic coupling vector $\mathbf{A}(\boldsymbol{r})$ with element $A_{a\mu}{}^{\nu}(\boldsymbol{r})$ from electronic states ν to μ along nuclear coordinate direction ${\rm R}_a$

$$A_{a\mu}{}^{\nu}(\boldsymbol{r}) = \int {\rm d}\boldsymbol{r}_{\rm e}\, \psi_\mu(\boldsymbol{r}, \boldsymbol{r}_{\rm e}) \frac{\partial \psi^\nu(\boldsymbol{r}, \boldsymbol{r}_{\rm e})}{\partial r_{\rm n}^a}, \tag{2.3}$$

where obviously $\psi_\mu(\boldsymbol{r}, \boldsymbol{r}_{\rm e} = (\psi^\mu(\boldsymbol{r}, \boldsymbol{r}_{\rm e}))^*$ is the complex conjugate; $\mathbf{A}(\boldsymbol{r})$ has dimension k as a vector, same as $\boldsymbol{r}$; also has dimensions equal to the operators acting on the Hilbert space spanned by electronic basis set $\{\psi^l(\boldsymbol{r}, \boldsymbol{r}_{\rm e})\}$. Using nonadiabatic coupling vectors we can rewrite Hamiltonian $\hat{\mathcal{H}}$ in the gauge invariant form. We also want to preserve time reversal symmetry of our question as the system we would like to investigate is a closed shell even-number-electron system. By limiting our discussion a two-level system, the electronic eigenfunction basis set is two dimensional, and the corresponding Hamiltonian is

$$\hat{\mathcal{H}}(\boldsymbol{r}) = -\frac{\hbar^2}{2m}(\boldsymbol{\nabla} + {\rm i}\hat{\sigma}_y \mathbf{A}(\boldsymbol{r}))^2 + \mathbf{V}(\boldsymbol{r}), \tag{2.4}$$

in which the eigenfunction is no longer $\Psi(\boldsymbol{r}, \boldsymbol{r}_\mathrm{e})$ as in Eq. (2.1), but $\boldsymbol{\chi}(\boldsymbol{r})$; while energy $E(\boldsymbol{r})$ remains the same. $\mathbf{V}(\boldsymbol{r})$ is now represented by Pauli matrices $\hat{\sigma}_x$, $\hat{\sigma}_y$, and $\hat{\sigma}_z$ as $\mathbf{V}(\boldsymbol{r}) = V_0(\boldsymbol{r})\hat{\sigma}_0 + V_x(\boldsymbol{r})\hat{\sigma}_x + V_z(\boldsymbol{r})\hat{\sigma}_z$, $\hat{\sigma}_0$ is simply the 2×2 identity matrix, and V_0 is the auxiliary condition upon which potential is defined. Now we can apply Legendre transform to obtain the corresponding $\hat{\mathcal{L}}$ from Eq. (2.4) and calculate the propagator $\hat{\mathcal{K}}(\tau_j, \tau_i)$ from time τ_i to τ_j with initial and final nuclear configurations $\boldsymbol{r}(\tau_i)$ and $\boldsymbol{r}(\tau_j)$ over all paths $\boldsymbol{\xi}$'s:

$$\hat{\mathcal{K}}(\tau_j, \tau_i) = \int_{\boldsymbol{\xi}} \mathcal{D}\boldsymbol{\xi} \exp\left(\frac{\mathrm{i}}{\hbar} \int_{\tau_i}^{\tau_j} \mathrm{d}\tau\, \mathcal{L}_0\right) \hat{U}(\boldsymbol{\xi}), \tag{2.5}$$

where we separate the action into abelian part, for which the integration can be calculated normally, and define the scalar Lagrangian $\mathcal{L}_0(\boldsymbol{r}, \dot{\boldsymbol{r}}_\mathrm{n}, \tau) = m\dot{\boldsymbol{r}}_\mathrm{n}^2(\tau)/2 - V_0(\boldsymbol{r}(\tau))$, and non-abelian part, which needs be integrated as time-ordered exponential $\hat{U}(\boldsymbol{\xi})$:

$$\hat{U}(\boldsymbol{\xi}) = \mathrm{Texp}\left(-\frac{\mathrm{i}}{\hbar} \int_{r(\tau_i)}^{r(\tau_j)} \mathrm{d}r^k\, \hat{A}_k\right), \tag{2.6}$$

where we define $\hat{A}_k = (\bar{\mathbf{V}}(\boldsymbol{r}), \hbar\hat{\sigma}_y \mathbf{A}(\boldsymbol{r}))$, and $\bar{\mathbf{V}}(\boldsymbol{r}) = V_x(\boldsymbol{r})\hat{\sigma}_x + V_z(\boldsymbol{r})\hat{\sigma}_z$ which is the potential matrix without auxiliary condition V_0.

2.3 Two-level scattering model

Now to study the scattering dynamics of a two-level system with conical intersection, we consider a schematic model of one particle where the conical intersection is represented by using two linear adiabatic potentials $V_\beta(\boldsymbol{r}) = f|\boldsymbol{r}|$ and $V_\alpha(\boldsymbol{r}) = -f|\boldsymbol{r}|$, where we let $f > 0$, $\boldsymbol{r}$ is the nuclear coordinate. The auxiliary potential V_0 is obviously 0 in this model. Since the angular momentum is conserved so the space in which this particle's trajectory lies is reduced to a 2-dimensional surface, denoted as the xz-plane. We are interested in the process where a wavepacket starts to approach the conical intersection from far away, while passing the wavepacket itself remains on the same adiabatic PES, scattered at some angle and after that goes on to somewhere far from the conical intersection; our question is, how would such a wavepacket be scattered at the conical intersection, given by our two-level model?

To answer this question, we first define the adiabatic region, which is far enough from the conical intersection such that nonadiabatic coupling vector $\mathbf{A}$ between our two states is small

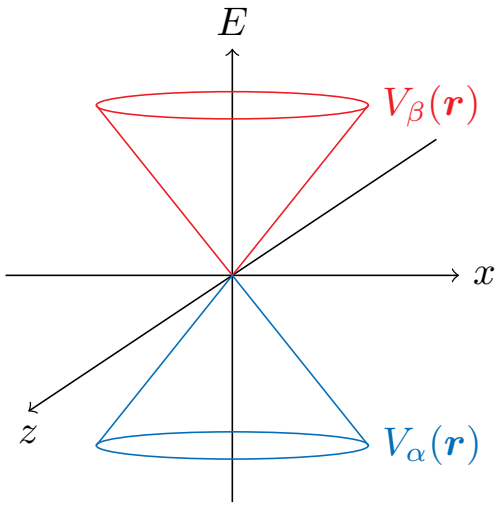

Figure 2.1: A two-level adiabatic PES model shown in 2-dimensional Cartesian coordinate system. Upper adiabatic PES $V_\beta(\boldsymbol{r}) = f|\boldsymbol{r}|$ shown in red, and lower adiabatic PES $V_\alpha(\boldsymbol{r}) = -f|\boldsymbol{r}|$ shown in blue. Two nuclear degrees of freedom, longitudinal direction x and transversal direction z, nuclear distance vector $\boldsymbol{r}$ satisfies $\boldsymbol{r}^2 = x^2 + z^2$.

enough that can be neglected, then we can treat the propagation in this region semiclassically and adiabatically using Van Vleck propagator; we also define the *scattering region*, which is essentially in the vicinity of conical intersection, in which the adiabatic approximation becomes invalid and we need to calculate the propagator using Eq. (2.5) in diabatic basis set, the wavepacket propagation is treated ballistically as $V_0 = 0$ in $\mathcal{L}_0$, with quantum fluctuation included in $\hat{U}$. Now we claim the following conjecture: In the intersection where adiabatic and scattering regions overlap with each other, we can either calculate the propagation adiabatically using Van Vleck propagator, or diabatically using Eq. (2.5).

To prove this conjecture, we first introduce two paths representing the aforementioned process, considered and plotted in Cartesian coordinate (x, z): first is the reference path, shown in Fig. 2.2 by the purple trajectory, along which a wavepacket propagates from initial point $(-r', 0)$, at where the center of the wavepacket is located, to conical point $(0, 0)$, then get scattered at classical angle θ, which is sufficiently small such that its momentum is still conserved within the semiclassical limit, and propagates from the conical intersection to final point $(r'' \cos\theta, r'' \sin\theta)$, which is approximately $(r'', r''\theta)$ and will be used from now on; second is the actual path, shown in Fig. 2.2 by the teal trajectory, the wavepacket propagates from $(-r', 0)$ to the vicinity of conical point, then goes through the scattering region ballistically, i.e. in a straight line which does not pass the

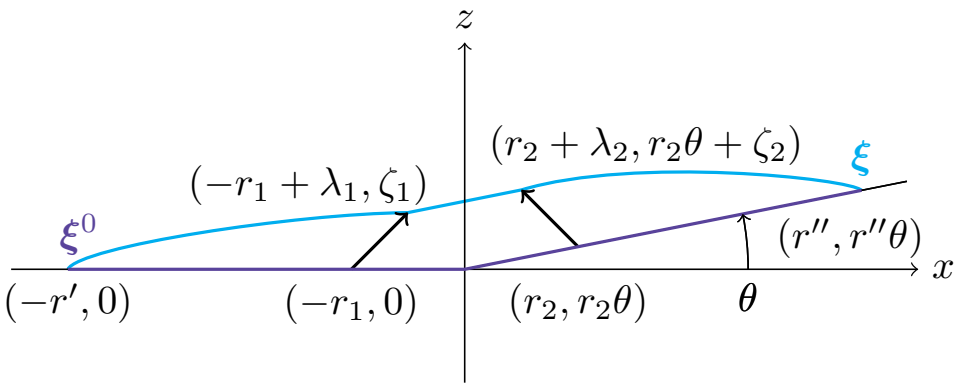

Figure 2.2: The actual and reference path of wavepacket propagation. The cyan trajectory represents the actual path, denoted $\boldsymbol{\xi}$; The violet trajectory represents the reference path, denoted $\boldsymbol{\xi}^0$; Initial point $(-r', 0)$ and final point $(r'', r''\theta)$ are far from the conical point and in the adiabatic region. Intermediate points $(-r_1, 0)$ and $(r_2, r_2\theta)$ are in the proposed overlapping region.

conical point $(0, 0)$, to the other side of scattering region, and then propagates adiabatically to the destination $(r'', r''\theta)$. We suggest two reference points: $(-r_1, 0)$ and $(r_2, r_2\theta)$, which lie in between the adiabatic and scattering region. Introduce local coordinates (λ_1, ζ_1) around $(r_1, 0)$ and (λ_2, ζ_2) around $(r_2, r_2\theta)$, so now the wavepacket goes through the scattering region from $(-r_1 + \lambda_1, \zeta_1)$ to $(r_2 + \lambda_2, \zeta_2)$, then we can define the scattering length: $r_s = \sqrt{\hbar(r_2 + r_1 + \lambda_2 - \lambda_1)/f(t_2 - t_1)}$, adopted and updated from previous study [126].

Denote the initial time as t_0, final time as t, at t_1 the wavepacket reaches $(-r_1 + \lambda_1, \zeta_1)$ and at t_2 it reaches $(r_2 + \lambda_2, \zeta_2)$, also for convenience let $\tau = 0$ at the instance the wavepacket arrives at $z = 0$. Then in this model, by considering the variables in powers of $\hbar$, we have 1. $r', r'', v, f \sim \hbar^0$; 2. $r_1, r_2, t_1, t_2 \sim \hbar^{(1/2)-\epsilon}$, where ϵ is some small positive number; 3. $g_s, \lambda_1, \lambda_2, \zeta_1, \zeta_2, \theta \sim \hbar^{1/2}$. So r_s is automatically of order $\hbar^{1/2}$, while the inf of r_s is smaller than the typical length of scattering region, and sup of r_s is far enough from the conical intersection for adiabatic approximation to be valid. In the semiclassical limit, $\hbar \to 0$, since we need to calculate the propagator as $\exp(\mathrm{i}S/\hbar)$, in the action we only have to keep the terms of order no more than $\hbar$, anything of order higher than $\hbar$ would be insignificant when actually calculating the propagation numerically and can thus be neglected.

Consider the dynamics of a wavepacket traveling along the actual path as in Fig. 2.2 while staying on surface β, before and after the conical intersection, the Lagrangian $\mathcal{L}(\boldsymbol{\xi})$ described in

polar coordinate is

$$\mathcal{L}(\boldsymbol{\xi}) = \frac{m}{2}(\dot{r}^2 + r^2\dot{\vartheta}^2) - fr, \quad r > 0. \tag{2.7}$$

This Lagrangian is then used to evaluate the associated stability matrix $\mathrm{M_C}(\tau_j, \tau_i)$. For reference path, the angular momentum is $\mathbf{0}$ in this case and we have

$$p_r(\tau) = m\dot{r}(\tau) = \pm\sqrt{2m(E - fr(\tau))}, \tag{2.8}$$

$p_r(\tau)$ is negative when approaching the conical intersection, and positive when leaving it. Lagrangian of the system (in 1-dim) is

$$\mathcal{L} = \frac{m}{2}\dot{x}^2 + fx. \tag{2.9}$$

We can write the total action along actual path on surface β, $S(\boldsymbol{\xi}) = \int_{\tau_i}^{t} \mathcal{L}(\boldsymbol{\xi})\,\mathrm{d}\tau$, which is then separated into three parts, where we further denote $S_1(\boldsymbol{\xi}) = \int_{\tau_i}^{t_1} \mathcal{L}(\boldsymbol{\xi})\,\mathrm{d}\tau$, at time t_1 the wavepacket reaches the scattering region at $(-r_1+\lambda_1, \zeta_1)$; $S_2(\boldsymbol{\xi}) = \int_{t_2}^{t} \mathcal{L}(\boldsymbol{\xi})\,\mathrm{d}\tau$, at time t_2 the wavepacket leaves the scattering region from $(r_2 + \lambda_2, \zeta_2)$; from t_1 to t_2 we have the ballistic action, denoted $S_b(\boldsymbol{\xi})$ and considered as a free propagation from $(-r_1 + \lambda_1, \zeta_1)$ to $(r_2 + \lambda_2, \zeta_2)$; the reason why we can treat the action in scattering region as ballistic propagation is given by Eq. (2.5), as $S_b(\boldsymbol{\xi})$ is just the action from scalar Lagrangian $\mathcal{L}_0$, where $V_0 = 0$. According to the scales we defined, in the semiclassical limit we can treat the local coordinates as variations, by keeping up to the second order terms, we can expand $S_1(\boldsymbol{\xi})$ as

$$S_1(\boldsymbol{\xi}) = S_1(\boldsymbol{\xi}^0; t_1, t_0) + p_x(t_1)\lambda_1 + p_z(t_1)\zeta_1 + \Lambda_x\lambda_1^2 + \Lambda_z\zeta_1^2, \tag{2.10}$$

and $S_2(\boldsymbol{\xi})$ as

$$S_2(\boldsymbol{\xi}) = S_2(\boldsymbol{\xi}^0; t, t_2) - p_x(t_2)\lambda_2 - p_z(t_2)\zeta_2 + \Theta_x\lambda_2^2 + \Theta_z\zeta_2^2, \tag{2.11}$$

momenta are calculated by expanding Eq. (2.8) to the first order of r_j's then converted into Cartesian coordinate. Second derivatives of actions are denoted by Λ's and Ξ's, which are defined in

appendix D using parts from the stability matrix $\mathrm{M_C}(\tau_j, \tau_i)$:

$$\mathrm{M_C}(\tau_j, \tau_i) = \begin{pmatrix} A(\tau_j, \tau_i) & B(\tau_j, \tau_i) \\ C(\tau_j, \tau_i) & D(\tau_j, \tau_i) \end{pmatrix}, \tag{2.12}$$

evaluated from initial τ_i to final τ_j in Cartesian coordinate, definitions of each submatrix are included in appendix D, so the components in $\mathrm{M_C}$ of our interests are $A(\tau_j, \tau_i)$, $B^(\tau_j, \tau_i)$, and $D(\tau_j, \tau_i)$, which can be calculated by first calculating the stability matrix $\mathrm{M_P}(\tau_j, \tau_i)$ in polar coordinate then converting into Cartesian coordinate. Actions $S_1(\boldsymbol{\xi}^0; t_1, t_0)$ and $S_2(\boldsymbol{\xi}^0; t, t_2)$ are taken along the reference path in Fig. 2.2 which can be calculated in the following way:

The action $S_1(\boldsymbol{\xi}^0; t_1, t_0)$ can be calculated using the abbreviated action since energy is conserved

$$\begin{aligned} S_1(\boldsymbol{\xi}^0; t_1, t_0) &= \int_{\boldsymbol{q}(t_0)}^{\boldsymbol{q}(t_1)} \boldsymbol{p}\, \mathrm{d}\boldsymbol{q} - \int_{t_0}^{t_1} E\, \mathrm{d}t \\ &= \int_{r'}^{r_1} \mathrm{d}r\, (-\sqrt{2mE - 2mfr}) - E(t_1 - t_0) \\ &= \frac{2\sqrt{2m}}{3f}\Big((E - fr_1)^{3/2} - \big(E - fr'\big)^{3/2}\Big) - E(t_1 - t_0). \end{aligned} \tag{2.13}$$

Similarily the action along reference trajectory $S_2(\boldsymbol{\xi}^0; t, t_2)$ is given by

$$\begin{aligned} S_2(\boldsymbol{\xi}^0; t, t_2) &= \int_{\boldsymbol{q}(t_2)}^{\boldsymbol{q}(t)} \boldsymbol{p}\, \mathrm{d}\boldsymbol{q} - \int_{t_2}^{t} E\, \mathrm{d}t \\ &= \frac{2\sqrt{2m}}{3f}\Big((E - fr_2)^{3/2} - \big(E - fr''\big)^{3/2}\Big) - E(t - t_2). \end{aligned} \tag{2.14}$$

Ballistic action $S_b(\boldsymbol{\xi})$ can be calculated easily since it's a free propagation,

$$S_b = \frac{m(r_2 + r_1)^2}{2(t_2 - t_1)} + \delta S_\lambda + \delta S_\zeta, \tag{2.15}$$

and its local corrections are:

$$\delta S_\lambda = \frac{m(r_2 + r_1)(\lambda_2 - \lambda_1)}{t_2 - t_1} + \frac{m(\lambda_2 - \lambda_1)^2}{2(t_2 - t_1)}, \tag{2.16a}$$

and

$$\delta S_\zeta = \frac{mr_2\theta(\zeta_2 - \zeta_1)}{t_2 - t_1} + \frac{m(\zeta_2 - \zeta_1)^2}{2(t_2 - t_1)}. \tag{2.16b}$$

To evaluate the propagator in Eq. (2.5) from time t_0 to t staying on surface β for our model, we can split the propagator according to the way we treat these actions, and connect them by integrating over local coordinates from $-\infty$ to $+\infty$, which is the collection of all paths passing through the scattering region. Now we have $\mathcal{K}(t,t_0)$ equals to

$$\mathcal{K}(t,t_0)=\int \mathcal{D}\boldsymbol{\xi}\mathcal{K}(t,t_2)\mathcal{K}(t_2,t_1)\mathcal{K}(t_1,t_0). \tag{2.17}$$

By splitting the propagator, each of them can be calculated using the corresponding actions and appropriately approximated, according to the domain in which they are defined. For $\mathcal{K}(t_1,t_0)$ and $\mathcal{K}(t,t_2)$, since they are away from the conical intersection with distance no smaller than the order of $\hbar^{(1/2)-\epsilon}$, we can use the adiabatic basis set and calculate them as Van Vleck propagators [46]. Here we have:

$$\mathcal{K}(t_1,t_0)=\exp\left(\frac{\mathrm{i}\pi n_1}{2}\right)\frac{\exp(\mathrm{i}S_1(\boldsymbol{\xi};t_1,t_0)/\hbar)}{2\mathrm{i}\pi\hbar\sqrt{|\det(B(t_1,t_0))|}}, \tag{2.18}$$

and

$$\mathcal{K}(t,t_2)=\exp\left(\frac{\mathrm{i}\pi n_2}{2}\right)\frac{\exp(\mathrm{i}S_2(\boldsymbol{\xi};t,t_2)/\hbar)}{2\mathrm{i}\pi\hbar\sqrt{|\det(B(t,t_2))|}}, \tag{2.19}$$

n_1 and n_2 are the Maslov indexes of each propagator [128]. For $\mathcal{K}(t_2,t_1)$, the ballistic action is considered in the vicinity of conical intersection so we choose diabatic basis set where nonadiabatic coupling vector is $\mathbf{0}$, to avoid the difficulty that when approaching the conical intersection in adiabatic basis set nonadiabatic coupling would rapidly increase to infinity. Since we have chosen the diabatic basis set for ballistic region, so the off-diagonal terms of matrix $\hat{U}(\boldsymbol{\xi})$ correspond to the same surface wavepacket propagation. For our model studying traveling and staying on surface β, we need $U_{12}(\boldsymbol{\xi})$. Hence the ballistic propagation is

$$\mathcal{K}(t_2,t_1)=\frac{m\exp(\mathrm{i}S_b(\boldsymbol{\xi};t_2,t_1)/\hbar)U_{12}(\boldsymbol{\xi})}{2\mathrm{i}\pi\hbar(t_2-t_1)}, \tag{2.20}$$

To evaluate these path integrals, we define $\lambda_-=(-\kappa\zeta_2+(1-\kappa)\zeta_1)/2\kappa(1-\kappa)$ and $\lambda_+=\kappa\zeta_2+(1-\kappa)\zeta_1$, where $\kappa=r_1/(r_1+r_2)$. We immediately realize that λ_+ is the impact parameter of our ballistic path by geometry. The time-ordered exponential $\hat{U}(\boldsymbol{\xi})$ can be calculated as described in previous study [12], for our model we define $l_1=\sqrt{2}(-r_1+\lambda_1)/r_s$, $l_2=\sqrt{2}(r_2+\lambda_2)/r_s$, and

$\alpha = \sqrt{2}\lambda_+/r_s$. Calculate $\exp(\mathrm{i}S(\boldsymbol{\xi};t,t_0)/\hbar)U_{12}(\boldsymbol{\xi})$ in the semiclassical limit by applying saddle point method to λ_- and calculating Gaussian integrals of λ_1 and λ_2, with the saddle point determined as $\bar{\lambda}_- = (1-2\kappa)\lambda_+$ we arrived at the expression of $\mathcal{K}(t,t_0)$:

$$\mathcal{K}(t,t_0) = \frac{a(t,t_0)}{\sqrt{r'r''}} K_{\mathrm{cl}}(t,t_0) \int_{-\infty}^{+\infty} \mathrm{d}\lambda_+ \, I_{\lambda_+}, \tag{2.21}$$

while the integrand I_{λ_+} equals to

$$I_{\lambda_+} = \sqrt{P}\exp\left(\frac{mv\theta\lambda_+}{\mathrm{i}\hbar} + \omega\ln\frac{g_s^2}{2} - \mathrm{i}\arg\Gamma(\omega)\right), \tag{2.22}$$

where $\omega = -\mathrm{i}f\lambda_+^2/2\hbar v$ is the dimensionless phase factor which is of order $\hbar^0$, dimensionless scaling parameter $g_s = \sqrt{m^2v^3/\hbar f}$, and $P = 1-\exp(2\pi\omega/\mathrm{i})$ is the possibility amplitude introduced from time-ordered exponential calculation [12]. $\mathcal{K}_{\mathrm{cl}}$ is the classical propagator along the reference path staying on surface β:

$$K_{\mathrm{cl}}(t,t_0) = \exp\left(\frac{\mathrm{i}}{\hbar}S_{\mathrm{cl}}(t,t_0)\right). \tag{2.23}$$

So we can conclude that the propagator, in Eq. (2.21), we derived governed by the Lagrangian, in Eq. (2.7), is independent of the *midway* points we assumed at where the propagation enters and leaves the vicinity of conical intersection at which we would consider the nonadiabatic coupling is too strong that we have to use diabatic basis set to describe the physical processes, without actually finding and using diabatic basis set.

2.4 Conclusion

We have delivered a newer semiclassical model to compute the diabatic wavepacket propagation along the same PES in a two-level system of potential functions $V_\alpha(\boldsymbol{r}) = -f|\boldsymbol{r}|$ and $V_\beta(\boldsymbol{r}) = f|\boldsymbol{r}|$. A propagation process is proposed, from adiabatic propagation, then to ballistic propagation, and last back to adiabatic propagation. The corresponding actions are calculated using Van Vleck propagator and stability matrices. We have proven that for our model, in the semiclassical limit, there is an overlapping region near the scattering region where both the adiabatic propagator and ballistic propagator for nonadiabatic dynamics are valid. We look forward to develop algorithm based on this theory and do computational study. We would also like to generalize this result to

two-level systems with potential energy surfaces of certain local symmetry in the vicinity of conical intersection.

CHAPTER 3 DYNAMICAL CONSEQUENCES OF TIME-REVERSAL SYMMETRY IN NONADIABATIC DYNAMICS

Reproduced from Chem. Phys., Volume 515, 2018, Pages 3-20, with the permission of Elsevier B.V.

3.1 Overview

The goal of the presented study is to identify the implications of time-reversal symmetry and topology, associated with unavoidable crossings, on wavepacket dynamics, with focus on half-integer spin case. This is achieved via (i) investigating electronic structure using group invariance under real structure transformations, (ii) establishing the topological invariants, associated with a CS, (iii) extending the semiclassical approach of [126] to the half-integer spin case, characterized by the Kramers permanent degeneracy, by addressing the Kramers permanent degeneracy for the adiabatic Born-Oppenheimer dynamics, as well generalizing the ballistic approach that describes the wavepacket evolution when passing a CS, and (iv) finally identifying the topological implications on the scattered wavepacket shape. The chapter is organized as follows. In section 3.2 we discuss the time-reversal symmetry for non-relativistic (with spin-orbit corrections) many electron systems, with focus on the half-integer spin (odd electron number) case, and the major differences between the aforementioned situation and the integer spin or no time-reversal symmetry (strong effects of magnetic fields) counterparts. To provide a formulation, ready for studies of the dynamical consequences of time-reversal symmetry, we identify the orthogonal SO(n), unitary U(n), and symplectic groups Sp(n) as the ones, responsible for the symmetry in the integer-spin, no-symmetry, and half-integer spin situations, naturally referring to them as the orthogonal, unitary, and symplectic cases. We also provide a description of local structures of CSs in all three cases, within a unique fashion, which is achieved by introducing the gamma-matrices, associated with spinors in lower an higher dimensions, namely $d = 2$, $d = 3$, and $d = 5$. In section 3.3 we introduce the topological invariants associated with CSs for all three aforementioned cases, represented by the first Stiefel-Whitney, first Chern, and second Chern classes, respectively, focusing on their properties that unveil the topological effects in wavepacket dynamics. The presentation is done on an intuitive level, keeping

it to minimum, needed to understand the topological dynamical implications, using calculus and linear algebra only, so it does not require from a reader any knowledge in topology or geometry. We also describe a geometrical effect, associated with Kramers permanent degeneracy, and relate it to "non-abelian Berry phase". In section 3.4 we extend the Born-Oppenheimer, and corresponding semiclassical approximations to the symplectic case, introduce the wavefunction polarization, appearing as a consequences of Kramers degeneracy, and apply the parallel transport concept to describe semiclassical evolution of the polarization. In section 3.5 we present the ballistic approximation, the main tool of studying the asymptotically exact semiclassical limit of wavepacket evolution while it passes a CS, in a unique fashion, in particular allowing to apply the standard expressions of the celebrated 2-state Landau-Zener problem to its 5-state counterpart, occurring in the symplectic case, which is achieved by making use of the (Clifford) algebra of gamma-matrices, which, in particular, justifies the formulation of time-reversal symmetry, given in section 3.2. In section 3.6 we present an explicit analytical expression for the wavepacket that just passed through a conical seam, analyze its shape, identify the topological nature of the latter, and connect it to the topological invariants of CSs, described in section 3.3.

3.2 Time-Reversal Symmetry in Many-Electron Systems

Time-reversal symmetry that occurs in the absence of external magnetic fields, which is usually the case in dynamics of molecular systems, has important implementations on the system dynamics. In the simplest case of no spin the time-reversal transformation j is defined by $j\psi(\boldsymbol{r}) = \psi^*(\boldsymbol{r})$, and it commutes $j\hat{H} = \hat{H}j$ with the system Hamiltonian $\hat{H}$. Such symmetry is coined time-reversal due to the fact that if $\psi(t)$ satisfies the dynamical Schrödinger equation $i\hbar\partial_t\psi(t) = \hat{H}\psi(t)$ then, due to the above commutation property $j\psi(t) = \psi^*(t)$ satisfies the Schrödinger equation with the same Hamiltonian, but for reversed time.

Since, by simple intuitive reason, presented above, time-reversal symmetry involves complex conjugation, it is represented by an *antilinear* map j acting in the space of the system quantum states, which means

$$j(u+v) = j(u) + j(v), \quad j(\lambda u) = \lambda^* j(u) \tag{3.1}$$

for any two states u, v and complex number λ. Note that antilinear is different from a "standard" linear map through the second condition that in the linear case map reads $j(\lambda u) = \lambda j(u)$.

Time-reversal symmetry for spin 1/2 has been identified by Kramers, and can be described in the following way. One can ask a question: How does an antilinear map j, referred to as a real structure, look like that acts in a 2-dimensional complex vector space of the spin 1/2 and commutes with the group $SU(2)$ action? The latter property is equivalent to commuting with the generators of the corresponding Lie algebra $su(2)$, represented by $-\mathrm{i}\boldsymbol{\sigma} = -(\mathrm{i}\sigma_x, \mathrm{i}\sigma_y, \mathrm{i}\sigma_z)$, with

$$\sigma_0 = \mathbb{I} = \begin{pmatrix} 1 & 0 \\ 0 & 1 \end{pmatrix}, \quad \sigma_x = \sigma_1 = \begin{pmatrix} 0 & 1 \\ 1 & 0 \end{pmatrix}, \quad \sigma_y = \sigma_2 = \begin{pmatrix} 0 & -\mathrm{i} \\ \mathrm{i} & 0 \end{pmatrix}, \quad \sigma_z = \sigma_3 = \begin{pmatrix} 1 & 0 \\ 0 & -1 \end{pmatrix} \tag{3.2}$$

being the Pauli matrices in on of their standard representations. A real structure j that satisfies the aforementioned commutation property is represented by a matrix

$$j = \eta \mathrm{i}\sigma_y = \begin{pmatrix} 0 & \eta \\ -\eta & 0 \end{pmatrix}, \quad j \begin{pmatrix} c_1 \\ c_2 \end{pmatrix} = \begin{pmatrix} \eta c_2^* \\ -\eta c_1^* \end{pmatrix}, \quad j^2 = -1. \tag{3.3}$$

with $\eta \in \mathrm{U}(1)$ being a unimodular factor. The commutation properties follow from the commutation relations $\sigma_x\sigma_y = -\sigma_x\sigma_y$, $\sigma_y\sigma_z = -\sigma_z\sigma_y$, and $\sigma_z\sigma_x = -\sigma_x\sigma_z$, combined with the anti-linearity of j. The real structure, defined by Eq. (3.3) possesses two important properties: it preserves scalar products in the sense

$$(j(u), j(v)) = (u, v)^*, \tag{3.4}$$

and $j^2 = -1$. A straightforward argument that involves the Schur's lemma shows that Eq. (3.3) completely classifies the real structures with $j^2 = -1$ that preserve the scalar product. Hereafter we choose $\eta = 1$. It is straightforward to verify that the Breit-Pauli Hamiltonian [129] commutes with the real structure j obtained by applying j, defined by Eq. (3.3), to the spin variables of all electrons. An obvious, bur extremely important consequence of the property of the spin 1/2 real structure [see Eq. (3.3)] is $j^2 = (-1)^N$ with N being the number of electrons, so that we have $j^2 = 1$ and $j^2 = -1$ for the even and odd number of electrons, respectively, which leads to very different electronic structure symmetry properties for molecules and radicals.

To describe a situation when a finite number of Potential Energy Surfaces (PES) are taken

into account we should consider an n-dimensional complex vector space V (or, equivalently, a $2n$-dimensional real vector space) that describes the space of electronic states for a given nuclear configuration, n being the number of PES, taken into consideration, with an action $j : V \to V$ of a real structure on it, and further identify the space of allowed electronic Hamiltonians, represented by Hermitian operators h acting in V and commuting with j.

To recover a well-known picture, we start with the $j^2 = 1$ case that corresponds to an even number of electrons. The analysis is very simple: we consider V as a $2n$-dimensional real vector space with $i : V \to V$ representing multiplication with the imaginary unit i. Note that i and j can be viewed as just linear maps acting in the $2n$-dimensional real vector space V. Since j preserves the scalar product in the real space it is an orthogonal operator. Generically an orthogonal operator has pairs of mutually complex conjugated eigenvalues, however, due to the $j^2 = 1$ condition, all eigenvalues are ± 1 and hence j is diagonalizable within the real space. Due to anti-linearity of j we have $ji = -ij$, which means that if u is an eigenvector of j then $i(u)$ is also an eigenvector, but with an opposite eigenvalue. This implies that the space of states can be decomposed into a direct sum $V = W \oplus i(W)$, where $W \subset V$ is an n-dimensional real subspace of the eigenvectors of j with the unit eigenvalue. Equivalently it can be represented as

$$V = \mathbb{C} \otimes_{\mathbb{R}} W, \quad j(\lambda \otimes u) = \lambda^* \otimes u, \tag{3.5}$$

and the allowed electronic Hamiltonians are represented by real hermitian matrices that represent operators acting in W. We can always choose the basis sets to belong to W, so that the basis set transformations that preserve the scalar product are orthogonal, i.e., belong to the orthogonal group $\mathrm{O}(n)$; therefore, hereafter we refer to this case as orthogonal. Note that such orthogonal transformations are the ones that commute with the real structure j.

In the simplest case of $n = 2$ we have

$$h(\boldsymbol{r}) = h_0(\boldsymbol{r})\sigma_0 + h_x(\boldsymbol{r})\sigma_x + h_z(\boldsymbol{r})\sigma_z, \tag{3.6}$$

with σ_0 being the unit 2×2 matrix, so that for the two PES to intersect in a generic (maximal rank) situation, referred to as CSs, two conditions $h_x(\boldsymbol{r}) = h_z(\boldsymbol{r}) = 0$ should be satisfied, so that

the CSs have codimension 2, as well known.

Before we switch to the $j^2 = -1$ case we consider the case of no time-reversal symmetry (in the presence of magnetic field) For n PES in the absence of time-reversal symmetry an orthonormal basis set can be chosen up to a unitary transformation, so that we are dealing with the unitary symmetry described by the unitary group $\mathrm{U}(n)$; therefore, hereafter we refer to this case as unitary. In the case under consideration electronic Hamiltonians are described by just Hermitian operators (matrices) without any further conditions, so that in the simplest $n = 2$ case Eq. (3.6) adopts a form

$$h(\boldsymbol{r}) = h_0(\boldsymbol{r})\sigma_0 + h_x(\boldsymbol{r})\sigma_x + h_y(\boldsymbol{r})\sigma_y + h_z(\boldsymbol{r})\sigma_z, \tag{3.7}$$

and the CSs have codimension 3.

At this point we turn to the case of odd number of electrons, i.e., half-integer total electron spin, which corresponds to $j^2 = -1$. Similar to the integer spin case we consider an n-dimensional complex vector space of states V and view it as a $2n$-dimensional real vector space equipped with two linear maps $i, j : V \to V$. We further introduce the third linear map $k : V \to V$ by $k = ij$. It is verified in a straightforward way that i, j, and k anti-commute, and $i^2 = j^2 = k^2 = -1$, as well as $ki = j$ and $jk = i$. This implies that we have a well-defined action of the non-commutative *division ring* $\mathbb{H}$ of quaternions on V. We reiterate that a quaternion is represented $q = a_0 + a_1 i + a_2 j + a_3 k$, with $(a_s | s = 0, \ldots, 3)$ being a set of four real numbers; addition and multiplication of quaternions is defined in an obvious way. As a vector space $\mathbb{H} \cong \mathbb{C}^2 \cong \mathbb{R}^4$. A conjugate q^* to q quaternion is naturally defined as

$$(a_0 + a_1 i + a_2 j + a_3 k)^* = a_0 - a_1 i - a_2 j - a_3 k. \tag{3.8}$$

The term division ring means that each nonzero element has an inverse with respect to multiplication, so that sometimes $\mathbb{H}$ is referred to as a non-commutative field.

Although quaternions are non-commutative, their "field" property provides a very simple and universal structure of quaternion spaces, e.g., our space of states V, it allows for basis sets, and in particular orthonormal basis sets, and a unique decomposition of any state as a linear superposition

of the basis set elements with quaternion coefficients. A choice of a basis set allows a representation

$$V = \mathbb{H} \otimes_{\mathbb{R}} W, \quad q(\lambda \otimes u) = (q\lambda) \otimes u, \tag{3.9}$$

for $u \in W,\ q, \lambda \in \mathbb{H}$, where W is an m-dimensional real vector space with $n = 2m$.

Due to the basis set decomposition property transformations between the basis sets are represented by $m \times m$ matrices with quaternion entries. We can, however, further narrow down the class of preferred basis sets. We can apply the analysis of appendix A and note that there is a naturally defined action of the group $\mathrm{Sp}(m)$ on the space V of electronic states. We can also consider a class of *real orthonormal* basis sets (see appendix A for some details) that are defined as orthonormal basis sets of a special form

$$(e_1, \ldots, e_m, e'_1, \ldots, e'_m) = (e_1, \ldots, e_m, j(e_1), \ldots, j(e_m)). \tag{3.10}$$

Obviously, an invertible linear map $A : V \to V$ belongs to $\mathrm{Sp}(m)$ if and only if it transfers any real orthonormal basis set to the basis set of the same kind. In physics terms we can say that in the case of time-reversal symmetry and $j^2 = -1$ (odd number of electrons), when we have $n = 2m$ PES, we are dealing with symplectic symmetry, described by the group $\mathrm{Sp}(m)$; therefore, hereafter we refer to this case as symplectic. Note that since $[j, \hat{H}] = 0$ an adiabatic basis set can be always chosen to be real orthonormal, and all PES are double degenerate, being represented by pairs of adiabatic states $(e_a, j(e_a))$.

We are now in a position to identify the electronic Hamiltonians h, represented by Hermitian operators that commute with j. Using the quaternionic representation we find that they are given by $m \times m$ quaternionic matrices with $h_{ba} = h^*_{ab}$. In the simplest $m = 2$ case of $n = 2m = 4$ double degenerate PES, and omitting the unit matrix that has nothing to do with the intersections, so that we can deal with traceless matrices, we obtain a 5-dimensional space of matrices with a basis

set to be chosen, e.g., as

$$\gamma_1 = \begin{pmatrix} 0 & i \\ -i & 0 \end{pmatrix}, \quad \gamma_2 = \begin{pmatrix} 0 & j \\ -j & 0 \end{pmatrix}, \quad \gamma_3 = \begin{pmatrix} 0 & k \\ -k & 0 \end{pmatrix},$$
$$\gamma_4 = \begin{pmatrix} 0 & 1 \\ 1 & 0 \end{pmatrix}, \quad \gamma_5 = \begin{pmatrix} -1 & 0 \\ 0 & 1 \end{pmatrix}, \quad \gamma_0 = \begin{pmatrix} 1 & 0 \\ 0 & 1 \end{pmatrix}. \tag{3.11}$$

A straightforward computation yields

$$\gamma_a\gamma_b + \gamma_b\gamma_a = 2\delta_{ab}\gamma_0, \quad \gamma_5 = \gamma_1\gamma_2\gamma_3\gamma_4, \tag{3.12}$$

with γ_0 being the unit 2×2 quaternionic matrix. By implementing a standard 2×2 matrix representation of quaternion units

$$1 \mapsto \sigma_0, \quad i \mapsto i\sigma_x, \quad j \mapsto i\sigma_y, \quad k \mapsto i\sigma_z, \tag{3.13}$$

we can view the 2×2 quaternionic matrices as 4×4 complex matrices that represent linear operators acting in V in a real orthonormal basis set. Upon substitution of Eq. (3.13) into Eq. (3.11) one can recognize $(\gamma_a|a = 1, \ldots, 4)$ as Euclidean Dirac gamma-matrices, written in the so-called chiral representation, with γ_5 being the product of four Dirac γ-matrices, so that $(\gamma_a|a = 1, \ldots, 5)$ represent the five gamma-matrices, associated with the spinors in 5-dimensional space This implies that an electron Hamiltonian (with the unit matrix omitted) that preserves time-reversal symmetry adopts a form

$$h = \boldsymbol{h} \cdot \boldsymbol{\gamma} = \sum_{a=1}^{5} h_a\gamma_a, \tag{3.14}$$

with real coefficients h_a.

For the Hamiltonians in Eq. (3.14) we have two double-degenerate PES with the energies $\varepsilon = \pm\sqrt{(\boldsymbol{h}, \boldsymbol{h})}$, and the CI (Dirac) point at $\boldsymbol{h} = 0$. Since for the conical points, associated with the nuclear configurations, five equations $\boldsymbol{h}(\boldsymbol{r}) = 0$, should be satisfied, the CSs for the time-reversal symmetry with an odd number of electrons have codimension 5.

3.3 Conical Points and Associated Topological Invariants

We are now in a position to describe and compare the topological invariants associated with CSs. We start with the orthogonal case that corresponds to systems of even number of electrons with time-reversal symmetry. Consider a 2-dimensional vector space of electronic Hamiltonians $h = h_x\sigma_x + h_z\sigma_z$, with the unit matrix that has nothing to do with the PES intersections omitted from Eq. (3.6). We have for the electronic energies $\varepsilon = \pm\sqrt{h_x^2 + h_z^2}$, so that we have a CS at the origin $h_x = h_z = 0$. We further surround the origin with a circle S^1, defined say by $h_x^2 + h_z^2 = \varepsilon^2$. With each point (h_x, h_z) of the circle one can associate a 1-dimensional real space of real eigenstates, say with the higher eigenvalue $\sqrt{h_x^2 + h_z^2}$, and further ask a question whether one can identify globally an adiabatic real normalized basis set, i.e., associate with each 1-dimensional eigenspace a unit length vector in a continuous way. The answer is negative, since upon going over the circle the eigenstate changes the sign. In physics/chemistry literature it is known as the topological Berry phase, which assumes discrete values $0, \pi$. In geometry/topology language one would say that the aforementioned 1-dimensional bundle has a nontrivial *first Stiefel-Whitney class* w_1 [130], which is binary, rather than integer i.e., resides in $\mathbb{Z}_2$, rather than $\mathbb{Z}$, or in other words is represented by a sign ± 1 factor. If we wind a circle around the conical seam, it will be mapped to the space of electronic Hamiltonians by means of Eq. (3.6), which will give rise to the topological Berry phase in its conventional sense (gaining a -1 factor upon winding around the conical seam). In other words the topological Berry phase in the space of nuclear configurations $\boldsymbol{r}$ is completely induced by its counterpart in the space of electronic Hamiltonians, the latter being described above.

In the unitary case of no time-reversal symmetry (e.g., in a famous example of a single spin 1/2 in a magnetic field) we consider a 3-dimensional vector space of electronic Hamiltonians $h = h_x\sigma_x + h_y\sigma_y + h_z\sigma_z$, with the unit matrix that has nothing to do with the PES intersections omitted from Eq. (3.7). Similar to the time-reversal case we have the electronic energies $\varepsilon = \pm\sqrt{h_x^2 + h_y^2 + h_z^2}$, so that we have a conical (sometimes also referred to as *diabolic*) intersection at the origin $h_x = h_y = h_z = 0$. We further surround the origin with a (2-dimensional) sphere S^2, defined say by $h_x^2 + h_y^2 + h_z^2 = \varepsilon^2$. With each point (h_x, h_y, h_z) of the sphere one can associate a 1-dimensional complex space of eigenstates, say with the higher eigenvalue ε, and further ask a question whether one can identify globally a normalized adiabatic basis set, i.e., associate with each

1-dimensional eigenspace a unit length vector in a continuous way. The answer is negative again, and this can be rationalized as follows.

Denoting $\boldsymbol{h} = \varepsilon(\boldsymbol{n}, n_z)$ and $n_\pm = n_x \pm i n_y$, we can recast the eigenvalue problem $(\boldsymbol{h}\cdot\boldsymbol{\sigma})\boldsymbol{\psi} = \varepsilon\boldsymbol{\psi}$, for $\boldsymbol{\psi} = (\psi_1, \psi_2)$ in a form

$$\begin{aligned} (1 - n_z)\psi_1 - n_-\psi_2 = 0, \\ -n_+\psi_1 + (1 + n_z)\psi_2 = 0, \end{aligned} \tag{3.15}$$

where the two equations are equivalent. Two equivalent solutions can be naturally identified as

$$\begin{aligned} (\psi_1^-, \psi_2^-) = (n_-, 1 - n_z), \\ (\psi_1^+, \psi_2^+) = (1 + n_z, n_+) \end{aligned} \tag{3.16}$$

with $\bar{\boldsymbol{\psi}}^\pm = (1/\sqrt{2(1 \pm n_z)})\,\boldsymbol{\psi}_\pm$ being the normalized counterparts. The solutions $\boldsymbol{\psi}^\pm$ turn to zero at the south and north poles of the sphere, respectively, which already provides evidence of an impossibility of building a global adiabatic basis set.

We can extend the aforementioned evidence to a more rigorous argument. To that end we note that the two normalized solutions, both representing a normalized adiabatic state should be connected $\bar{\boldsymbol{\psi}}^+ = g\bar{\boldsymbol{\psi}}^-$ with $g(\boldsymbol{n}, n_z)$ being a function that admits values in unimodular complex numbers. We can easily see from Eq. (3.16) that $g(\boldsymbol{n}, n_z) = n_+\sqrt{n_+^* n_+}$. Restricting g to any circle that misses both poles, e.g., to equator we obtain the map $g : S^1 \to \mathrm{U}(1)$ that is topologically non-trivial, have a nonzero *degree* $\deg g = 1$, where the degree can be defined in an integral form

$$\deg g = \frac{1}{2\pi}\int_{S^1} g^{-1}\frac{dg}{dx}dx, \tag{3.17}$$

or equivalently as the winding number that measures how many times $g(s)$ winds around the target circle that represents U(1), while s winds once around the domain circle S^1. This implies that an adiabatic basis set ψ^- that is defined globally on the southern hemisphere, being recast on the equator in terms of ψ^+, defined globally on the northern counterpart, using a topologically non-trivial map g may not be contracted on the northern hemisphere, so that a global basis set on the whole sphere does not exist.

Similar to the orthogonal case, there is a topological obstruction to having a global adiabatic

basis set, induced by the conical seam, however in the unitary case it is the first *Chern class* c_1 [130] that is integer-valued, rather than the binary first Stiefel-Whitney class. To demonstrate that we consider the diagonal components of the nonadiabatic coupling terms, defined with respect to the adiabatic basis sets $\psi^{\pm}$ on the northern and southern hemispheres, and represented by vector potentials/gauge fields $A_j^{\pm}$, respectively. By Stokes theorem we have

$$\int_{S^1} A_j^{\pm} dx^j = \pm \int_{D_{\pm}} dA^{\pm} = \pm \int_{D_{\pm}} \varepsilon^{jk} F_{jk} d^2x \tag{3.18}$$

with $F_{jk} = (1/2)(\partial_j A_k - \partial_k A_j)$ and ε^{jk} being the vector potential curvature (magnetic field) and Levi-Civita symbol, respectively. The vector potentials are naturally connected by the gauge transformation

$$A_j^{+} = A_j^{-} + g^{-1}\partial_j g, \tag{3.19}$$

Integrating Eq. (3.19) over the equator, followed by making use of Eqs. (3.18) and (3.17) we arrive at

$$\frac{1}{2\pi} \int_{S^2} \varepsilon^{jk} F_{jk} d^2x = \deg g. \tag{3.20}$$

The l.h.s. of Eq. (3.20) is known as an integral representation of the first Chern class c_1 [130], so that we have $c_1 = \deg g$, which identifies the first Chern class as the topological invariant, associated with conical intersections in the unitary case.

The symplectic case of time-reversal symmetry for systems with odd number of electrons is treated very similar to the unitary case: in the relevant situation of two Kramers doublets we surround a conical point $\boldsymbol{h} = 0$ with a 4-dimensional sphere S^4, defined, say, by a condition $(\boldsymbol{h}, \boldsymbol{h}) = \varepsilon^2$. With each point $\boldsymbol{h}$ of the sphere one can associate a 2-dimensional complex subspace of double-degenerate eigenstates, say with the higher eigenvalue, in the 4-dimensional complex state of electronic states under consideration, which, according to the quaternionic approach, presented in section 3.2, is equivalent to associating with each point a 1-dimensional quaternion vector subspace of the 2-dimensional quaternion space of electronic states. We further ask a question whether one can identify a global real orthonormal adiabatic basis set, i.e., associate with each 2-dimensional

eigenspace a real orthonormal basis set, i.e. a pair $(\boldsymbol{e}, j(\boldsymbol{e}))$ with $|\boldsymbol{e}| = 1$, in a continuous way, which is equivalent to identifying a quaternion vector function $\boldsymbol{\psi}(\boldsymbol{h})$, with $\boldsymbol{\psi} = (\psi_1, \psi_2)$, that satisfies the eigenvalue problem. The answer is negative again, and this can be rationalized exactly in the same way as for the unitary case.

Indeed, denoting $\boldsymbol{h} = \varepsilon(\boldsymbol{n}, n_z)$ and $n_\pm = n_4 \mp i n_1 \mp j n_1 \mp k n_3$, the eigenvalue problem $(\boldsymbol{h}\cdot\boldsymbol{\gamma})\boldsymbol{\psi} = \varepsilon\boldsymbol{\psi}$, with the gamma-matrices given by Eq. (3.11) adopts the form of Eq. (3.15) and naturally has the same solution as in the unitary case, given by Eq. (3.16), with the only difference that $n_\pm$ are quaternions, rather than complex numbers, and $(\boldsymbol{n}, n_z)$ resides in the 4-dimensional sphere S^4, rather than its 2-dimensional counterpart S^2. In particular, the solutions $\boldsymbol{\psi}^\pm$ have zeros at the south and north pole of S^4, while their normalized counterparts are connected

$$\bar{\boldsymbol{\psi}}^+ = g\bar{\boldsymbol{\psi}}^-, \quad g(\boldsymbol{n}, n_z) = \frac{n_+}{\sqrt{n_+^* n_+}} \tag{3.21}$$

via the function g that admits values in unit length quaternions, the latter forming the group Sp(1), which by construction, as a space, forms a 3-dimensional sphere S^3. Note that Eq. (3.13) establishes an isomorphism $\mathrm{Sp}(1) \cong \mathrm{SU}(2)$, so that being restricted to $S^3 \subset S^4$, say, by fixing the value of $n_z \neq \pm 1$, e.g., to the equator for $n_z = 0$, we obtain a map $g : S^3 \to \mathrm{SU}(2)$, which is, in complete analogy with the unitary case is topologically non-trivial, which can be established by generalizing the notion of the degree of a map $g : S^n \to S^n$ from the case $n = 1$, considered earlier, and given by the winding number, to the case of any natural n. To that end we note that the winding number of $g : S^1 \to S^1$ can be measured by performing weighted counting of how many times $g(s)$ crosses some arbitrarily chosen reference point in the target S^1, while s winds once along the domain S^1, with the weights represented by ± 1 sign factors depending on the direction in which $g(s)$ goes through the reference point. The described procedure can be easily generalized to the arbitrary dimension case by looking at the generically finite set $g^{-1}(\{s_0\})$ of preimages of some arbitrary chosen reference point $s_0 \in S^n$ and counting the preimages, weighting them with sign factors, given by the signs of the Jacobian of g at the corresponding points. More formally we define $\deg g = \sum_{s \in g^{-1}(s_0)} \mathrm{sgn}(\det(\partial g(s)/\partial s))$. In complete analogy with the unitary case, we see that the map $g : S^3 \to S^3$, defined above, is one-to-one, and therefore, having a non-zero degree $\deg g = 1$, is topologically non-trivial, so that all arguments on the topologically nontrivial structure, introduced

by a CS, presented above for the unitary case, work in the symplectic situation in the exactly same way.

Similar to the unitary case the degree of g can be related to the Chern class, however, for the symplectic situation it is the second Chern class c_2 [130]. To see that we note that, in complete analogy with the unitary case, there is an integral representation for the degree of our map $g : S^3 \to \mathrm{SU}(2)$

$$\deg g = \frac{1}{24\pi^2} \int_{S^3} \mathrm{Tr}(g^{-1}dg \wedge g^{-1}dg \wedge g^{-1}dg), \tag{3.22}$$

rationalized by the fact (see appendix C for a more formal argument) that, up to a normalization constant, the integrand is given by the Jacobian of g. Therefore, the original integral over the domain of g can be interpreted as the integral of a constant function (whose value is determined by the aforementioned normalization constant) over the target space of g, multiplied by an integer factor that accounts for the multiplicity of the preimages of points in the target space. Recalling the definition of the map degree presented above, it becomes intuitively clear that this factor is given by $\deg g$. Using a similar to the unitary, still more technically involved approach (see appendix C for some details), and treating g as a gauge transformation of the diagonal nonadiabatic coupling terms, the latter being considered as a non-abelian (Yang-Mills) SU(2) gauge field, described by the matrix vector potential $A_j = -i \sum_{a=1}^{3} A_j^a \sigma_a$ Eq. (3.22) can be recast in a form

$$\frac{1}{8\pi^2} \int_{S^4} \mathrm{Tr}(F \wedge F) = \deg g. \tag{3.23}$$

with $F = F_{jk} dx^j \wedge dx^k$, where $F_{jk} = (1/2)(\partial_j A_k - \partial_k A_j + [A_j, A_k])$ is the non-abelian curvature. One recognizes the l.h.s. as a standard integral representation of the second Chern class c_2 [130], identifying it as the topological invariant, associated with conical intersections in the symplectic case. Some details of a derivation of Eq. (3.23) from Eq. (3.22), more formal rationalization of the latter, explanation why Eq. (3.23) reproduces the second Chern class, as well as necessary facts and concepts, associated with differential forms, including wedge products and Stokes theorem, involved in the aforementioned derivations, are presented in appendix C.

We conclude this section with noting that as opposed to the orthogonal, in the unitary and

symplectic cases the proper adiabatic states are defined up to a continuous degree of freedom, which sits in U(1) and SU(2), respectively, giving rise to diagonal components of the nonadiabatic coupling terms. The corresponding vector fields A_j are geometrically non-trivial, i.e., they have non-zero curvature F_{jk}, so that in the unitary case the effect of geometric (i.e., path-dependent) Berry phase takes place. A similar effect occurs in the symplectic case, where instead of the phase, as an element of U(1), we have an element of SU(2), hereafter referred to as *non-abelian Berry phase* [131]. The latter will be discussed in some detail in section 3.4.

3.4 Born-Oppenheimer Approximation for Half-Integer Spin Ca-se, Semiclassical Propagation, and Non-Abelian Berry Phase

The easiest way to rationalize semiclassical adiabatic dynamics for systems with time-reversal symmetry and odd number of electrons (symplectic case) is no bring in the partial path integral representation with matrix action, introduced, e.g., in [126], where the path integration is performed over the nuclear position variables $\boldsymbol{r}$, whereas the electronic counterparts are treated explicitly. Being focused on the case of two (both double-degenerate) potential surfaces, and following [126], we represent the Hamiltonian in a form

$$H = -\sum_{j=1}^{d} \frac{\hbar^2 \nabla_j^2}{2m_j} + \sum_{\alpha=0}^{5} \mathcal{U}_\alpha(\boldsymbol{r})\gamma_a, \tag{3.24}$$

with $\nabla_j = \partial/\partial r_j - A_j$ being the "long" gauge-invariant derivatives. The Hamiltonian in Eq. (3.24) can be viewed as a generalized 2-state Born-Oppenheimer (BO) approximation, with two double-degenerate PES. It treats adequately intersections of the two chosen PES, and requires only the rest of PES to be separated energetically, so that nonadiabatic coupling to them can be neglected. It is obtained by projecting the original Hamiltonian to the electronic subspace spanned onto the adiabatic states, which results in the standard expressions $A_j^{ab} = \langle \psi_a(\boldsymbol{r}) | \partial \psi_b(\boldsymbol{r})/\partial r_j \rangle$, where $\psi_a(\boldsymbol{r})$, with $a = 1, \ldots, 4$ being some position-dependent orthonormal real (in the sense of section 3.2) basis set in the space of electronic sates.

Assuming we are far away from CSs, we further apply the complete BO approximation, which boils down to choosing an adiabatic basis set and neglecting the block off-diagonal components of A_j^{ab}, i.e. the ones with a and b belonging to different adiabatic surfaces, making evolution on both

surfaces independent of each other. The corresponding BO Hamiltonians have a form

$$H = -\sum_{j=1}^{d} \frac{\hbar^2 \nabla_j^2}{2m_j} + \mathcal{U}(\boldsymbol{r}), \tag{3.25}$$

with

$$\mathcal{U}(\boldsymbol{r}) = \mathcal{U}_0(\boldsymbol{r}) \pm |\boldsymbol{\mathcal{U}}(\boldsymbol{r})| \tag{3.26}$$

being the adiabatic energies, whereas the diagonal, in the aforementioned sense components A_j are represented by 2×2 matrices A_j^{ab}, defined with respect to an orthonormal real basis set $\psi_a(\boldsymbol{r})$, with $\psi_2 = j\psi_1$, and therefore,

$$A_j(\boldsymbol{r}) = -\mathrm{i} \sum_{\mu=1}^{3} A_j^{\mu}(\boldsymbol{r}) \sigma_{\mu}. \tag{3.27}$$

The difference between the adiabatic evolution in the orthogonal and symplectic cases is that in the latter the wavefunction has a 2-component vector character and there is a non-abelian matrix gauge field that elongates the spatial derivatives.

Applying the path-integral representation to the evolution operator, associated with the adiabatic Hamiltonian [Eq. (3.25)] in a way, described in the beginning of this section, we obtain

$$\hat{G}(\boldsymbol{r}'', \boldsymbol{r}'; t) = \int_{\boldsymbol{x}(0)=\boldsymbol{r}'}^{\boldsymbol{x}(t)=\boldsymbol{r}''} \mathcal{D}\boldsymbol{x} \exp\left(\frac{\mathrm{i}}{\hbar} S(\boldsymbol{x})\right) \hat{U}(\boldsymbol{x}) \tag{3.28}$$

with

$$S(\boldsymbol{x}) = \int_0^t d\tau \left(\frac{m\dot{\boldsymbol{x}}^2(\tau)}{2} - \mathcal{U}_0(\boldsymbol{x}(\tau))\right), \quad \hat{U}(\boldsymbol{x}) = T \exp\left(\int_{\boldsymbol{x}} d\boldsymbol{r} \cdot \boldsymbol{A}\right). \tag{3.29}$$

The semiclassical adiabatic propagator is obtained by neglecting the trajectory fluctuations around the classical counterpart in computing $\hat{U}(\boldsymbol{x})$, so that the path integral represent just the standard adiabatic propagator, followed by applying the van Vleck semiclassical approximation to

the latter, resulting in

$$\hat{G}(\boldsymbol{r}'', \boldsymbol{r}'; t) = G_0(\boldsymbol{r}'', \boldsymbol{r}'; t)\hat{U}(\boldsymbol{x}_{\rm cl}(\boldsymbol{r}'', \boldsymbol{r}'; t)) \tag{3.30}$$

with G_0 denoting the van Vleck semiclassical propagator,so that Eq. (3.30) solves the problem of adiabatic dynamics in the semiclassical approximation. Semiclassical evolution near CSs, where the adiabatic approximation breaks down is considered in section 3.5.

The vector character of a Kramers doublet, considered in this section is naturally described in terms of the wavepacket polarization $\zeta(\boldsymbol{r})$ defined by the conditions $\Psi(\boldsymbol{r}) = |\Psi(\boldsymbol{r})|\zeta(\boldsymbol{r})$ and $|\zeta(\boldsymbol{r})| = 1$, so that the polarization is represented by a nuclear position dependent unit vector in the 2-dimensional complex vector space of electronic states of a Kramers doublet, so that the polarization $\zeta(\boldsymbol{r}) \in S^3$ resides in a 3-dimensional sphere. Obviously the second (matrix) factor in the r.h.s. of Eq. (3.30) affects the polarization only, keeping $|\Psi(\boldsymbol{r})|$ unchanged. However, the first (scalar) factor that represents the standard Van Vleck propagator, also affects the polarization, e.g., due to the phase factor $e^{i\hbar^{-1}S_{\rm cl}}$ that originates from the classical action. Still the evolution of polarization dynamics can be completely decoupled from the scalar Van Vleck evolution via introducing the reduced polarization $\bar{\zeta}(\boldsymbol{r})$ by considering two values of polarization ζ and ζ', represented by two unit 2-dimensional complex vectors, the same, if the latter differ by a unimodular factor. The reduced space of the described above equivalence classes is represented by the complex projective line $\mathbb{C}P^1$, the latter being topologically equivalent to the 2-sphere S^2. The reduction map $S^3 \to S^2$ that maps the polarization to its reduced counterpart is known in topology as a Hopf map. The aforementioned unimodular factor can be absorbed by the scalar part of the nuclear wavefunction, so that the latter can be represented by a complex-valued scalar wavefunction and reduced polarization $\bar{\zeta}$, instead of the polarization ζ and a real "wavefunction" $|\Psi|$, so that within the new (reduced polarization) representation picture, the scalar (Van Vleck) and polarization evolution are completely decoupled.

It follows immediately from Eq. (3.30) that semiclassical evolution of the wavepacket (reduced) polarization is of completely geometric nature, and is related to multiple phenomena, which, in particular include adiabatic propagation of a spin in time-dependent magnetic field, rotating cats/astronauts, stochastic current, generated by adiabatic driving, and are often referred to as Berry phase phenomena. Indeed, the geometrical meaning of the vector potential/gauge field that

represents the diagonal component of the nonadiabatic coupling terms is that it determines the parallel transport of the electronic state along a trajectory, as illustrated in Fig. 3.1. This is why in differential geometry it is referred to as a *connection*. The same connection appears in a different setting when the electronic Hamiltonian depends not on additional variables, in our case nuclear coordinates, but rather just on time. In the unitary case this would be a problem of a spin in a time-dependent magnetic field; in this case $\hat{U}(C)$, with C being a path in the 3-dimensional space of electronic Hamiltonians $\boldsymbol{h}$, belongs to U(1) and for a closed path (loop) reproduces exactly the celebrated Berry phase. In the symplectic case the phase becomes non-abelian, i.e., it belongs to SU(2), as outlined in [131].

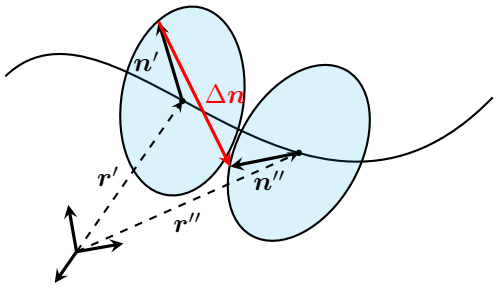

Figure 3.1: Geometric nature of wavepacket polarization evolution, described by parallel transport. The wavepacket polarizations $\boldsymbol{n}'$ and $\boldsymbol{n}''$ at different times belong to different subspaces. The new polarization value $\boldsymbol{n}''$, interpreted as a result of parallel transport over an infinitesimal time period, is uniquely determined by two conditions: $\boldsymbol{n}''$ should be normalized, and the polarization change $\Delta\boldsymbol{n}$ should be orthogonal to its initial value $\boldsymbol{n}'$.

3.5 Semiclassical Theory for Nuclear Wavepacket Propagation Through a Conical Seam

In this section we obtain explicit asymptotically exact expressions for the evolution of nuclear wavepackets in the presence of CSs in the semiclassical regime for all three situations, with focus on the symplectic case that corresponds to the half-integer spin. Compared to the integer-spin counterpart the half-integer situation is treated in a similar way, it is just technically more involved. As outlined in [126] for the "standard" integer spin case, as long as the wavepacket is not close to a CS, i.e., outside of the conical scattering region, it is moving adiabatically, which means that in the semiclassical regime a standard Van Vleck semiclassical propagator can be applied for asymptotically exact description of the system evolution (we reiterate that the Van Vleck propagator

approach is equivalent to the Gaussian Ansatz for wavepackets). When the wavepacket passes through the CS, ballistic approximation is valid in the semiclassical regime. The described approach in fact works due to the overlap of the adiabatic and ballistic regions, as clearly demonstrated in [126]. The semiclassical approach for the adiabatic region has been extended to the half-integer spin case in section 3.4, including effects of the non-abelian Berry phase.

Since the goal of [126] was to extend the Van Vleck semiclassical propagator to the case of the presence of CSs, evolution in the scattering region was described on the level of the ballistic propagator, which was obtained by bringing in the path-integral approach with matrix contribution to the action, followed by neglecting the fluctuation of the nuclear trajectory in computing the time-ordered exponential, associated with the matrix component of the action. Of course the wavepacket evolution in the vicinity of a CS can be readily obtained by applying the ballistic propagator to the incoming wavepacket, however, in this chapter we will derive explicit expressions for the wavepacket evolution directly from the dynamical Schrödinger equation. The advantages of this way include simplicity of the derivation, bypassing additional integration involved in applying the propagator to the incoming wavepacket, as well as relative easiness in connecting the ballistic and adiabatic solutions in the overlap region.

The ballistic approximation starts with switching to a diabatic basis set (the use of the indefinite article is important), defined by a condition $\boldsymbol{A}(\boldsymbol{r}_0) = 0$, with the point $\boldsymbol{r}_0$, where the wavepacket, whose size scales $\sim \sqrt{\hbar}$, crosses the conical seam, being well defined in the semiclassical $\hbar \to 0$ limit, followed by introducing the time-dependent wavepacket position $\boldsymbol{R}(t) = \boldsymbol{R}_0 + \boldsymbol{v}(t - t_0)$, and representing the system wavefunction in a form

$$\Psi(\boldsymbol{r}, t) = \exp\big(i\hbar^{-1}\boldsymbol{p} \cdot (\boldsymbol{r} - \boldsymbol{R}(t))\big)\bar{\Psi}(\boldsymbol{r} - \boldsymbol{R}(t), t), \tag{3.31}$$

with $\boldsymbol{p} = m\boldsymbol{v}$ and $\boldsymbol{v}$ being the wavepacket momentum and velocity, respectively. Upon substitution of Eq. (3.31) into the dynamical Schrödinger equation we obtain

$$\mathrm{i}\hbar\frac{\partial\bar{\Psi}(\boldsymbol{r}, t)}{\partial t} = (H_{\mathrm{B}}(t) + H_1)\bar{\Psi}(\boldsymbol{r}, t) \tag{3.32}$$

with

$$H_{\mathrm{B}}(t) = -\frac{\boldsymbol{p}^2}{2m} + \hat{h}(\boldsymbol{r}_{\mathrm{L}}(\boldsymbol{r},t)), \quad H_1 = -\frac{\hbar^2\partial^2}{2m}, \tag{3.33}$$

$\boldsymbol{r}_{\mathrm{L}}(\boldsymbol{r},t) = \boldsymbol{R}(t)+\boldsymbol{r}$, $\hat{h}(\boldsymbol{r}_{\mathrm{L}}) = \boldsymbol{h}(\boldsymbol{r}_{\mathrm{L}})\cdot\boldsymbol{\gamma}$, and ∂^2 being the Laplace operator. The ballistic approximation boils down to neglecting the H_1 term in the r.h.s. of Eq. (3.32) turning the PDE [Eq. (3.32)] into a family of ODE parameterized by $\boldsymbol{r}$, whose solutions can be explicitly represented in terms of time-ordered exponentials, resulting in:

$$\bar{\Psi}(\boldsymbol{r},t) = \mathrm{e}^{\mathrm{i}S_{\mathrm{B}}/\hbar}T\exp\left(-\frac{\mathrm{i}}{\hbar v^2}\int_C \hat{h}(\boldsymbol{r}')\boldsymbol{v}\cdot d\boldsymbol{r}'\right)\bar{\Psi}(\boldsymbol{r},t_0), \tag{3.34}$$

with C and

$$S_{\mathrm{B}} = \frac{m\boldsymbol{v}^2(t-t_0)}{2} \tag{3.35}$$

being the straight (ballistic) path that connects $r_{\mathrm{L}}(\boldsymbol{r},t_0)$ to $r_{\mathrm{L}}(\boldsymbol{r},t)$, and the ballistic action, respectively.

An explicit expression for the evolution in the ballistic approximation [Eq. (3.34)] has a very simple and natural interpretation, namely there are two factors that affect the evolution: (i) the wavepacket is moving ballistically, i.e., with a constant velocity $\boldsymbol{v}$, and (ii) the (vector) value of the wavefunction for any position $\boldsymbol{r}$ in the moving frame is evolving according to the value $\hat{h}(\boldsymbol{r}_{\mathrm{L}}(\boldsymbol{r},t))$ of the matrix Hamiltonian at the corresponding point in the laboratory frame. The aforementioned interpretation is illustrated in Fig. 3.2.

We will apply the ballistic approximation to the region around the conical seam, where the position dependence $\hat{h}(\boldsymbol{x})$ can be linearized, We further note that the expression for ballistic propagation [Eq. (3.34)] is valid for short enough times for any matrix Hamiltonian $\hat{h}(\boldsymbol{x})$ and a configuration space of any dimension. In particular, the aforementioned expression is capable of handling all three, namely the orthogonal, unitary, and symplectic, cases in the configuration space of arbitrary dimension. On the other hand, during the ballistic process of the wavepacket crossing a CS, nothing happens to the wavepacket shape along the CS, with all changes occurring in the transverse directions. Therefore, for the sake of presentation clarity/simplicity, and to avoid notational clutter we

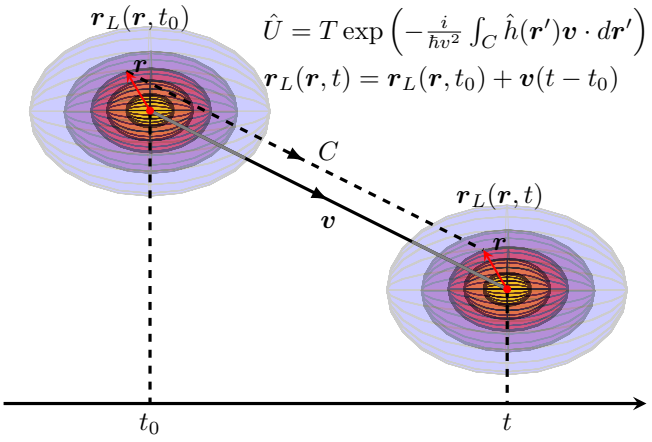

Figure 3.2: Illustration of ballistic wavepacket propagation, using the laboratory frame, in which the wavepacket moves with a constant velocity $\boldsymbol{v}$, i.e., ballistically. The molecular configuration vector $\boldsymbol{r}$ in the proper frame, associated with a moving wavepacket, shown as red, stays unchanged, while its laboratory frame counterpart changes from $\boldsymbol{r}_L(\boldsymbol{r},t_0)$ to $\boldsymbol{r}_L(\boldsymbol{r},t)$. The dashed line represents the integration path C in Eq. (3.34).

will set the configuration space dimension to $d = 2$, $d = 3$, and $d = 5$, for the orthogonal, unitary, and symplectic cases, respectively, postponing a very simple discussion of a truly straightforward extension to the arbitrary dimension case to section 3.6. In all three cases, for the aforementioned dimensions, the CS is represented by a single point, located at the coordinate origin. The derivations, as well as the final expressions, become most compact upon implementing an appropriate coordinate system $\boldsymbol{r} = (\boldsymbol{x}, z)$ in the configuration space and an appropriate basis set in the relevant subspace of electronic states.

We start with the simplest orthogonal case, in particular setting $d = 2$. We first linearize the dependence $\hat{h}(\boldsymbol{x})$. We then choose the direction $\boldsymbol{e}_z$ of the z-axis in the wavepacket velocity direction, and further rotate the basis set in the 2-dimensional electronic space to achieve $\hat{h}(\boldsymbol{e}_z) = f\sigma_z$ for some f. We further identify the direction $\boldsymbol{e}_x$ of the x-axis by imposing the condition $\hat{h}(\boldsymbol{e}_x) = f\sigma_x$, to arrive at

$$\hat{h}(x,z) = f(x\sigma_x + z\sigma_z), \tag{3.36}$$

with f being a (scalar) force constant. Note that it is due to the coordinate/basis choices, described above, we were able to replace a 2×2 force constant matrix with a single scalar counterpart.

In the unitary case we choose $\boldsymbol{e}_z$ and rotate the basis set in exactly the same way as in the

orthogonal situation, achieving $\hat{h}(\boldsymbol{e}_z) = f\sigma_z$, whereas $\boldsymbol{e}_x$ and $\boldsymbol{e}_y$ are identified in a similar way from the conditions $\hat{h}(\boldsymbol{e}_x) = f\sigma_x$ and $\hat{h}(\boldsymbol{e}_y) = f\sigma_y$, resulting in

$$\hat{h}(\boldsymbol{x}, z) = f(\boldsymbol{x} \cdot \boldsymbol{\sigma} + z\sigma_z), \tag{3.37}$$

with $\boldsymbol{x} = (x, y)$ and $\boldsymbol{\sigma} = (\sigma_x, \sigma_y)$.

For the symplectic case, in a similar way, we choose $\boldsymbol{e}_5$ to be along the wavepacket velocity and further achieve $\hat{h}(\boldsymbol{e}_5) = f\gamma_5$ via the electronic space basis set choice, and further identify $\boldsymbol{e}_j$ from the conditions $\hat{h}(\boldsymbol{e}_j) = f\gamma_j$, for $j = 1, 2, 3, 4$. This results in

$$\hat{h}(\boldsymbol{x}, z) = f(\boldsymbol{x} \cdot \boldsymbol{\gamma} + z\sigma_z), \tag{3.38}$$

with $\boldsymbol{x} = (x_1, x_2, x_3, x_4)$ and $\boldsymbol{\gamma} = (\gamma_1, \gamma_2, \gamma_3, \gamma_4)$. Note that the unitary case [Eq. (3.37)] can be represented in the form of Eq. (3.38) by setting $\boldsymbol{\gamma} = (\sigma_x, \sigma_y)$ and $\gamma_5 = \sigma_z$.

Following [126] we introduce the scattering r_s and ballistic r_B length scales

$$r_\mathrm{s} = \sqrt{\hbar v/f}, \quad r_\mathrm{B} = \left(m\hbar v^3/f^2\right)^{1/3}, \tag{3.39}$$

so that the matching region, where both the ballistic and adiabatic approximation are valid is defined by

$$r_\mathrm{s} \ll r \ll r_\mathrm{B}, \tag{3.40}$$

and the overlap $r_\mathrm{s} \ll r_\mathrm{B}$ of the ballistic and adiabatic regions is provided by the condition $g_\mathrm{s} \ll 1$, with the dimensionless parameter that controls applicability of our semiclassical approach given by

$$g_\mathrm{s} = \sqrt{f\hbar/m^2v^3}, \quad r_\mathrm{s}/r_\mathrm{B} = g_\mathrm{s}^{1/3}. \tag{3.41}$$

for the orthogonal case, we further introduce the dimensionless parameter l that parameterizes ballistic trajectories and the dimensionless impact parameter α

$$l = (\sqrt{2}/r_\mathrm{s})(z_0 + vt), \quad \alpha = \sqrt{2}x/r_\mathrm{s}, \tag{3.42}$$

so that the time-ordered exponential in Eq. (3.34) is obtained by solving a linear ODE

$$\mathrm{i}\frac{\mathrm{d}}{\mathrm{d}l}\Psi(l)=\frac{1}{2}(\alpha\sigma_x+l\sigma_z)\Psi(l). \tag{3.43}$$

The time-ordered exponential in Eq. (3.34) is therefore given by the evolution operator, associated with Eq. (3.43),

$$\hat{U}(l_2,l_1)=\begin{pmatrix} u_{\mathrm{d}}(l_2,l_1) & u_{\mathrm{a}}(l_2,l_1) \\ -u_{\mathrm{a}}^{*}(l_2,l_1) & u_{\mathrm{d}}^{*}(l_2,l_1)\end{pmatrix} \tag{3.44}$$

which, in the relevant for us limit $l_1\to-\infty$ and $l_2\to\infty$, is given by the scattering matrix of the celebrated Landau-Zener (LZ) problem

$$u_{\mathrm{d}}=\sqrt{P_{\mathrm{d}}}e^{-i\Phi_{\mathrm{d}}},\quad u_{\mathrm{a}}=\sqrt{1-P_{\mathrm{d}}}e^{-i\Phi_{\mathrm{a}}},\quad \Phi_{\mathrm{d}}=\Phi_2-\Phi_1,\quad \Phi_{\mathrm{a}}=\Phi_2+\Phi_1-\delta(\alpha), \tag{3.45}$$

with $P_{\mathrm{d}}(\alpha)=\exp\bigl(-\pi\alpha^2/2\bigr)$, $\Phi_j=(l_j^2+\alpha^2\ln|l_j|)/4=\Phi(l_j;\alpha)$ are the LZ probability to stay on a diabatic level and the adiabatic phases, respectively with $j=1$ and $j=2$ corresponding to the initial and final points of a ballistic trajectory. The nonadiabatic phase shift $\delta(\alpha)=\pi/4-\arg\Gamma(-\mathrm{i}\alpha^2/4)$ is expressed in terms of the Euler gamma function $\Gamma(z)$.

The expressions, provided by Eqs. (3.44) and (3.45), being substituted into Eq. (3.34) fully describe the asymptotically exact semiclassical scattering of a wavepacket on a conical scheme for the orthogonal case. In order to apply them to the unitary and symplectic cases in an almost straightforward way we recast them in a form

$$\hat{U}=\sqrt{P_{\mathrm{d}}}(\gamma_0\cos\Phi_{\mathrm{d}}-\mathrm{i}\gamma_5\sin\Phi_{\mathrm{d}})+\sqrt{1-P_{\mathrm{d}}}(\gamma_5\gamma\cos\Phi_{\mathrm{a}}-\mathrm{i}\gamma\sin\Phi_{\mathrm{a}}), \tag{3.46}$$

with $\gamma_0=\sigma_0$, $\gamma=\sigma_x$, and $\gamma_5=\sigma_z$. Using the introduced notation Eq. (3.43) is naturally represented in a form

$$\mathrm{i}\frac{d}{dl}\Psi(l)=\frac{1}{2}(\alpha\gamma+l\gamma_5)\Psi(l). \tag{3.47}$$

The key observation on the way of extending our expressions to the unitary and symplectic cases is that both Eq. (3.47) and the associated evolution operator [Eq. (3.46)] are expressed in terms of an algebra, generated by γ_0, γ, and γ_5 with the relations $\gamma^2=\gamma_5^2=\gamma_0$, $\gamma_5\gamma=-\gamma\gamma_5$ (anticommute),

and γ_0 being the unit. Therefore, for any matrices with the described above relations the evolution operator, associated with Eq. (3.47), is given by Eq. (3.46).

In the unitary and symplectic cases, when the position is described by $(\boldsymbol{x}, z)$, the impact parameter $\boldsymbol{x}$, associated with a ballistic trajectory is of vector nature, and is naturally represented as $\boldsymbol{x} = x\boldsymbol{n}$, with $\boldsymbol{n}$ being a unit vector, so that x can be interpreted as a scalar impact parameter. For the unitary case, defining $\gamma = \boldsymbol{n} \cdot \boldsymbol{\gamma}$ with, as described above $\gamma_0 = \sigma_0$, $\boldsymbol{\gamma} = (\sigma_x, \sigma_y)$, and $\gamma_5 = \sigma_z$, we find that the equation that describes the relevant time-ordered exponential is given by Eq. (3.47), which immediately implies that the associated evolution operator $\hat{U}$ is given by Eq. (3.46) with the described above values of the γ-matrices, so that after some straightforward algebra we arrive at

$$\hat{U} = \begin{pmatrix} \sqrt{P_{\rm d}} \mathrm{e}^{-\mathrm{i}\Phi_d} & \sqrt{1-P_{\rm d}} \mathrm{e}^{-\mathrm{i}\Phi_a} n_+ \\ -\sqrt{1-P_{\rm d}} \mathrm{e}^{\mathrm{i}\Phi_a} n_- & \sqrt{P_{\rm d}} \mathrm{e}^{\mathrm{i}\Phi_d} \end{pmatrix} \tag{3.48}$$

with $n_\pm = n_x \pm \mathrm{i} n_y$.

The symplectic case is treated exactly in the same way setting $\gamma = \boldsymbol{n} \cdot \boldsymbol{\gamma}$, with γ_0, $\boldsymbol{\gamma} = (\gamma_1, \gamma_2, \gamma_3, \gamma_4)$, and γ_5 given by Eq. (3.11). Using a standard matrix representation of the quaternionic units in terms of the Pauli matrices [Eq. (3.13)], we obtain upon its substitution into Eq. (3.46), followed by straightforward algebra

$$\hat{U} = \begin{pmatrix} \sqrt{P_{\rm d}} \mathrm{e}^{-\mathrm{i}\Phi_d} \sigma_0 & \sqrt{1-P_{\rm d}} \mathrm{e}^{-\mathrm{i}\Phi_a} u(\boldsymbol{n}) \\ -\sqrt{1-P_{\rm d}} \mathrm{e}^{\mathrm{i}\Phi_a} u^\dagger(\boldsymbol{n}) & \sqrt{P_{\rm d}} \mathrm{e}^{\mathrm{i}\Phi_d} \sigma_0 \end{pmatrix} \tag{3.49}$$

with $\boldsymbol{n} = (\boldsymbol{\eta}, n_4)$, so that $\boldsymbol{\eta}^2 + n_4^2 = 1$ and

$$u(\boldsymbol{n}) = n_4 \sigma_0 + i \boldsymbol{\eta} \cdot \boldsymbol{\sigma} \tag{3.50}$$

being a direction dependent unitary matrix. Note that Eq. (3.50) provides a standard global parameterizations of the unitary group, in particular establishing an isomorphism $S^3 \cong \mathrm{SU}(2)$. It is useful to note that Eq. (3.48) can be represented in the form of Eq. (3.49) by introducing $u(\boldsymbol{n}) = n_+$, so that $u(\boldsymbol{n})$ denote the maps $u : S^1 \to \mathrm{U}(1)$ and $u : S^3 \to \mathrm{SU}(2)$ for the unitary and symplectic cases, respectively, and in both cases the degree of the relevant map is $\deg(u) = 1$.

Since the expressions in Eqs. (3.48) and (3.49) are represented in a diabatic basis set, the diagonal and off-diagonal elements of the 2×2 and block 2×2 matrices describe the nonadiabatic and adiabatic processes, respectively, so that that the wavepacket components that changes the adiabatic surface does not show any dependence on the direction $\boldsymbol{n}$ of the impact parameter, whereas the counterpart that stays on it shows a topologically nontrivial dependence on $\boldsymbol{n}$, which will be discussed in some detail in section 3.6.

3.6 Topological Properties of a Scattered Wavepacket

In this section we obtain analytical expressions for the wavepacket, right after passing the CS, with focus on its polarization structure, and study the topological properties of the latter. We start with deriving an explicit expression for the scattered wavepacket,which can be readily obtained by substituting Eq. (3.48) or Eq. (3.49) into Eq. (3.34), as explained in section 3.5.

Indeed, let $\bar{\Psi}_1(\boldsymbol{x}; z) = \bar{\Psi}_1(\boldsymbol{n}, x; z)$ be the incident wavepacket at the initial time t_0; the coordinates are relative to the wavepacket position that by definition lies on the ballistic trajectory that goes exactly through the conical point, which means that the position is completely defined by $z_1 < 0$, so that the actual position of a configuration in the wavepacket is $(\boldsymbol{x}; z_1 + z)$. Note that if a wavepacket has a well-defined center, e.g., in the Gaussian case, the position is generically shifted with respect to the center by the impact parameter of the ballistic trajectory, associated with the center. Let $z_2 > 0$ be the position of the scattered wavepacket, at time t, with the obvious relation $z_2 = z_1 + v(t - t_0)$, and let $\bar{\Psi}_2(\boldsymbol{x}; z) = \bar{\Psi}_2(\boldsymbol{n}, x; z)$ be the scattered wavepacket, with the coordinates naturally defined relative to the new position.

Being focused on a more interesting case of the wavepacket staying on an adiabatic surface we obtain, e.g., for the upper adiabatic surface

$$\bar{\Psi}_2(\boldsymbol{n}, x; z) = \mathrm{e}^{\mathrm{i}S_\mathrm{B}/\hbar}\sqrt{1 - P_\mathrm{d}(\sqrt{2}x/r_\mathrm{s})}\mathrm{e}^{-\mathrm{i}\Phi_a} u(\boldsymbol{n})\bar{\Psi}_1(\boldsymbol{n}, x; z), \tag{3.51}$$

with

$$\Phi_\mathrm{a} = \Phi(\sqrt{2}(z_1 + z)/r_\mathrm{s}; \sqrt{2}x/r_\mathrm{s}) + \Phi(\sqrt{2}(z_2 + z)/r_\mathrm{s}; \sqrt{2}x/r_\mathrm{s}) - \delta(\sqrt{2}x/r_\mathrm{s}), \tag{3.52}$$

so that evaluating the r.h.s. of Eq. (3.51) we arrive at the following explicit expression

$$\begin{aligned}\bar{\Psi}_2(\boldsymbol{n},x;z) = {}& \mathrm{e}^{\mathrm{i}S_{\mathrm{cl}}/\hbar}\mathrm{e}^{-\mathrm{i}(z_1+z_2)z/r_{\mathrm{s}}^2-\mathrm{i}(x^2/(2r_{\mathrm{s}}^2))\ln\left(2|z_1z_2|/r_{\mathrm{s}}^2\right)} \\ & \times\sqrt{1-\exp(-\pi x^2/r_{\mathrm{s}}^2)}\mathrm{e}^{\mathrm{i}\pi/4-\mathrm{i}\arg\Gamma(-\mathrm{i}x^2/(2r_{\mathrm{s}}^2))-\mathrm{i}z^2/r_{\mathrm{s}}^2} \\ & \times u(\boldsymbol{n})\bar{\Psi}_1(\boldsymbol{n},x;z),\end{aligned} \tag{3.53}$$

with the classical action

$$S_{\mathrm{cl}} = \frac{mv^2(t-t_0)}{2} - \frac{fz_1^2+fz_2^2}{2}v. \tag{3.54}$$

The final expression for the wavepacket scattering [Eqs. (3.53) and (3.54)] can be interpreted in the following way. The scalar and matrix factors in the second and third lines of the r.h.s. of Eq. (3.53) are independent of the initial z_1 and final z_2 positions and describe strong nonadiabatic effects, associated with the wavepacket passing through the conical seam. The action S_{cl} is easily identified as the action, associated with a classical particle of mass m ballistic propagation exactly through the conical point in the potential $V(z) = f|z|$ of the upper adiabatic surface, taken in the diabatic approximation. The remaining factor in the first line of the r.h.s. provides a z_1- and z_2-dependent correction to the wavepacket momentum, and a Gaussian correction to its shape, represented by the first and second terms in the exponent, respectively. They are responsible for the semiclassical adiabatic dynamics of the wavepacket in the matching region $r_{\mathrm{s}} \ll r \ll r_{\mathrm{B}}$, where the ballistic approximation also holds. This factor plays an important role in connecting the wavepacket dynamics in the adiabatic and ballistic region, ensuring the independence of the final result on a particular choice of the intermediate points z_1 and z_2, as long as both belong to the matching region.

We reiterate that, as observed earlier, Eq. (3.53) describes both the unitary and symplectic cases by interpreting u as $u : S^1 \to \mathrm{U}(1)$ and $u : S^3 \to \mathrm{SU}(2)$. We further note that the orthogonal case also fits the aforementioned expression by setting $u : S^0 \to \mathbb{Z}_2$ to an identity map, making use of $S^0 = \{-1, 1\} = \mathbb{Z}_2$.

We are now in a position to identify the topological properties of the scattered wavepacket that are completely determined by the matrix factor in the last line of Eq. (3.53). We start with

the simpler unitary case in its minimal dimension $d = 3$. In the frame, moving together with the wavepacket, hereafter referred to as the proper frame, the conical point moves with a constant velocity $-\boldsymbol{v}$, pinching the wavepacket along a segment of a straight line, hereafter referred to as the conical trajectory, as shown in Fig. 3.3. According to the earlier agreement the wavepacket position should be chosen as a point that belongs to the conical trajectory. The z-axis in Fig. 3.3 is not orthogonal to the $\boldsymbol{x} = (x, y)$ plane, since, as explained in section 3.5, we use a coordinate system that diagonalizes the matrix of the force constants at the conical point, rather than the mass matrix m_{ij}, with the second one usually referred to as the reduced coordinate system. By the same reason the lines of constant values of z and $x = |\boldsymbol{x}|$ appear to be ellipses, rather than circles; however they are still circles topologically and therefore will be denoted S^1. Recalling our definition of polarization, given at the end of section 3.4 for the symplectic case, adopting it to the unitary case, and applying it to $\bar{\Psi}$, rather than Ψ, with the two related via Eq. (3.31), we have $\bar{\Psi}(\boldsymbol{x}, z) = \zeta(\boldsymbol{x}, z)|\bar{\Psi}(\boldsymbol{x}, z)|$, and further observe from Eq. (3.53) that, if the polarization of the incident wavepacket is $(\boldsymbol{x}, z)$-independent, than the phase of ζ acquires 2π upon performing a full rotation over the circle S^1, reflecting the fact that the degree of the map $\zeta : S^1 \to \mathrm{U}(1)$ is $\deg \zeta = 1$. The fact that the degree of a map is a topological (strictly speaking, homotopy) invariant, makes it robust. In particular, we will still have $\deg \zeta = 1$ for any, generically curved path that winds along the trajectory of the conical point once. Secondly, the topologically nontrivial structure of the scattered wavepacket will still be in place if the initial polarization is not necessarily homogeneous, but also in the case when its phase is well-defined, which happens, e.g., in the case when the wavefunction does not have zeros within its support. This is true, e.g., for a very relevant example of a Gaussian wavepacket, and not true for the scattered counterpart that has zeros on the conical point trajectory. Third, if one finds even a single circle with the nontrivial associated $\deg \zeta = 1$, this immediately implies that the wavefunction will turn to zero on some line within the wavepacket, which follows from the argument that the wavefunction should turn to zero at at least one point on any disc, spanned onto the circle. The latter follows from a standard topological argument and is intuitively obvious.

The topologically non-trivial structure of the scattered wavepacket, namely, $\deg u = 1$, for the map u, associated with a circle, that winds around the conical trajectory, is directly related to the non-trivial value $c_1 = 1$ of the first Chern class, which represents the relevant topological

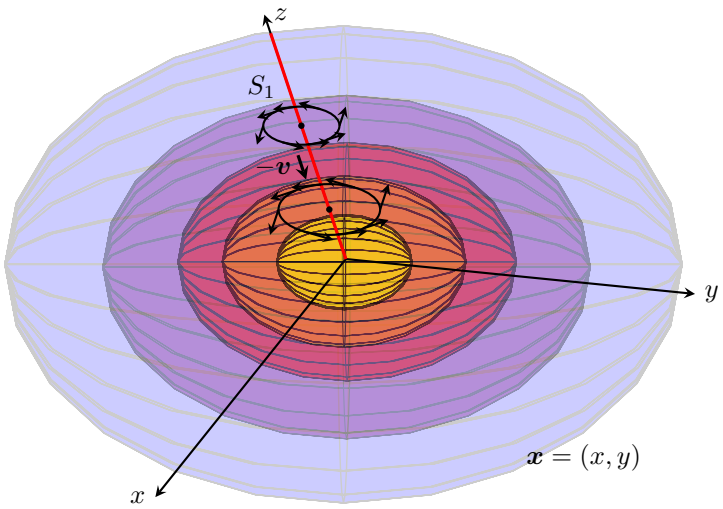

Figure 3.3: Nontrivial topological structure of the scattered wavepacket. The red line represents the conical trajectory that, in the proper frame, associated with the wavepacket, pinches the wavepacket along z-axis, where the wavefunction turns to zero (nodal line). The polarization vector performs a complete 2π rotation along any circle that surrounds the conical trajectory (two are shown).

invariant associated with conical seams in the unitary case. An argument that demonstrates the aforementioned relation is illustrated in Fig. 3.4. It is based on considering a circle that lies inside the wavepacket in its adiabatic region, and winds around the conical trajectory, e.g., by fixing the value of z, say to $z = 0$. In the laboratory frame, upon ballistic motion of the wavepacket, this circle will span a cylinder, as shown in Fig. 3.4. Spanning 2-dimensional discs D^2 on the initial and final circles we obtain a surface, topologically equivalent to S^2, that winds around the conical point, and therefore, the upper adiabatic level, associated with the surface, has Chern class $c_1 = 1$. Fixing the phase of the adiabatic state on the initial disc according to the actual wavefunction, we can then extend it to the cylinder by applying adiabatic propagation, resulting in a well defined basis, defined on the surface, except for the final disc. As for the final disc, it is natural to fix the phase to be position independent. By the arguments, presented in section 3.3, the latter basis set, being restricted to the circle is connected to its counterpart, restricted from the cylinder, i.e., obtained from solving the dynamical problem, via a map $g : S^1 \to \mathrm{U}(1)$ with degree $\deg g = c_1$, so that the topological structure of the final wavepacket, namely $\deg \zeta = \deg g = 1$ for its polarization ζ, is determined by the value $c_1 = 1$ of the topological invariant, associated with the conical seam.

The more relevant symplectic case is analyzed in an absolutely similar way. In fact all arguments, presented above for the unitary case, stay conceptually the same, with just a couple of differences in

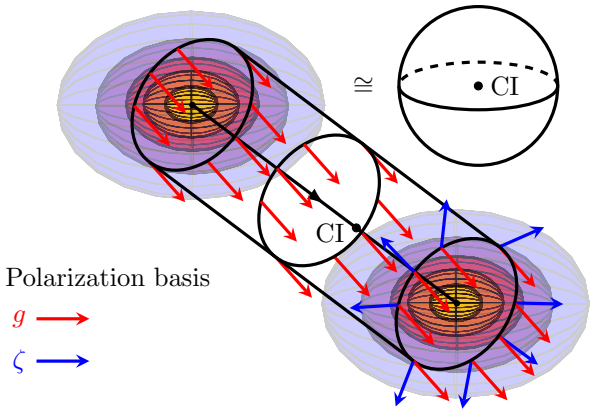

Figure 3.4: Illustration of the argument that connects the topologically non-trivial structure of the scattered wavepacket to the Chern class, associated with a CS, represented by a single point. Red vectors show the wavepacket polarization in the adiabatic region, using an appropriate adiabatic basis set that does not have singularities inside the initial wavepacket. In the adiabatic region polarization is preserved by ballistic evolution. Blue vectors show the final polarization using an alternative and appropriate basis set that is regular within the scattered wavepacket. By the topological argument polarization in the appropriate basis set shows nontrivial topological structure.

details. Namely, the minimal space dimension should be changed from $d = 3$, to $d = 5$, the circles S^1 that surrounds the conical trajectory and the discs D^2, spanned on them, are replaced by the 3-dimensional spheres S^3 and 4-dimensional discs D^4, respectively. Also the map $g : S^1 \to \mathrm{U}(1)$ and the related first Chern class c_1 are replaced by $g : S^3 \to \mathrm{SU}(2)$ and second Chern class c_2, as follows from material, presented in section 3.3. The aforementioned strong similarity of the two cases (which borders with identity, at least in the conceptual sense), together with dealing with much more intuitive 3-dimensional case, compared to 5-dimensional counterpart, was the actual reason why we chose to focus on the unitary case in our presentation.

We are now in a position to briefly discuss the topology of the ballistic case for arbitrary dimension $d \geq 3$ and $d \geq 5$, for the unitary and symplectic cases, respectively, now focusing on the symplectic situation, with the unitary being interpreted by analogy. The local coordinate system is chosen by slightly modifying the approach, presented in section 3.5 for the minimal dimension $d = 5$ case. We chose the z axis along the velocity direction and achieve $\hat{h}(\boldsymbol{e_5}) = f\gamma_5$ in exactly the same way. We further choose some orthonormal, with respect to the mass-weighted scalar product, basis set $(\boldsymbol{e}_k \,|\, 6 \leq k \leq d)$ along the conical seam. We further impose the conditions $\hat{h}(\boldsymbol{e}_j) = f\gamma_j$, for $j = 1, \ldots, 4$, which, together with the requirement of orthogonality to the conical seam, completely identify $(\boldsymbol{e}_j \,|\, 1 \leq j \leq 4)$. It is natural to denote the corresponding coordinate

components $\boldsymbol{x} = (x_1, x_2, x_3, x_4)$ The conical trajectory becomes a $(d-4)$-dimensional plane that pinches the wavepacket along a $(d-4)$-dimensional disc D^{d-4}, where the wavepacket position should be chosen, and where the wavefunction of the scattered wavepacket turns to zero. This disc can be winded by 3-dimensional spheres, e.g., restricting them to the $\boldsymbol{x}$ spaces, so that on each of these spheres the polarization is topologically non-trivial, same as in the minimal dimension case. On a more general note, in the semiclassical/ballistic approximation, with the aforementioned coordinate choice the wavepacket evolves only along the 5 essential coordinates $(\boldsymbol{x}, z)$ with nothing happening to its dependence on the rest of coordinates, chosen along the conical seam.

The topological nature of the scattered wavepacket structure is an important observation, due to robustness of topological features with respect to continuous parameter changes, which implies that when the parameter g_{s} becomes larger, so that the ballistic approximation does not hold quantitatively, the main features, i.e., the wavefunction turning to zero on some $(d-4)$-dimensional disc, generically curved, and the topological feature of the polarization around it, will preserve, at least in the region from small to modest values of g_{s}, providing strong, topologically protected evidence of the wavepacket to have passed through a conical seam.

3.7 Conclusion

In this chapter we addressed nonadiabatic effects in photoinduced dynamics of molecules with odd number of electrons (radicals), with focus on semiclassical treatment. Similar to [126], where spin has been not considered at all, we built a semiclassical theory that accounts for nonadiabatic transitions, which is asymptotically exact in the $\hbar \to 0$ limit. Similar to the simpler integer spin case, in the proper semiclassical limit nonadiabatic transitions occur only in the neighborhood of the conical seam, whose transverse size is given by the scattering length r_{s}. In our earlier work nonadiabatic transitions have been accounted for via modification of the Van Vleck semiclassical propagator, in the region where a classical trajectory passes by the conical seam. Here we developed an equivalent, still more intuitive approach, formulated using wavepacket dynamics in the following way. While far away from the conical seam, a wavepacket moves adiabatically and semiclassically, according to Van Vleck picture, in particular preserving a Gaussian shape. The conical seam is passed ballistically, with the wavepacket experiencing completely local changes, according to a multistate (in the half-integer spin case 4-state) Landau-Zener evolution.

There are still some important differences, implied by time-reversal symmetry, in particular Kramers permanent degeneracy of the electronic levels/potential energy surfaces. To identify the dynamical consequences of the aforementioned permanent degeneracy and interpret them in a clear and intuitive way, in section 3.2 we have formulated time-reversal symmetry using proper terms, reformulating the results of Mead [132, 133] and Matsika-Yarkony [134–137] in a form ready for dynamical implementation. In particular, representing the electronic Hamiltonians in the vicinity of unavoidable crossings as a linear combination of gamma-matrices, represented by σ_z and σ_x, all three Pauli matrices, and four Dirac gamma matrices together with γ_5, in the orthogonal (integer spin), unitary (no time-reversal symmetry), and symplectic (half-integer spin) cases, respectively, allowed later (in section 3.5) the ballistic propagation to be treated within the same framework, in particular express the results in terms of a "standard" 2×2 Landau-Zener problem, by making use of the gamma-matrix algebra.

We have identified the symplectic group Sp(1) as the one being responsible for Kramers degeneracy, and pointed to its isomorphism to special unitary group SU(2), the latter being more common in the chemical physics community. In section 3.4 we have extended the Born-Oppenheimer approximation to the permanent degeneracy case, and have demonstrated that, in the semiclassical limit, the wavefunction polarization that defines the value of the function in the double-degenerate electronic space, and is represented by a unit length 2-component complex vector, evolves completely geometrically, according to parallel transport, the latter effect leading to a non-abelian Berry phase, represented by an SU(2) rotation, if one moves over a close loop trajectory.

We further demonstrated, using the ballistic approximation, that once completely passed through a conical seam, the wavepacket component that stays on the same adiabatic surface adopts a topologically non-trivial structure: the wavefunction turns to zero on a $(d-4)$-dimensional surface, represented by the points in the wavepacket that went exactly through the $(d-5)$-dimensional CS, and that in the transverse directions the polarization shows a topologically nontrivial structure. We have demonstrated that the latter is directly related to the topological invariant of CSs in the symplectic case, namely the second Chern class c_2, whereas in the orthogonal and unitary cases the corresponding invariant, responsible for the wavepacket structure, is represented by the first Stiefel-Whitney w_1 and first Chern class c_1, respectively. Such identification is an important observation since, due to robust character of topology, the structure, described above, will not dis-

appear when the semiclassical/ballistic approximation is no longer valid, just the aforementioned $(d-4)$-dimensional node surface will get curved, so that the topologically non-trivial polarization structure can be viewed as a strong experimental evidence of the wavepacket to have passed through a CS, for the measurements, sensitive to the wavefunction polarization [138], e.g., in spin-sensitive fragment angular distributions upon photo-dissociation of half-integer spin radicals. We reiterate that, in the integer spin case, state-of-art numerically exact propagation of nuclear wavepackets with nonadiabatic effects accounted for explicitly, combined with the Landau-Zener spirit analysis showed the sensitivity of photo-dissociation data, available from experiments to the specific details of the wavepacket shape, characteristic to passing through a conical seam, as well as an excellent agreement between the Landau-Zener analysis and numerically exact results [139, 140]. Furthermore, an apparently more complicated case of triple-state crossing have been studied for both half-integer and integer spin systems [21, 141–143]. It is worth mentioning that, the CS in a triple crossing integer spin system has codimension 5 which equals to the CS in a double crossing half-integer spin system, despite the different local structures of their Hamiltonian in the vicinity of the CSs.

Obviously the ballistic approximation allows not only the shapes of the scattered wavepackets to be determined, but also the evolution of the complete wavefunction during whole the scattering process to be followed. This can be easily achieved by replacing the limiting values of the matrix elements in Eq. (3.44), given by Eq. (3.45), with the actual values, expressed in terms of the parabolic cylinder functions, as presented in [126]. These should provide a clear semiclassical interpretation of the recently proposed time-resolved X-ray experiments [144, 145], capable of providing detailed dynamical information on the nuclear wavepacket passage through a CS. It is worth noting that in the proper adiabatic (i.e., diabatic) basis set, associated with the reference trajectory, the wavepackets that stay and change the diabatic surface, will have a topologically plain and topologically non-trivial polarization structure, respectively.

Finally, it would be of interest to explore a possibility of combining the presented semiclassical dynamical view of scattering at conical intersections with widely used surface hopping algorithms, especially the ones that properly account for the quantum phase effects, see, e.g., [58,59], to improve their performance in the situation when conical intersections are involved.

CHAPTER 4 SEMICLASSICAL MONTE-CARLO APPROACH TO MODELING NONADIABATIC DYNAMICS

Reproduced from J. Chem. Phys. 141, 184101 (2014), with the permission of AIP Publishing.

4.1 Overview

In this chapter we describe a method based on Monte-Carlo sampling of the semiclassical time-dependent wavefunction of a molecule. The method was first reported in [**Tretiak S. et al. Semiclassical Monte-Carlo Approach for modelling non-adiabatic dynamics in extended molecules. Nat. Commun. 4:2144 doi: 10.1038/ncomms3144 (2013)**]. It was shown that the results obtained with our method are in a very good agreement with numerically exact results for three standard sample problems (the so-called Tully problems). [52] Additionally, comparison of the results for 1-D and 2-D test problems, [58] demonstrated that the convergence of the method does not deteriorate with the an increase in the number of nuclear degrees of freedom. This is a consequence of a fact that the stochasticity of the Monte-Carlo procedure is related purely to the non-determinism in the subspace of the electronic states (between the hops nuclei propagate according to the classical equations of motion, i.e., deterministically). This chapter is organized as follows: In section 4.2, we will formulate the problem and describe the theory behind the numerical method. In Section 4.3 we describe, in detail, how to carry out the SCMC simulation, and provide an algorithm for a system with two PES. In Section 4.4 we analyze the results of the SCMC method when applied to Tully's 1-D test problems.

4.2 Theory

Consider a Hamiltonian with nuclear and electronic degrees of freedom:

$$H = \frac{\hat{\mathbf{P}}^2}{2M} + \hat{H}_{\mathrm{el}}(\boldsymbol{r}), \tag{4.1}$$

where $\hat{\mathbf{P}}$ is the N-component nuclear momentum operator (N is the number of independent nuclear coordinates, $\mathbf{R} \equiv (R_1, ..., R_N)^T$), M is the nuclear mass (for simplicity of notation we assume that all nuclear degrees of freedom have the same mass, extension to different masses is straightforward)

and $H_{\rm el}$ is the electronic Hamiltonian (which includes electronic kinetic energy and all interactions and depends parametrically on $\mathbf{R}$). The dynamics of the nuclear degrees of freedom can be conveniently represented in the adiabatic basis in terms of the effective Hamiltonian (see Ref. 146, 147 for details)

$$\hat{H}_{\rm eff} = \frac{(\hat{\mathbf{P}} - \hat{\mathbf{d}}(\boldsymbol{r}))^2}{2M} + \hat{E}(\boldsymbol{r}). \tag{4.2}$$

Here $\hat{E}(\boldsymbol{r})$ is diagonal matrix with elements being the eigenstates of the Hamiltonian $H_{\rm el}$ and $\hat{\mathbf{d}}(\boldsymbol{r})$ is the nonadiabatic (derivative) coupling matrix, $d_{ij}(\mathbf{R}) = \langle \Psi_i(\boldsymbol{r}) | \nabla_{\boldsymbol{r}} | \Psi_j(\boldsymbol{r}) \rangle$.

In the absence of the nonadiabatic coupling the PES's are decoupled and the nuclei propagate on a potential landscape given by a particular $E_i(\boldsymbol{r})$. Formally, in order to describe quantum dynamics for a system of N particles corresponding to Hamiltonian $H_0 = (\hat{\mathbf{P}}^2/2m) + \hat{E}(\boldsymbol{r})$, one needs to solve $N+1$ dimensional Schrodinger equation (for a given PES, i.e., $E_i(\boldsymbol{r})$), which is an impossible task for $N \gg 1$. However, in the classical limit, the problem reduces to solving N coupled Newton's equations, which is not too difficult, even for a reasonably large number of degrees of freedom. Furthermore, in this classical or semiclassical limit one can easily construct a wavefunction of the nuclei by utilizing a gaussian approximation:

$$\Psi_i(\boldsymbol{r}, t) \sim \prod_{\alpha=1}^{N} \mathrm{e}^{-\frac{(R^\alpha - R_c^\alpha(t))^2}{2\sigma_\alpha^2(t)} + \mathrm{i}P_c^\alpha(t)(R^\alpha - R_c^\alpha(t)) + \mathrm{i}S_i(t)}. \tag{4.3}$$

That is, the gaussian wavepacket with average momentum $\mathbf{P}_c(t)$ is centered around positions $\boldsymbol{r}_c(t)$, is evaluated according to the classical equations of motion, with $S_i(t)$ being the classical action of the system produced during a time, t. For simplicity in this chapter we assume that the dispersion of the gaussian wavepacket corresponds to that of a free particle, $\sigma^2(t) = \sigma^2(0) + i\hbar t/M$. While this approximation is clearly violated for PESs with sufficient curvature, for dynamics in realistic molecules this is practically never the case. Indeed, a typical spread of the nuclear wavepacket is of the order of nuclear zero point motion associated with the vibrational ground states of a molecule, which is at least an order of magnitude smaller than the size of a typical electronic bond (which sets the length scale of $E_i(\boldsymbol{r})$) due to large mass, M, of the nuclei. Furthermore, this approximation did not lead to significant deviation from exact solution in the scattering results considered below. Thus, instead of solving a $N+1$ dimensional Schrodinger equation, a problem reduces to solving

N ordinary second order differential equations.

Unfortunately, for $\hat{\mathbf{d}} \neq 0$ this is no longer the case. One way to proceed is to use the mean field approach and neglect the spacial dependence of the wavefunction. Such approach is easy to implement, but it is well known that it leads to significant errors when branching of trajectories is important. Another approach was proposed by Pechukas in the late 1960's, [60, 61] which is an attempt to apply the semiclassical approximation to the $\hat{\mathbf{d}} \neq 0$ situation. Unfortunately in such case one can only formulate an iterative procedure (which is not necessarily well convergent) that leads to the saddle point (*i.e.* semiclassical) solution to the Schrodinger equation for the molecule. Instead we propose a different approach: We write down solution to the Schrodinger equation as a perturbative expansion in powers of $\hat{\mathbf{d}}$:

$$\begin{aligned} |\Psi(t)\rangle &= \mathrm{e}^{-\mathrm{i}\hat{H}_0 t/\hbar}\,|\Psi(0)\rangle + \int_0^t \mathrm{d}t_1 \mathrm{e}^{-\mathrm{i}\hat{H}_0(t-t_1)/\hbar}\frac{-\mathrm{i}}{2m}(\hat{\mathbf{d}}\mathbf{P} + \mathbf{P}\hat{\mathbf{d}})\mathrm{e}^{-\mathrm{i}\hat{H}_0 t_1/\hbar}\,|\Psi(0)\rangle \\ &+ \int_0^t \mathrm{d}t_1 \int_0^{t_1} dt_2 \ldots . \end{aligned} \tag{4.4}$$

Eq. (4.4) is an infinite series with second and higher order terms being time ordered integrals and containing second and higher orders of perturbation. Here we neglected the $\hat{\mathbf{d}}^2/2M$ term, which is small (compared to the systems kinetic energy) in the semiclassical approximation. Moreover, this term is diagonal and therefore it may be included in the definition of $\hat{H}_0$ if needed.

Suppose that the state $|\Psi(0)\rangle$ is a gaussian wavepacket localized on the PES 1. Furthermore let us assume that the electronic subspace is two dimensional, i.e., there are only two close PES, the remaining PESs are separated by large gaps so that transition probabilities are infinitesimally small due to rapid oscillations of the integrands in Eq. (4.4). In fact such situation is usually the case; typically only two PES cross in a relevant region of the phase space. Then $\hat{\mathbf{d}} = d_{12}(\boldsymbol{r})\hat{\sigma}_y$, where $\hat{\sigma}_y$ is a Pauli matrix and $\mathbf{d}_{12}$ is a scalar function of $\boldsymbol{r}$. According to the above discussion of the $\hat{\mathbf{d}} = 0$ situation, the first term in the right hand side (r.h.s.) of Eq. (4.4) is just a gaussian wavepacket that have propagated along the first PES according to classical equations of motion.

Let us consider the second term in the r.h.s. of Eq. (4.4) which corresponds to a "piece" of the wavefunction that has hopped once at time t_1 from PES 1 to PES 2. It is clear that the wavepacket right before the hopping event at t_1 can be approximated as a gaussian. It is reasonable to assume that after the scattering event at t_1 the wavepacket retains its gaussian shape, but acquires an

amplitude c (proportional to d_{12} at $\boldsymbol{r}_c(t_1)$). Similar assumptions apply to the higher order integrals. That is, we approximate the wavefunction in Eq. (4.4) as

$$
\begin{aligned}
|\Psi(\boldsymbol{r},t)\rangle = \mathcal{N}\Big(& \mathrm{e}^{-\frac{(\boldsymbol{r}-\boldsymbol{r}_c^{(0)}(t))^2}{2\sigma^2(t)}+\mathrm{i}\mathbf{P}_c^{(0)}(t)(\boldsymbol{r}-\boldsymbol{r}_c^{(0)}(t))+\mathrm{i}S^{(0)}(t)}\,|1\rangle \\
& -\mathrm{i}\int_0^t dt_1 c[\boldsymbol{r}_c^{(0)}(t_1)]\mathrm{e}^{-\frac{(\boldsymbol{r}-\boldsymbol{r}_c^{(1)}(t))^2}{2\sigma^2(t)}+\mathrm{i}\mathbf{P}_c^{(1)}(t)(\boldsymbol{r}-\boldsymbol{r}_c^{(1)}(t))+\mathrm{i}S^{(1)}(t)}\,|2\rangle \\
& +(-\mathrm{i})^2\int_0^t dt_1\int_0^{t_1} dt_2\, c[\boldsymbol{r}_c^{(0)}(t_1)]\, c[\boldsymbol{r}_c^{(1)}(t_2)]\mathrm{e}^{-\frac{(\boldsymbol{r}-\boldsymbol{r}_c^{(2)}(t))^2}{2\sigma^2(t)}+\mathrm{i}\mathbf{P}_c^{(2)}(t)(\boldsymbol{r}-\boldsymbol{r}_c^{(2)}(t))+\mathrm{i}S^{(2)}(t)}\,|1\rangle \\
& +\ldots\Big).
\end{aligned}
\tag{4.5}
$$

where the normalization constant $\mathcal{N} = \pi^{-N/4}[\sigma(t)]^{-N/2}$ and from now on we will set $\hbar = 1$ unless stated otherwise. In Eq. (4.5) the superscript indices for the "classical" variables, $\boldsymbol{r}_c$, $\mathbf{P}_c$, and S_c, indicate the number of jumps. For example, $\boldsymbol{r}_c^{(2)}$ is a classical position for a trajectory of the nuclei with two hops: At time t_1 from PES 1 to PES 2 and back at time t_2, so that $\boldsymbol{r}_c^{(2)}$ is a function not only of t, but also of t_1 and t_2.

Eq. (4.5) is incomplete on itself: One needs to specify the $c[\boldsymbol{r}_c(t)]$ as well as the value of the momentum right after the hop. (Here we assume that neither the position nor the dispersion of the wavepacket change immediately after the hop, which is easy to check by a simple calculation similar to the one discussed below.) For that let us divide the time integrals in Eqs. (4.4, 4.5) into integrals over smaller time intervals Δt, where Δt is smaller than the timescale at which the particle moves over the distance at which potential $E_{1,2}(\mathbf{R})$ varies significantly. Let us consider dynamics of the wavepacket at such interval Δt. Assume that at the beginning of the interval the shape of the wavepacket (for the nuclei) is $\phi_1(\boldsymbol{r},0)$ (which is not necessarily gaussian) with electrons being in state 1. Furthermore, we assume that the wavepacket is in the semiclassical regime: On one hand it is sufficiently localized so that it's width, σ, is smaller than the distance at which potential $E_{1,2}(\mathbf{R})$ varies significantly; on the other hand its momentum is well defined so that it is much greater in magnitude than its uncertainty (σ^{-1}). Then the parameters $c[\boldsymbol{r}_c(t)]$ and $\mathbf{P}_2$ (the momentum after the hop, i.e. at the PES 2) must be such that the descriptions of the wavefunction in Eq. (4.4) and Eq. (4.5) match. That is, Eq. (4.4) on the time interval, Δt, describes dynamics of a wavepacket according to an effective Hamiltonian in Eq. (4.2), where, within a small Δt, we may determine the wavefunction as $|\Psi_{ex}(t)\rangle = \mathrm{e}^{-it\hat{H}_{\mathrm{eff}}}\phi_1(\boldsymbol{r},0)\,|1\rangle$ by expanding in powers of t and setting $\mathbf{d}$ and E to

be independent of $\boldsymbol{r}$. Similarly we may evaluate the wavefunction for the gaussian approximation in Eq. (4.5). Up to the second order in t, which is sufficient for our purposes, we may write

$$|\Psi_g(t)\rangle = (1 - c^2t^2/2)\phi_1(\boldsymbol{r}, t)\,|1\rangle - \mathrm{i}ct\phi_2(\boldsymbol{r}, t)\,|2\rangle\,, \tag{4.6}$$

where $\phi_2(\boldsymbol{r}, t)$ is a normalized wavepacket at the second PES. The t^2 term in Eq. (4.6) arises due to two hop contribution in Eq. (4.5). Note that the wavefunction in Eq. (4.6) is normalized up to $O(t^2)$. Since c and $\mathbf{P}_2 = \int d\boldsymbol{r}\phi_2^*(\boldsymbol{r}, t)\hat{\mathbf{P}}\phi_2(\boldsymbol{r}, t)$ define occupation probabilities and system's momentum, we require that

$$\langle\Psi_g(t)|\sigma_z|\Psi_g(t)\rangle = \langle\Psi_{ex}(t)|\sigma_z|\Psi_{ex}(t)\rangle\,, \tag{4.7}$$

$$\langle\Psi_g(t)|\hat{\mathbf{P}}|\Psi_g(t)\rangle = \langle\Psi_g(t)|\hat{\mathbf{P}} - \mathbf{d}_{12}\sigma_y|\Psi_g(t)\rangle\,. \tag{4.8}$$

Eqs. (4.7, 4.8) provide the matching (boundary) conditions that determine values of c and $\mathbf{P}_2$. Note that in the r.h.s. of Eq. (4.8) we have used the "true" momentum of the system, which is given by its velocity $M\dot{\boldsymbol{r}} = \mathrm{i}M\left[\hat{H}_{\text{eff}}, \boldsymbol{r}\right] = \hat{\mathbf{P}} - \mathbf{d}_{12}\hat{\sigma_y}$. The left hand side (l.h.s.) of Eq. (4.8) gives $1 - 2(ct)^2$, while the r.h.s. results in $1 - 2(\mathbf{d}_{12}\mathbf{P}_1t)^2/M^2$, where $\mathbf{P}_1 = \int \mathrm{d}\boldsymbol{r}\phi_1^*(\boldsymbol{r}, t)\hat{\mathbf{P}}\phi_1(\boldsymbol{r}, t)$. Then we obtain that

$$c(\boldsymbol{r}) = (\mathbf{d}_{12}(\boldsymbol{r}) \cdot \mathbf{P}_1)/M = \mathbf{d}_{12}(t), \tag{4.9}$$

with $\mathbf{P}_1$ being the momentum right before the hop.

Similarly, the l.h.s. of Eq. (4.8) gives $\mathbf{P}_1 - (ct)^2(\mathbf{P}_2 - \mathbf{P}_1)$, where we have assumed that t is small enough and so the momenta $\mathbf{P}_1$ and $\mathbf{P}_2$ do not change during the evolution over the time interval t. The r.h.s. yields $\mathbf{P}_1 - \mathbf{d}_{12}(R)(E_2 - E_1)(\mathbf{d}_{12}(\boldsymbol{r}) \cdot \mathbf{P}_1)t^2/M$, so that

$$\mathbf{P}_2 - \mathbf{P}_1 = \frac{M(E_2 - E_1)\mathbf{d}_{12}(\boldsymbol{r})}{\mathbf{d}_{12}(\boldsymbol{r}) \cdot \mathbf{P}_1}. \tag{4.10}$$

Eq. (4.10) gives a condition for the re-scaling of momentum of the wavepacket which, at first glance, may seem to be in contradiction with that proposed by Herman [148] and used by Tully [52] in his surface hopping algorithm. Indeed, while in Eq. (4.10) the change in the momentum at the hop is along $\mathbf{d}_{12}$, Eq. (4.10) does not conserve the total energy at the hop. However, careful inspection

reveals that Eq. (4.10) is simply the zeroth and first order terms in an expansion, in powers of $\frac{E_2-E_1}{\mathbf{P}_1^2/2M}$, of the full energy conservation condition. This is, presumably, an artifact of the short time approximation that we used in the derivation of Eq. (4.10). Indeed, its easy to check that Eq. (4.10) conserves energy approximately, up to the leading order in $\Delta E = E_2 - E_1$. Furthermore, we have run the test problems considered below using condition of Eq. (4.10) as well as using the exact energy conservation condition at the hop and found very good agreement between the two in a very broad range of initial momenta. This is a consequence of a fact that the main contribution to the integrals in Eq. (4.5) comes from the region where ΔE is small and so the energy conservation at the hop is satisfied. Therefore we conclude that the two conditions are essentially identical and in the following we will be using the Herman/Tully criterion to re-scale the wavepacket's momentum at the hop. In the next section we will describe an efficient numerical algorithm that evaluates the wavefunction in Eq. (4.5) using Monte-Carlo technique.

4.3 SCMC Calculation

The SCMC provides a first principles method for calculating nonadiabatic molecular dynamics, with similar cost to surface hopping methods. The calculation occurs in two main steps: **A)** the nonadiabatic propagation of classical trajectories, and **B)** the use of trajectory data to sample the integrals in Eq. (4.5), with $c[\boldsymbol{r}_c(t)] = \mathbf{d}_{ij}(t)$. The classical propagation is similar to standard surface hopping algorithms. [2, 52, 148] For simplicity, we assume that we have only two electronic states to consider. Generalization to higher numbers of states is straightforward. [58] In the following subsections we describe, in algorithmic fashion, the surface-hopping dynamics, **A**, and the Monte Carlo calculation of the time-dependent semi-classical wavefunction, **B**. Figure 4.3 shows a diagrammatic map of the algorithm.

A1 All trajectories are initialized with the same position and momentum. Various tracked values are initialized (see Fig. 4.3). We begin propagation of the nuclear wavepackets.

A2 Begin time step. Supplied with a molecular geometry, $\boldsymbol{r}_c$, quantum chemistry methods (*e.g.* DFT and TDDFT) are used to calculate the electronic state energies, $E_i(t)$, the Hellmann-Feynman forces (electronic gradients), $\mathbf{F}_c$, the first order nonadiabatic coupling vectors (NA-CV), $\mathbf{d}_{ij}(\boldsymbol{r}_c) = \left\langle \Psi_i(\boldsymbol{r}_c) \middle| \frac{\partial}{\partial \boldsymbol{r}_c} \Psi_j(\boldsymbol{r}_c) \right\rangle$, and scalars $d_{ij}(t) = \left\langle \Psi_i(\boldsymbol{r}_c(t)) \middle| \frac{\partial}{\partial t} \Psi_j(\boldsymbol{r}_c(t)) \right\rangle = \mathbf{d}_{ij}(\boldsymbol{r}_c) \cdot \dot{\boldsymbol{r}}_c(t)$.

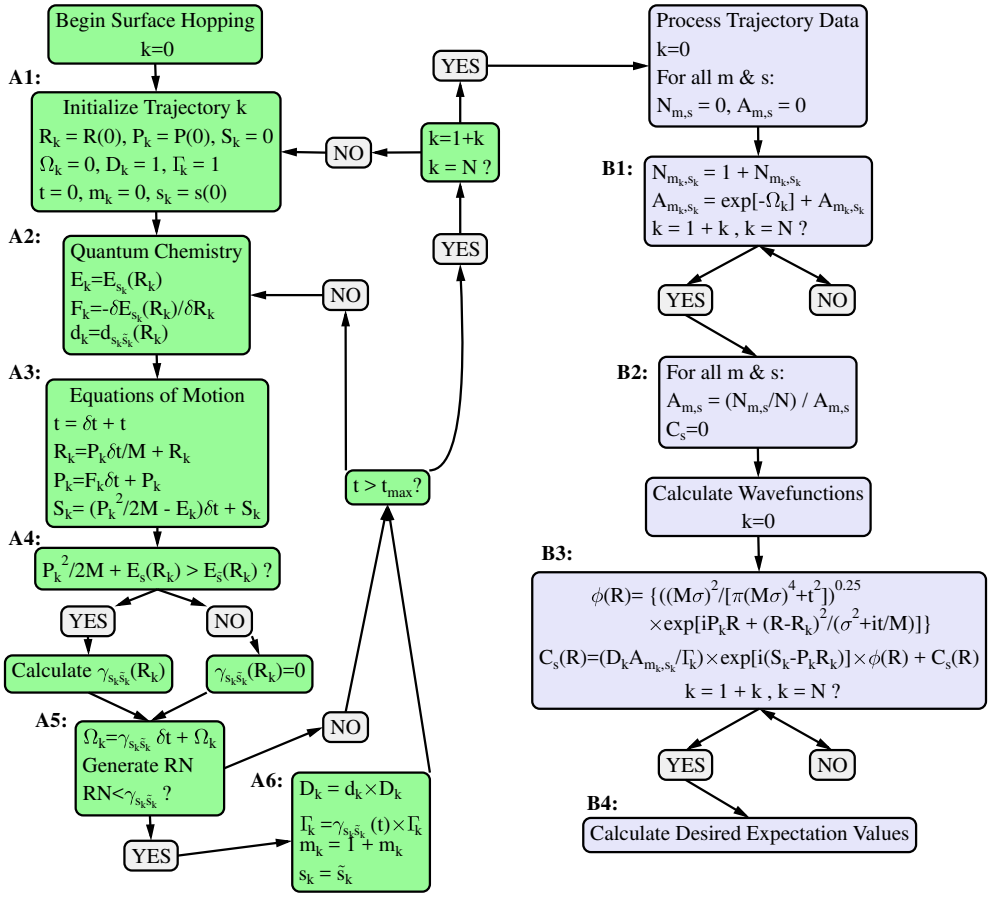

Figure 4.1: Example for semiclassical Monte-Carlo surface hopping algorithm for a two electronic state system. Green boxes - Part A (dynamics). Purple boxes - Part B (Wavefunction calculation). Definitions are same as text.

A3 The classical particles are propagate for one time step, ∂t, on the current adiabatic surface, i, using Newton/Lagrange equations of motion,

$$\frac{\partial}{\partial t}\mathbf{P}_c(t) = \mathbf{F}_c(t) = -\frac{\partial}{\partial \boldsymbol{r}_c} E_i(\boldsymbol{r}_c(t)), \tag{4.11}$$

by some numerical method, *e.g.* Verlet, Runga-Kutta. The classical action along the trajectory,

$$\begin{aligned} S(t) &= \int_0^t \mathrm{d}t' \sum_\alpha^N \frac{P_\alpha^2(t')}{2M_\alpha} - E(t') \\ &= \sum_\alpha^N \int_{R_c^\alpha(0)}^{R_c^\alpha(t)} \mathrm{d}\bar{R}_c^\alpha P_\alpha(\bar{R}_c^\alpha), \end{aligned} \tag{4.12}$$

is calculated for subsequent use in part B. We assume our propagated gaussian nuclear wavepackets are "free", *i.e.* they broaden with time, independent of the PES.

A4 At the end of the time step, we determine whether or not to hop to a new state, j. First, we determine whether the hop is allowed or frustrated by, the assumed, conservation of energy, *i.e.*

$$\frac{\mathbf{P}_c^2(t')}{2M} + E_i(\mathbf{R}_c) \geq E_j(\mathbf{R}_c). \tag{4.13}$$

If the hop is allowed the probability, $\gamma_{i\to j}(t)$, is calculated. If not $\gamma_{i\to j}(t) = 0$. Unlike other surface hopping methods, [2, 52, 148] the final result is formally independent of the choice of hopping rate, assuming that the hopping rate is nonzero everywhere $d_{ij}(t)$ is non-zero. However the choice of hopping rate is crucial to achieve rapid convergence of the result.

A5 At each time step the hopping probability to the new state is added to the integral:

$$\Omega(\mathbf{t}) = \sum_{l=0}^{l=m} \int_{t_l}^{t_{l+1}} \mathrm{d}t' \, \gamma_{s_l \to s_{l+1}}[\boldsymbol{r}_c(t')]. \tag{4.14}$$

Here, m is the number of hops over the course of the trajectory, and t_l is the time at which the lth hop occurs ($t_{m+1} \equiv t$, $s_{m+1} \equiv j$). If RN $< \gamma_{i\to j}$, where RN is a generated random number between 0 and 1, then the trajectory hops to state j.

A6 If a hop occurs, the products:

$$D(t_{m-1} \ldots t_0) = \prod_{l=0}^{m-1} d_{s_l \, s_{l+1}}(t_l), \tag{4.15}$$

$$\Gamma(t_{m-1} \ldots t_0) = \prod_{l=0}^{m-1} \gamma_{s_l \to s_{l+1}}(t_l) \tag{4.16}$$

are multiplied by $d_{ij}(t)$ and $\gamma_{i\to j}(t)$ respectively. The number of hops, m, is increased by one.

The procedure is repeated for the next time step on either the original or new state. These dynamics continue for the desired time. Once completed, the final position, $\boldsymbol{r}_c(t)$, and momentum, $\mathbf{P}_c(t)$, of the trajectory are stored. The process is repeated for the specified number of trajectories. In calculations of realistic molecular systems, **A2**, *i.e.* quantum chemistry calculation of state

energies, forces and nonadiabatic couplings, will be the most computationally demanding step. However, due to the independence of the dynamical trajectories, the loop beginning at **A1** is trivially parallelizable. This will greatly aid in the application of the method to larger systems.

4.3.1 Post-Processing

Information collected by the surface hopping dynamics is further analyzed in the second step at negligible computational expense when compared to part **A**. Namely we calculate the nuclear wavefunctions,

$$\mathbf{\Psi}_i(\boldsymbol{r},t) = \sum_m \int d^m\mathbf{t}\mathbf{I}_i^m(\boldsymbol{r},\mathbf{t}), \tag{4.17}$$

or probabilities, $P_i = \int \mathrm{d}\boldsymbol{r}\,|\mathbf{\Psi}_i(\boldsymbol{r},t)|^2$. Here $\mathbf{t} \equiv \{t_1,\ldots,t_m,t\}$ is the set of time integration variables and $\int \mathrm{d}^m\mathbf{t} \equiv \int_0^t \mathrm{d}t_m \int_0^{t_m} \mathrm{d}t_{m-1}\ldots\int_0^{t_2}\mathrm{d}t_1$. We independently sample integrals, $\int \mathrm{d}^m\mathbf{t}\,\mathbf{I}_i^m(\boldsymbol{r},\mathbf{t})$, which differ in the number of hops, m, and final state, i. Additionally, if there is significant separation between wavepackets, *e.g.* wavepackets which are reflected or transmitted in 1-D, then integrals contributing to those wavepackets are also sampled separately. While not required formally, this consideration of spacial overlap significantly improves convergence rates with minimal loss of information. Thus, trajectories are sorted by the number of hops and final electronic state, and grouped into spatially separated contributors of the partial wavefunctions.

Using the standard Monte Carlo approach, the integral $\int \mathrm{d}^m\mathbf{t}\,\mathbf{I}_i^m(\boldsymbol{r},\mathbf{t})$, can be expressed in terms of an expectation value:

$$\int \mathrm{d}^m\mathbf{t}\,\mathbf{I}_i^m(\boldsymbol{r},\mathbf{t}) = \int \mathrm{d}^m\mathbf{t}\,\frac{\mathbf{I}_i^m(\boldsymbol{r},\mathbf{t})}{\rho_i^m(\mathbf{t})}\times\rho_i^m(\mathbf{t}) \approx \frac{1}{N_i^m}\times\sum_{k=0}^{N_i^m}\frac{\mathbf{I}_i^m(\boldsymbol{r}_k,\mathbf{t}_k)}{\rho_i^m(\mathbf{t}_k)}\ . \tag{4.18}$$

Here, k is the index of a trajectory from step 1, N_k^m is the total number of trajectories with m hops and ending in state i. $\rho_i^m(\mathbf{t}_k)$ is the value of the probability distribution, $\rho_i^m(\mathbf{t})$, for the trajectory k.

The kth value of the probability distribution can be expressed as $\rho_i^m(\mathbf{t}_k) = \Gamma_i^m(\mathbf{t}_k)/A_i^m$. Here $\Gamma_i^m(\mathbf{t}_k)$ is given by Eq. (4.16), and $A_i^m = \int \mathrm{d}^m\mathbf{t}\,\Gamma_i(\mathbf{t})$ is the normalization coefficient for trajectories with m hops finishing in state i. A_i^m can be determined using statistical considerations of the stochastic process defined by the rate γ. We consider the probability of a single trajectory finishing

in state i with m hops for all values of $\mathbf{t}$ (see Supplemental of Ref. [58]):

$$\mathrm{p}_i = \int \mathrm{d}^m\mathbf{t}\,\Gamma_i(\mathbf{t})\mathrm{e}^{-\Omega_i(\mathbf{t})}. \tag{4.19}$$

This probability can also be expressed as an expectation value, using the same probability distribution, $\rho_i^m(\mathbf{t}) = \Gamma_i(\mathbf{t})/A_i^m$, from Eq. (4.18):

$$\mathrm{p}_i = \frac{A_i^m}{N_i^m}\sum_{k=0}^{N_i^m} e^{-\Omega_i(\mathbf{t}_k)}. \tag{4.20}$$

$\Omega_i(\mathbf{t}_i)$ is given by Eq. (4.14). We seek the value of A_i^m. Thus, we assume the number of trajectories, N_i^m, is sufficiently large so that we can replace p_i with N_i^m/N, and rearrange:

$$\begin{aligned} A_i^m &\approx (N_i^m)^2\left[N\sum_{k=0}^{N_i^m} e^{-\Omega_i^m(\mathbf{t}_k)}\right]^{-1}, \\ \text{and}\quad \rho_i^m(\mathbf{t}_k) &= \Gamma_i^m(\mathbf{t}_k)\frac{N}{(N_i^m)^2}\sum_{k=0}^{N_i^m}\mathrm{e}^{-\Omega_i^m(\mathbf{t}_k)}. \end{aligned} \tag{4.21}$$

B1 We first determine N_i^m and calculate the sum in Eq. 4.21 for every i/m pair.

B2 We calculate each A_i^m.

B3 For a given trajectory $\mathbf{I}_i^m(\boldsymbol{r}_k, \mathbf{t}_k)$ is easily calculated, see Eq. (4.5), from the surface hopping data, Eqs. (4.11,4.12,4.15).

$$\mathbf{I}_i^m(\boldsymbol{r}_k, \mathbf{t}_k) = D_k(\mathbf{t}_k) \times \mathrm{e}^{\mathrm{i}(S^i(\mathbf{t}_k) - \mathbf{P}^k(t)\boldsymbol{r}_c^k(t))} \times \boldsymbol{\phi}(\boldsymbol{r}, \boldsymbol{r}_c^k, \mathbf{P}_c^k, t), \tag{4.22}$$

where $\boldsymbol{\phi}$ is a "free" gaussian wavepacket,

$$\boldsymbol{\phi}(\boldsymbol{r}, \boldsymbol{r}_c^k, \mathbf{P}_c^k, t) = \sqrt[4]{\frac{M^2\sigma^2}{\pi(M^2\sigma^4 + t^2)}}\mathrm{e}^{\mathrm{i}\mathbf{P}^k(t)\boldsymbol{r}}\mathrm{e}^{\frac{(\boldsymbol{r}-\boldsymbol{r}_c^k(t))^2}{\sigma^2 + \frac{\mathrm{i}t}{M}}}, \tag{4.23}$$

with the final position and momentum of the trajectory k, and an initial width, σ. At this point the nuclear wave functions can be calculated by summing over all the trajectories, Eq. (4.18).

B4 Once $\mathbf{\Psi}_i(\boldsymbol{r},t)$ is known, expectation values (*e.g.* x, P, density matrix) can be calculated. When the number of trajectories is low, the random error in $\mathbf{\Psi}_i(\boldsymbol{r},t)$ can be reduced by normalization. However the effect is minimal in a well converged calculation.

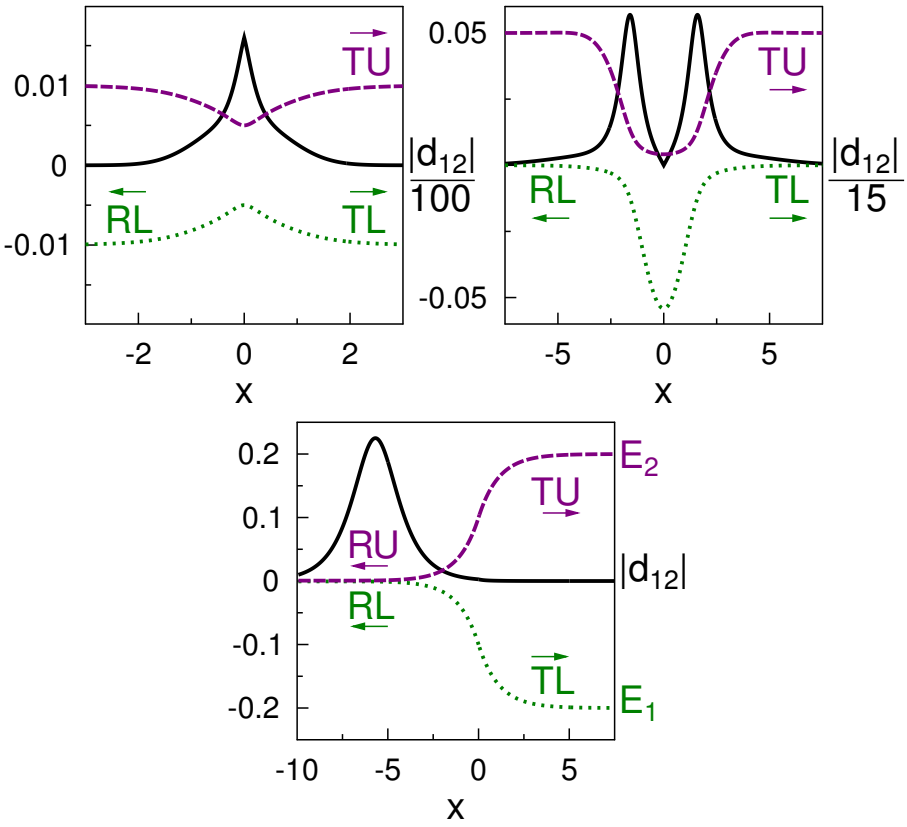

Figure 4.2: Tully's problem set. Top Left: Problem 1-Single avoided crossing. Top Right: Problem 2- Double avoided crossing. Bottom: Problem 3- Extended coupling with reflection. Green dotted (Purple dashed) line is lower (upper) electronic eigenstate, $E_{1(2)}$. Black solid line is the absolute value of the nonadiabatic coupling vector, $|d_{12}(x)|$. All values are in atomic units.

Some notes on the case of more than 2 electronic states: [1] The rate in Eq. (4.14) would be replace with a sum over the rates to all possible new states. [2] Eqs. (4.15, 4.16) remain unchanged. [3] Determination of which state to hop to can be determined as it is in Ref [52]. [4] For every possible path of intermediate electronic excited states, there is an integral which must be sampled independently. Thus each distinct path has a different probability distribution, Eq. (4.21).

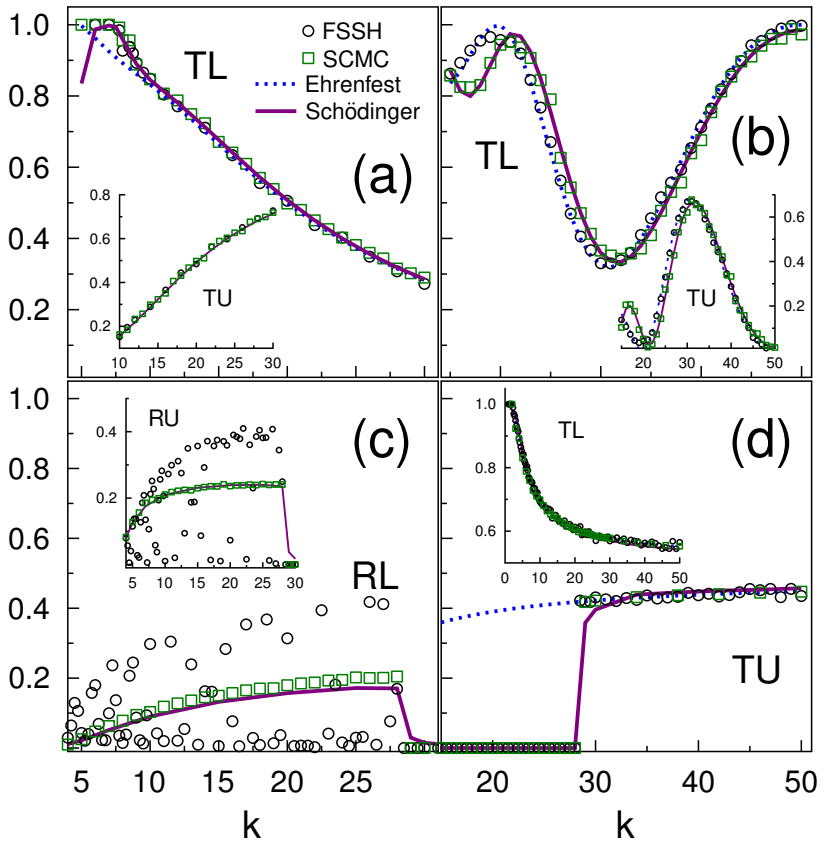

Figure 4.3: Scattering probabilities for Tully's problem set, using, time-dependent Schödinger equation (black solid line), Ehrenfest method (blue dotted line), fewest switching surface hopping (purple circles), and SCMC method (green squares). (a) Problem 1 - Transmission on lower (inset-upper) surface. (b) Problem 2 - Transmission on lower (inset-upper) surface. (c) Problem 3- Reflection on lower (inset-upper) surface. (d) Problem 3- Transmission on upper (inset-lower) surface.

4.4 Analysis of SCMC Method

In order to test the SCMC procedure we consider three two-level models proposed by Tully. [52] Figure 4.2 shows the energy eigenstates and NACV's of these three one-dimensional problems. For the exact form of the Hamiltonians see Ref. [52]. For these three problems, scattering probabilities calculated using the SCMC, FSSH, and Ehrenfest methods are compared to the exact time-dependent Schrödinger equation in Gorshkov *et. al.* [58] In Figure 4.3, we re-present those scattering results. For Problems 1 and 3: 25,000 and 10,000 trajectories were used for the SCMC and FSSH approaches respectively. For Problem 2: 75,000 trajectories were used in the SCMC calculation, while only 10,000 were used in the FSSH calculation. Here we seek to provide in-depth analysis of these results and insight into the method. All parameters and results in this section are in atomic units.

Problem 3 provides a simple model problem where the standard implementation of the FSSH quantitatively and qualitatively fails to reproduce the exact TD-Schrödinger result, see Fig. 4.3-c/d. It is well known that this failure is due to the lack of decoherence. [52, 149] The equation of motion for the electronic density matrix, or complex expansion coefficients, does not include the effect of bifurcation of nuclear wavepackets. Corrections can be introduced by hand into the FSSH algorithm to correct for this problem. [102, 104–116] In the SCMC approach, we do not need to propagate the electronic density matrix in order to determine hopping rates. We find the simple hopping rate $\gamma_{1\to 2}(t) = |d_{12}(t)|$ leads to accurate results for all of the test problems, see Fig. 4.3-4.4. Thus, since we do not utilize the electronic density matrix, we do not encounter the "over coherence" problem. The left (right) column of Figure 4.4 shows the results of the SCMC (time-dependent Schrödinger) calculation for Problem 3 with an initial wavefunction:

$$\Psi(t=0,x) = \begin{pmatrix} (\pi\sigma^2)^{-\frac{1}{4}} \times \exp\{\mathrm{i}kx - \frac{(x-x_0)^2}{2\sigma^2}\} \\ 0 \end{pmatrix}, \tag{4.24}$$

with initial position: $x_0 = -12$, momentum: $k = 10$, and width: $\sigma = \sqrt{200}/k$, starting on the lower eigenstate: $|\psi_1\rangle$. The snapshot is taken after the wavepacket has gone through the interaction region with a portion being transmitted on the lower adiabatic surface (bottom), or reflected on either the lower (middle) or upper (top) surface. The SCMC wavepackets have the same momentum, p, and positions, x, as the exact solution, indicating that our semi-classical dynamics, *i.e.* assumption of conservation of energy and Newtonian equations of motion, are reasonable. The transmitted wavepacket (bottom) calculated by SCMC shows significantly less broadening than the exact result. This is due to our "free" gaussian approximation, which ignores the increase in broadening due to the negative second derivative in the energy of the lower surface from $x = -5 \to 0$. In principle, this is simple to account for, [150] however calculation of the second derivative of the PES would be prohibitively expensive in a many-dimensional problem.

4.4.1 Role of Phases

While the SCMC method does a good job of reproducing the exact result, including when FSSH and Ehrenfest methods fail, it does so at an increased cost in trajectories. In order to determine the areas where SCMC is most applicable, we seek to understand how the convergence rate is

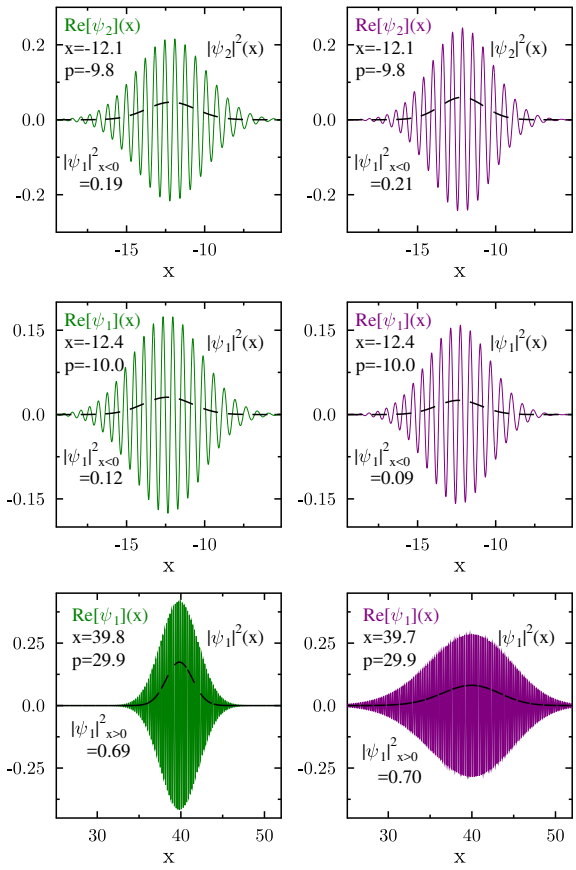

Figure 4.4: Scattered wavepackets problem 3 at $t = 4059$. Left column - SCMC method using 25000 trajectories. Right column - TD Schrödinger equation. Top (Center) - Reflected wavepacket on upper (lower) electronic eigenstate. Bottom- Transmitted wavepacket on lower electronic eigenstate. Colored Solid - Wavefunction. Black Dashed- Probability Density.

affected by different models and parameters. First, we look at the simple single level crossing, Problem 1. Figure 4.5 (Fig. 4.5-Inset) shows the relative error, δ_{rel}, in the calculated probabilities of transmission on the upper (lower) surfaces, TU (TL), as a function of the total number of trajectories, N. For all momentums and both probabilities, the convergence obeys an approximate power law of the form $\delta_{\text{Rel}} = \frac{a}{\sqrt{N}} + b$ (see line fits). This $\mathcal{O}(\frac{1}{\sqrt{N}})$ dependence of the error is standard to Monte-Carlo methods. For TU, we see faster convergence with increasing initial momentum.

This k dependence can be understood by looking at the phase in Eq. (4.22). Assuming a one dimensional system with two electronic states, we can calculate the phase for a trajectory which

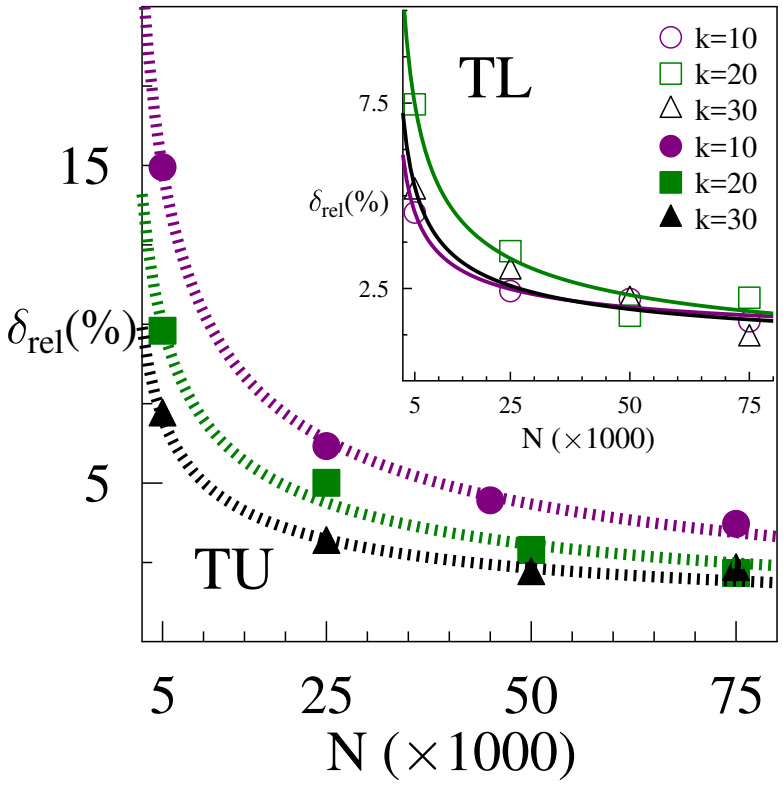

Figure 4.5: Average relative error percentage (δ_{Rel}) of SCMC calculation, without normalization, for Problem 1 as a function of the number of trajectories (N) for $k = 10$, 20, and 30. 20 calculations per data point. Filled (Empty) Markers - Transmission probability on the upper (lower) surface. Solid (Dashed) lines are respective fits to the data of the form $\delta_{\text{rel}} = \frac{a}{\sqrt{N}} + b$

begins on the lower surface and hops once:

$$F_1(t_f, t_1) = P_2(t_f)\left(\int_0^{t_1} dt \frac{P_1(t)}{M} + \int_{t_1}^{t_f} dt \frac{P_2(t)}{M} + x_0\right) + \int_0^{t_1} dt\left(\frac{P_1(t)^2}{2M} - E_1(t)\right) + \int_{t_1}^{t_f} dt\left(\frac{P_2(t)^2}{2M} - E_2(t)\right). \tag{4.25}$$

Since all trajectories have the same final and initial times we can subtract off any term which doesn't depend on the time or position of the hop. Additionally, if we assume that the initial momentum, k, is large enough that we do not have any reflection, and t_f is large enough that $P_2(t_f)$ is a constant, we can rewrite Eq. (4.25) as a relative phase that depends on the position of the hop:

$$\tilde{F}_1(x_1) = P_{2f} \int_{x_0}^{x_1} dx\left(1 - \frac{P_2(x)}{P_1(x)}\right) + \int_{x_0}^{x_1} dx\left(P_1(x) - \frac{P_2(x)^2}{P_1(x)}\right). \tag{4.26}$$

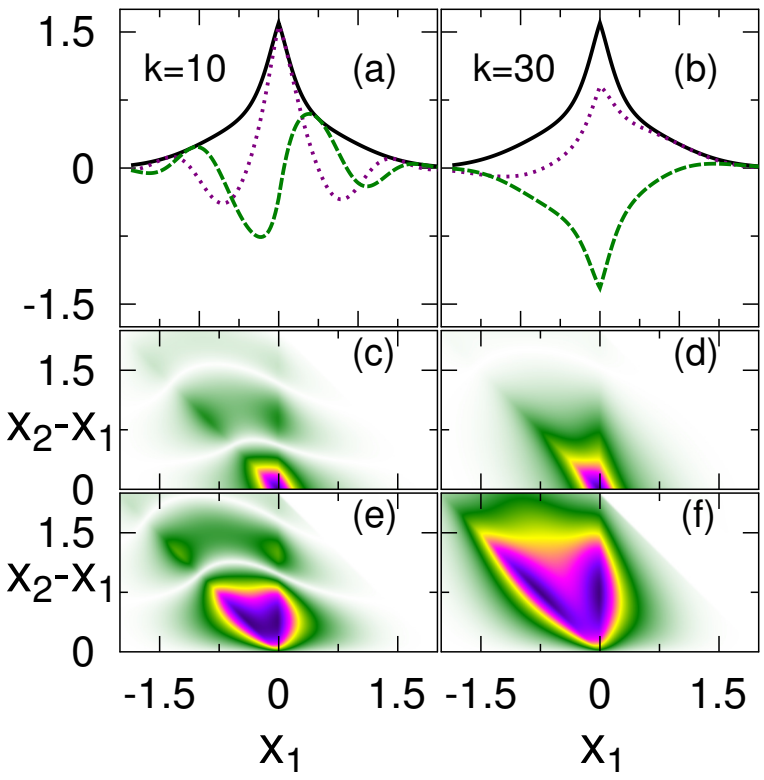

Figure 4.6: Problem 1 - Relative Phases, for single (a,b), Eq. (4.26), and double (c-f), Eq. (4.27), hop trajectories for k=10 (left) and k=30 (right). (a,b) Black solid - $|d_{12}(x)|$, Purple dotted - $d_{12}(x) \times \mathrm{Re}(\tilde{F}_1(x))$, Green dashed - $d_{12}(x) \times \mathrm{Im}(\tilde{F}_1(x))$. (c,d) Color map of $|d_{12}(x_1)d_{21}(x_2) \times \mathrm{Re}(\tilde{F}_2(x_1,x_2))|$. (e,f) Color map of $|d_{12}(x_1)d_{21}(x_2) \times \mathrm{Im}(\tilde{F}_2(x_1,x_2))|$. $\int \mathrm{d}x\, |d_{12}(x)| \simeq 1.57$.

With the same considerations we can write the relative phase for a trajectory with two hops:

$$\tilde{F}_2(x_1,x_2) = P_{1f} \int_{x_1}^{x_2} dx \left(1 - \frac{P_1(x)}{P_2(x)}\right) + \int_{x_1}^{x_2} dx \left(P_2(x) - \frac{P_1(x)^2}{P_2(x)}\right) . \tag{4.27}$$

In Figure 4.6 we can see that the number of oscillations, which must be sampled, is reduced in the one (a,b) and two (c-f) hop integrals when we go from the low momentum, $k = 10$, to the high momentum $k = 30$. Indeed for integrals of all numbers of hops the number of oscillations will decrease with an increasing momentum. The "smoother" integrands associated with higher momentum are easier to sample via Monte Carlo methods. For the TL in Figure 4.5, the effect competes with constant error sources, due to, *e.g*, the free gaussian approximation, which appears as an increasing relative error with decreasing average probability (probability of TL decreases with

increase k). This leads to the non-monotonic k dependence.

When going from a single (Problem 1) to double (Problem 2) crossing systems the integrated area of $|d_{12}(x)|$ increases from 1.57 to 2.60. The number of trajectories required to sample an integral with m hops will scale with $\int \mathrm{d}x\,|d_{12}(x)|$ as:

$$\frac{1}{m!}\left(\int \mathrm{d}x\,|d_{12}(x)|\right)^m. \tag{4.28}$$

However, integrals with more hops, generally, will contribute less to the total wavefunction. Additionally, oscillations due to the phases, Eq. (4.26, 4.27), increase for Problem 2 (see Fig. 4.7). These two, not independent, effects result in a much slower convergence rate for Problem 2 as compared to Problem 1 or 3. It was shown in Ref. [58] that ~ 3 times the number of trajectories are required to obtain similar precision for Problem 2 as for Problems 1 and 3.

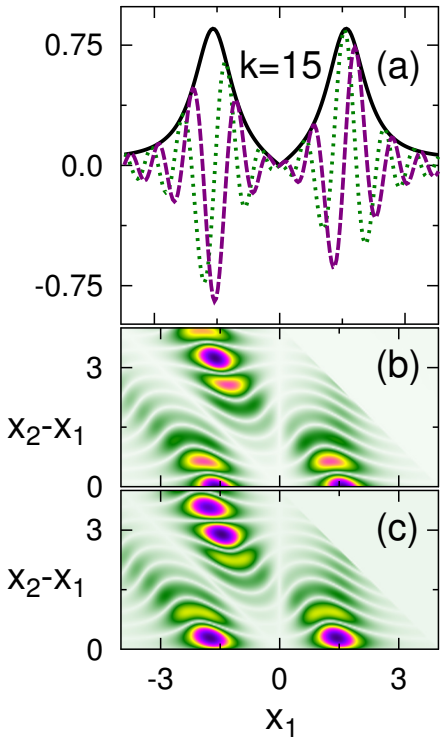

Figure 4.7: Problem 2 - Relative Phases, for single (a), Eq. (4.26), and double (b,c), Eq. (4.27), hop trajectories for $k = 15$. (a) Black solid - $|d_{12}(x)|$, Green dotted - $d_{12}(x) \times \mathrm{Re}(\tilde{F}_1(x))$, Purple dashed - $d_{12}(x) \times \mathrm{Im}(\tilde{F}_1(x))$. (b) Color map of $|d_{12}(x_1)d_{21}(x_2) \times \mathrm{Re}(\tilde{F}_2(x_1, x_2))|$. (c) Color map of $|d_{12}(x_1)d_{21}(x_2) \times \mathrm{Im}(\tilde{F}_2(x_1, x_2))|$. $\int \mathrm{d}x\,|d_{12}(x)| \simeq 2.60$.

4.4.2 Choice of hopping rate

In principle, the hopping rate, $\gamma_{i\to j}$, is arbitrary. It is simply the choice of a probability distribution for sampling the integral, Eq. (4.5). A better probability distribution leads to less samples being required to accurately calculate the correct result. The closer the probability distribution is to the absolute value of the normalized integrand, the better the sampling. If we knew the normalization factor for each integrand I_i^m, then we would not need to run simulations. Even if we could make a good estimate of these normalization factors, we would have to run separate sets of trajectories, with different hopping rates, to sample different outcomes. Additionally, it is not clear, in general, how to include the complex phases into a probability distribution, and it is difficult to know the phases in Eq. (4.22) *a priori*. However, by choosing $\gamma_{i\to j}(t) = |\mathbf{d}_{ij}(t)|$ we can at least include the factor $D(\mathbf{t})$ into the probability distribution. $D(\mathbf{t})$ provides bounds and amplitude to the integrands in Eq. (4.5). While there are methods to improve sampling of complex valued integrands, *e.g.* stationary phase approximation, [151, 152] they emphasize sampling in the same region as $D(\mathbf{t})$, *i.e.* regions with small ΔE between PES. This leads to minimal or no improvement. Investigating other hopping rate choices, which would effectively include the effects from the phases, is an ongoing project.

One choice which may come to the readers mind, is the fewest switches hopping rate from Tully [52]:

$$\gamma_{i\to j}^{\mathrm{FS}}(t) = \begin{cases} 2\,\mathrm{Im}\{a_{ji}(t)V_{ji}\} - 2\,\mathrm{Re}\left\{\frac{a_{ji}(t)\mathbf{d}_{ji}}{a_{ii}(t)}\right\} & \\ 0 & \text{if the value is smaller than 0} \end{cases} \tag{4.29}$$

with

$$\frac{\partial}{\partial t}a_{ji}(t) = \sum_k \left(\mathrm{i}(a_{jk}(t)V_{ki} - V_{jk}a_{ki}(t)) + a_{jk}(t)\mathbf{d}_{ki} - \mathbf{d}_{jk}a_{ki}(t)\right). \tag{4.30}$$

Here a is the electronic density matrix. Figure 4.8 shows the relative error of the SCMC calculation for the different hopping rates, $\gamma_{i\to j}^{\mathrm{FS}}$ and $\mathbf{d}_{ji}$. In both the case where FSSH method works (Problem 1- Fig. 4.8-a), and when the FSSH method fails (Problem 2- Fig. 4.8-b), the error is extreme (see Fig. 4.8-b inset) if the results are unnormalized, and still high even when normalized (Fig. 4.8). There is a problem with using $\gamma_{i\to j}^{\mathrm{FS}}$. After one surface hop, the returning hop is frustrated, for a

time, due to the resulting negative sign in $\gamma_{i\to j}^{\mathrm{FS}}$. This leads to regions of vanishing hop probability in trajectories with more than one hop. Even without the phases this would, in principle, lead to erroneous results.

Additionally, when the integrals are unevenly sampled without consideration of the phases, as they are when using $\gamma_{i\to j}^{\mathrm{FS}}$, the sensitive constructive/destructive behavior of the phases leads to the large error. We believe there will always be situations where any *ad hoc* hopping rate will lead to poor convergence due to the imperfect accounting of the phases. The difference in the result before (Fig. 4.5 and inset of 4.8-b) and after (Fig 4.8-a/b) normalization tells us how well the method is working. If the change is minimal (compare Figs. 4.5 and 4.8-a), the SCMC procedure is working well for the system. If the change is large (compare Fig. 4.8-b body and inset), the SCMC procedure is failing.

4.5 Conclusion

The semi-classical Monte-Carlo method provides an approach, which is not *ad hoc*, for calculating nonadiabatic dynamics in extended molecular systems. It is based on an expansion of the full molecular wavefunction into partial wave functions corresponding to the number of transitions between electronic states. The procedure involves standard surface hopping dynamics with an additional post-processing step (calculation of the wave functions from collected data). While in the surface hopping method the hopping probability controls all of the dynamics; in SCMC it is primarily interference between trajectories with different (or similar) phases that determines the final result. For this reason, the SCMC method does not suffer from the same "over coherence" problem as the FSSH approach.

Some notes on the applicability of this method: (1) While the phases lead to difficulty in sampling for small momentum, for higher momentums the sampling becomes easier. (2) Additionally, we believe that convergence rate does not increase with increased number of system coordinates. [58] (3) Increasing the number of crossing regions increases the number of trajectories required for sampling, see Eq. (4.28), due to an increase in the area of nonadiabatic coupling and an increase in the number of oscillations due to the phases. (4) While it has been shown that, in some systems, FSSH approach requires complete coupling, *i.e* the quantum mechanical electronic dynamics requires calculation of NACV for all combinations of states ($\frac{1}{2}N_s[N_s-1]$ NACV calculations), [153]

the SCMC method with a hopping rate of $|d_{i,j}(t)|$ requires only partial coupling ($N_s - 1$ NACV calculations). When N_s becomes large the calculation of NACV's can become the bottleneck of the calculation. Thus improved scaling in N_s may make up for the additional trajectories needed for sampling the wavefunction. (5) Alternatively, one could utilize this method only in the vicinity of non-negligible NAC, in essence attacking the multi-crossing problem one crossing at a time. We leave development of such a procedure, with comparison to full SCMC and TD-Schrödinger calculations, as well as continued efforts in improving convergence rates, and application of the SCMC approach to realistic systems for future work.

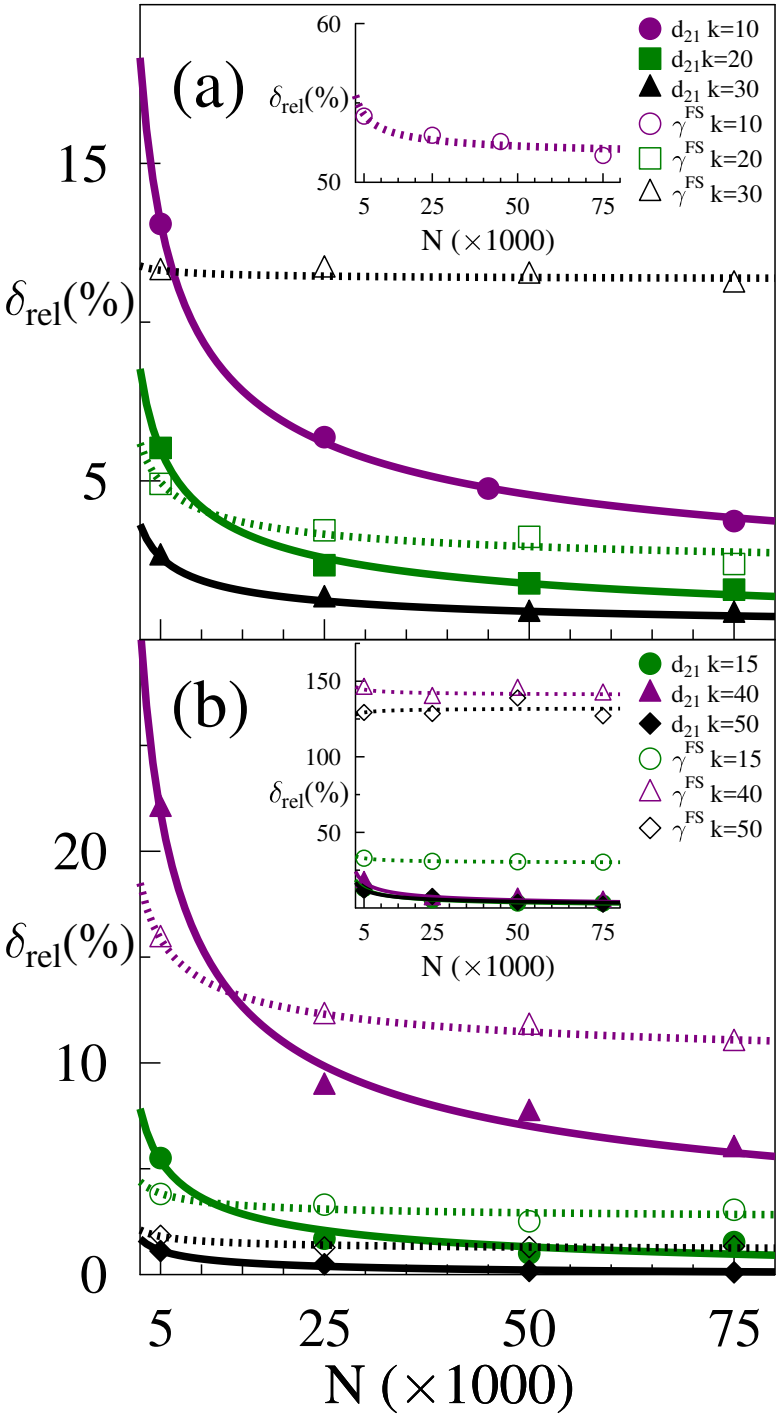

Figure 4.8: Averaged relative error percentage (δ_{Rel}) of SCMC calculation as a function of the number of trajectories (N). (a) Problem 1, Transmission probability on the upper surface with normalization for $k = 10$, 20, and 30 (b) Problem 2, Transmission probability on the lower surface with normalization for $k = 15$, 30, and 50. (b-inset) Averaged relative error percentage of unnormalized results. Filled markers are for $\gamma_{1\to2} = |d_{21}|$. Empty markers are for $\gamma_{1\to2} = \gamma^{FS}_{1\to2}$. Solid (Dashed) lines are respective fits to the data of the form $\delta_{\text{rel}} = \frac{a}{\sqrt{N}} + b$

APPENDIX A SCALAR PRODUCTS, SYMPLECTIC FORMS, AND SYMPLECTIC GROUPS

In this appendix we present certain notation, definitions, and properties of *symplectic* groups, together with some derivations. One of the reasons we wrote this appendix is that there is an ambiguity in the notation used by several various sources.

The symplectic group $\mathrm{Sp}(2m;\mathbb{F})$, with $\mathbb{F}$ being a field, is the group of invertible linear operators acting in the $2m$-dimensional vector space $V \cong \mathbb{F}^{2m}$, equipped with a symplectic form ω, preserved by the aforementioned linear operators. Usually the cases $\mathbb{F} = \mathbb{R}$ or $\mathbb{F} = \mathbb{C}$ are considered. We will focus on the case $\mathrm{Sp}(2m;\mathbb{C})$ that is relevant for our applications. A natural question arises: why and in what way are symplectic groups closely related to time-reversal symmetry in quantum systems? The answer can be formulated as follows. By definition, a symplectic form is just a non-degenerate bilinear form in a (complex) vector space V, which is skew-symmetric, i.e., it satisfies the property $\omega(u \otimes v) = -\omega(v \otimes u)$, for $u, v \in V$.

We further observe that a Hermitian scalar product, which is always a part of a game for a quantum system, establishes a one-to-one correspondence between antilinear maps and bilinear forms (not necessarily skew-symmetric) that is uniquely determined by the condition

$$\omega(u \otimes v) = (u, j(v)) \quad \forall u, v \in V. \tag{A.1}$$

We will say that ω is compatible with the scalar product if the corresponding antilinear map j preserves the scalar product in the sense of Eq. (3.4). In this case we have

$$\omega(u \otimes v) = (u, j(v)) = (j(u), j^2(v))^* = (j^2(v), j(u)) = \omega(j^2(v) \otimes u), \tag{A.2}$$

which implies that in our compatible case the skew-symmetry of ω is equivalent to $j^2 = -1$. Therefore, there is a one-to-one correspondence between the symplectic forms compatible with the scalar product and $j^2 = -1$ real structures that preserve the scalar product. Stated differently, and in more physics terms, we are considering a situation when time-reversal symmetry respects the scalar product, the latter being the most important structure in quantum mechanics.

In view of the above we can define a symplectic group $\mathrm{Sp}(m)$, also often referred to as a *compact symplectic* group (since it is in fact compact), in the following way. Let V be a complex vector space of even dimension $2m$, equipped with a Hermitian scalar product and a symplectic form, compatible with the scalar product (or equivalently a $j^2 = -1$ real structure that preserves the scalar product). The group $\mathrm{Sp}(m)$ then consists of all linear operators A acting in V that are unitary and preserve the symplectic form (or, equivalently, commute with the corresponding real structure):

$$(A(u), A(v)) = (u, v), \quad \omega(A(u) \otimes A(v)) = \omega(u \otimes v), \quad jA = Aj. \tag{A.3}$$

Stated in more physics terms operators that belong to $\mathrm{Sp}(m)$ represent unitary operators (i.e., a quantum version of variable changes) that respect time-reversal symmetry.

At this point we would like to note that sometimes $\mathrm{Sp}(m)$ are denoted $\mathrm{USp}(2m)$ to emphasize that it is isomorphic $\mathrm{Sp}(m) \cong \mathrm{U}(2m) \cap \mathrm{Sp}(2m; \mathbb{C})$ of unitary symplectic matrices with complex entries. This definition is somewhat sloppy due to the following reason. The notion of unitarity can exist only if a Hermitian scalar product is defined. The symplectic group can be properly defined only if the symplectic form ω is compatible with the scalar product in the sense, explained above. The compatibility condition is also often dropped out of the definition of the $\mathrm{Sp}(m)$ groups, since they are usually defined in terms of matrices, using an orthonormal basis set in which the symplectic form has a standard (canonical) form

$$\omega = \begin{pmatrix} 0 & I \\ -I & 0 \end{pmatrix}, \tag{A.4}$$

with I being the unit $m \times m$ matrix, and it can be straightforwardly verified that the canonical symplectic form [Eq. (A.4)] is compatible with the canonical scalar product (associated with an orthonormal basis set).

There is another standard, and also very convenient model for the $\mathrm{Sp}(m)$ group, referred to as the unitary quaternionic group $U(m; \mathbb{H})$ that consists of all invertible $m \times m$ matrices with quaternionic entries that preserve the standard Hermitian scalar product

$$\langle \boldsymbol{u} | \boldsymbol{v} \rangle = \sum_{a=1}^{m} u_a v_a^* \in \mathbb{H}. \tag{A.5}$$

The isomorphism $\mathrm{Sp}(m) \cong U(m;\mathbb{H})$ can be established by using *real orthonormal* basis sets, i.e., orthonormal basis sets of a form $(e_1, \ldots, e_m, j(e_1), \ldots, j(e_m))$. Such basis sets can be actually built by applying an obvious extension of the Gram-Schmidt orthogonalization procedure that on each step builds a new pair $(e_a, j(e_a))$ of the basis set elements, orthogonal to the previously chosen ones. One then can choose $(e_1, \ldots, e_m)$ as the basis set, forming the m-dimensional quaternionic space $\mathbb{H}^m$, to represent the linear operators acting in V that commute with the real structure j using $m \times m$ quaternionic matrices and show directly that an operator A preserves a Hermitian scalar product in the $2m$-dimensional complex vector space V if and only if the corresponding $m \times m$ quaternionic matrix preserves the quaternionic scalar product, given by Eq. (A.5).

A quaternionic scalar product in a complex vector space V equipped with a Hermitian scalar product and a real structure that preserves the latter can be introduced in an invariant way

$$\langle u, v\rangle = (u, v) + (u, J(v))j, \quad \langle u, v\rangle \in \mathbb{H}; \tag{A.6}$$

here for the sake of clearness of the derivations, presented below we do not overload the notation for j, by still denoting with j the element of the quaternion algebra $j \in \mathbb{H}$, while using J for the real structure anti-linear map $J : V \to V$. The introduced scalar product has the following important properties. First, and though obvious, still very important: the quaternionic scalar product $\langle u, v\rangle$ provides two Hermitian scalar products (u, v) and $(u, J(v))$. Second, for an invertible operator A the property of preserving the quaternionic scalar product is equivalent to preserving the Hermitian scalar product and the real structure, the latter meaning $[J, A] = 0$. This can be demonstrated as follows. The preservation of the quaternionic scalar product means

$$\begin{aligned} (A(u), A(v)) &= (u, v), \\ (A(u), JA(v)) &= (u, J(v)), \quad \forall u, v \in V. \end{aligned} \tag{A.7}$$

The first relation means preservation of the Hermitian scalar product, whereas applying the first relation to the r.h.s. of the second one we obtain

$$(A(u), JA(v)) = ((A(u), AJ(v)), \quad \forall u, v \in V, \tag{A.8}$$

which is equivalent to $AJ = JA$. Finally the following bilinear properties are in place

$$\langle \lambda u, v\rangle = \lambda\langle u, v\rangle, \quad \langle u, \lambda v\rangle = \langle u, v\rangle\lambda^*, \tag{A.9}$$

for $u, v \in V$ and $\lambda \in \mathbb{H}$. To verify the properties, presented in Eq. (A.9), it is enough to verify them for $\lambda \in \mathbb{C} \subset \mathbb{H}$ and for $\lambda = j$. For $\lambda \in \mathbb{C}$ we have

$$\begin{aligned}
\langle \lambda u, v\rangle &= (\lambda u, v) + (\lambda u, J(v))j \\
&= \lambda(u, v) + \lambda(u, J(v))j = \lambda\langle u, v\rangle, \\
\langle u, \lambda v\rangle &= (u, \lambda v) + (u, \lambda^* J(v))j \\
&= \lambda^*(u, v) + \lambda(u, J(v))j \\
&= (u, v)\lambda^* + (u, J(v))j\lambda^* = \langle u, v\rangle\lambda^*,
\end{aligned} \tag{A.10}$$

whereas for $\lambda = j$

$$\begin{aligned}
\langle ju, v\rangle &= \langle J(u), v\rangle = (J(u), v) + (J(u), J(v))j \\
&= -(u, J(v))^* + (u, v)^* j \\
&= j^2(u, J(v))^* + (u, v)^* j \\
&= j(u, J(v))j + j(u, v) = j\langle u, v\rangle,
\end{aligned} \tag{A.11}$$

$$\begin{aligned}
\langle u, jv\rangle &= \langle u, J(v)\rangle = (u, J(v)) + (u, J^2(v))j \\
&= -(u, v)j + (u, J(v)) \\
&= -(u, v)j - (u, J(v))j^2 \\
&= -\langle u, v\rangle j = \langle u, v\rangle j^*.
\end{aligned} \tag{A.12}$$

The bilinear properties [Eq. (A.9)] imply that if the vectors $u, v \in V$ are decomposed using an orthonormal, with respect to the quaternionic scalar product, quaternionic basis set, and quaternionic coefficients $u_a, v_a \in \mathbb{H}$

$$u = \sum_{a=1}^{m} u_a e_a, \quad v = \sum_{a=1}^{m} v_a e_a, \quad \langle e_a, e_b\rangle = \delta_{ab}, \tag{A.13}$$

so that the quaternionic scalar product has a form of Eq. (A.5).

We further describe the notion of a linear operator H being quaternionically Hermitian, which naturally reads

$$\langle H(u)|v\rangle = \langle u|H(v)\rangle \quad \forall u, v \in V, \tag{A.14}$$

or explicitly

$$(H(u), v) + (H(u), J(v))j = (u, H(v)) + (u, J(H(v)))j, \tag{A.15}$$

or recasting further in components

$$\begin{aligned} (H(u), v) &= (u, H(v)), \\ (H(u), J(v)) &= (u, J(H(v))). \end{aligned} \tag{A.16}$$

The first equality in Eq. (A.16) simply means that H is Hermitian; applying it to the second one we arrive at

$$(u, HJ(v)) = (u, J(H(v))), \quad \forall u, v \in V, \tag{A.17}$$

which implies that $[J, H] = 0$. Summarizing, quaternionically Hermitian operators are exactly Hermitian operators that commute with J, i.e., preserve the real structure.

Since quaternions do not commute we need to describe carefully how to represent linear operators in the matrix form. Consider a linear operator H that preserves the real structure, hereafter referred to as a quaternionic operator that has the property $H(\lambda u) = \lambda H(u)$ for $\lambda \in \mathbb{H}$. For a quaternionic orthonormal basis $(e_1, \ldots, e_m)$ we can define the matrix elements with the condition

$$H(e_b) = \sum_{b=1}^{m} H_{ab} e_a, \quad H_{ab} \in \mathbb{H}, \tag{A.18}$$

so that

$$\begin{aligned} H(u) &= H\left(\sum_b u_b e_b\right) = \sum_{ab} u_b H_{ab} e_a, \\ H(u)_a &= \sum_b u_b H_{ab}, \quad u_a, u_b \in \mathbb{H}, \end{aligned} \tag{A.19}$$

which means that we can use standard matrix representation with the order of multiplication of the matrix elements with the vector components, prescribed by Eq. (A.19).

We conclude the discussion of the quaternionic scalar product by recalling a statement that orthonormal in the quaternionic sense [Eq. (A.13)] basis sets are in one-to-one correspondence with orthonormal real basis sets, introduced earlier: given a quaternionic orthonormal basis set $(e_1, \ldots, e_m)$ we can build a real orthonormal basis set $(e_1, \ldots, e_m, J(e_1), \ldots, J(e_m))$. Note that all basis set elements $e_1, \ldots, e_m, J(e_1), \ldots, J(e_m) \in V$.

It would be instructive to note that the group $\mathrm{Sp}(m)$ can be viewed as the compact real counterpart of $\mathrm{Sp}(2m; \mathbb{C})$ in the following sense. The latter group is complex analytical (and naturally, being non-abelian, is non-compact), i.e., as a space it is a complex-analytical manifold. The map $\bar{J} : \mathrm{Sp}(2m; \mathbb{C}) \to \mathrm{Sp}(2m; \mathbb{C})$, defined by $\bar{J}(A) = A^\dagger$ is a real structure, since it is anti-holomorphic, i.e., transforms holomorphic functions to anti-holomorphic, preserves the group action, and satisfies $\bar{J}^2 = \mathrm{id}$. The group $\mathrm{Sp}(m) \subset \mathrm{Sp}(2m; \mathbb{C})$ can be considered as the subspace of the real points of $\mathrm{Sp}(2m; \mathbb{C})$, i.e., the fixed points of $\bar{J}$. An elementary computation, based on identification of the Lie algebras, associated with the above Lie groups shows that $\mathrm{Sp}(2m; \mathbb{C})$, has complex dimension $m(2m + 1)$, whereas $\mathrm{Sp}(m)$ has real dimension $m(2m + 1)$, the latter in accordance with $\mathrm{Sp}(m)$ being the real counterpart of $\mathrm{Sp}(2m; \mathbb{C})$.

APPENDIX B ORTHOGONAL GROUPS, SPINORS, AND GAMMA-MATRICES

In this appendix we present some simple basic facts about spinors, necessary to formulate nice interpretation of the conical intersections. A nice and concise overview of the spinors and gamma-matrices for arbitrary dimension can be found in [154].

The orthogonal groups $\mathrm{SO}(n)$ with $n \geq 3$ are known to be connected, but not simply connected, the latter meaning that they have a not-contractible cycle. The group of equivalence classes (with respect to homotopy) of one-dimensional closed curves with a given origin in a space X is called its fundamental group, and denoted $\pi_1(X)$. As known $\pi_1(\mathrm{SO}(n)) = \mathbb{Z}_2$ for $n \geq 3$. For any topological group G there is a uniquely defined topological group $\tilde{G}$, referred to as the universal cover of G, that covers G, i.e., $\tilde{G} \to G$, with $\pi_1(\tilde{G}) = 0$ and the fiber, i.e., the inverse image of any point in G with respect to the cover map, being isomorphic to $\pi_1(G)$. The universal (double) cover of $\mathrm{SO}(n)$ is called $\mathrm{Spin}(n)$, so that we have $\mathrm{Spin}(n) \to \mathrm{SO}(n)$. A group $\mathrm{Spin}(n)$ has a canonical unitary representation, referred to as the *spinor representation* and a set of γ-matrices $(\gamma_a | a = 1, \ldots, n)$, acting in the space of the spinor representation, that satisfy the Clifford algebra relations

$$\gamma_a \gamma_b + \gamma_b \gamma_a = 2\delta_{ab}. \tag{B.1}$$

Under the action of $\mathrm{Spin}(n)$ the gamma-matrices transform linearly and preserve the natural (real) scalar product, so that elements of $\mathrm{Spin}(n)$ are represented by orthogonal operators acting in the n-dimensional space $\mathbb{R}^n$, spanned on the γ-matrices, which defines the cover $\mathrm{Spin}(n) \to \mathrm{SO}(n)$.

There is a well-known explicit construction for γ-matrices and $\mathrm{Spin}(n)$, the spinor representation, which we do not give here, but rather present some basic facts. The group $\mathrm{Spin}(n)$ for $n = 2m$ and $n = (2m + 1)$ acts in the same vector space of (complex) dimension 2^m, with the γ-matrices for $n = (2m + 1)$ obtained by extending the set of γ-matrices for $n = 2m$ with the product $\prod_{a=1}^{2m} \gamma_a$. There are the following identifications $\mathrm{Spin}(3) \cong \mathrm{SU}(2) \cong \mathrm{Sp}(1)$, with the well-known cover $\mathrm{SU}(2) \to \mathrm{SO}(3)$, and γ-matrices represented by the Pauli matrices $\boldsymbol{\sigma}$. For $n = 4$ we have $\mathrm{Spin}(4) \cong \mathrm{SU}(2) \times \mathrm{SU}(2)$, with the γ-matrices represented by the Dirac matrices. Finally

Spin(5) $\cong$ Sp(2), with the action of the latter in $V \cong \mathbb{C}^4$, equipped with a scalar product and a real structure j that preserves the latter, and the γ-matrices represented by Hermitian operators that commute with j, as described in some detail in appendix A.

APPENDIX C DIFFERENTIAL FORMS, WEDGE PRODUCT-S, STOKES THEOREM, AND CHERN CLASSES

In this appendix we present some basic facts and concepts, associated with differential forms, including wedge products and multidimensional Stokes theorem, as well as representation of Chern classes using differential forms, with applications to rationalizing Eq. (3.22) and deriving Eq. (3.23), starting with the former. Further details on differential forms, Stokes theorem, vector bundles and connections can be found in [155]. The original construction of Chern classes, developed by Chern, which uses differential forms, is adopted in Chapter 3 and briefly described in this appendix, can be found in [156].

A differential form A (of rank k) on space/manifold X is a smooth function on X, whose value at any point $x \in X$ is a skew-symmetric poly-linear (k-linear) form on the vector space of tangent to X vectors at x. Given a system of local coordinates it can be equivalently viewed as an expression

$$A = A_{j_1 j_2 \ldots j_k}(x) dx^{j_1} \wedge dx^{j_2} \wedge \ldots \wedge dx^{j_k}, \tag{C.1}$$

where the wedge product involved in Eq. (C.1) is simply a skew-symmetric product, which just means $dx^j \wedge dx^i = -dx^i \wedge dx^j$. We reiterate that throughout Chapter 3 we use the Einstein summation convention. A wedge product of forms A and B with ranks k and l, respectively, is a differential form $A \wedge B$, naturally defined as

$$\begin{aligned} A \wedge B &= A_{i_1 \ldots i_k}(x) B_{j_1 \ldots j_l}(x) dx^{i_1} \ldots \wedge dx^{i_k} \\ &\wedge \quad dx^{j_1} \wedge \ldots \wedge dx^{j_l}, \end{aligned} \tag{C.2}$$

An exterior differential dA of A is a $(k+1)$-rank form, defined also in a very natural way

$$dA = \frac{\partial}{\partial x^j} A_{i_1 \ldots i_k}(x) dx^j \wedge dx^{i_1} \ldots \wedge dx^{i_k}, \tag{C.3}$$

with the following easily verifiable properties in place

$$\begin{aligned} A \wedge B &= (-1)^{kl} B \wedge A, \\ \mathrm{d}(A \wedge B) &= \mathrm{d}A \wedge B + (-1)^k A \wedge \mathrm{d}B\,, \\ \mathrm{d}^2 A &= \mathrm{d}(\mathrm{d}A) = 0. \end{aligned} \tag{C.4}$$

We note that the exterior differential operator can be defined in an invariant, i.e., coordinate-free way, so that in any local coordinate system it reproduces Eq. (C.3). It is done by defining it for functions, i.e., 0-rank differential forms, as $df = (\partial f/\partial x^j)dx^j$ and extending it to arbitrary rank by requiring the properties, given by Eq. (C.4) to be satisfied. Also note, that, due to skew-symmetric character, the maximal rank of a form is given by the space dimension.

If $f : X \to Y$ is a map of manifolds, and A is a form over Y, we can introduce a form f^*A over X, called the pull-back of A along f, in a very natural way, as

$$f^*A = A_{\alpha_1 \ldots \alpha_k}(f(x)) \frac{\partial f^{\alpha_1}(x)}{\partial x^{j_1}} \ldots \frac{\partial f^{\alpha_k}(x)}{\partial x^{j_k}} dx^{j_1} \wedge \ldots \wedge dx^{j_k}. \tag{C.5}$$

Viewing f as a coordinate transformation, Eq. (C.5) can be also interpreted as the transformation law for differential forms under coordinate transformations.

One of the reasons why differential forms are so useful is that they are designed to be integrated, and, as opposed to just functions, they do not require an integration measure. Indeed, a maximal rank form can be always represented as $A = A(x)dx^1 \wedge \ldots \wedge dx^n$, with $A(x)$ being a function. On the other hand, as it follows from Eq. (C.5), under coordinate change $A(x)$ transforms via the Jacobian $J(x) = \det(\partial f/\partial x)$ of the coordinate transformation. Therefore, one can define an integral of the aforementioned differential form as

$$\int_X A = \int_X A(x) dx^1 \ldots dx^n, \tag{C.6}$$

since the r.h.s. of Eq. (C.6) does not depend on the coordinate choice, as long as the coordinate transformation preserves orientation, i.e., $J(x) > 0$. A careful reader would notice that the given definition works locally; to make it global one can use a standard argument that involves a so-called

partition of unity. The bottom line is that the integral of a maximal rank differential form over a compact oriented manifold is well defined.

Most importantly, forms of lower rank can be also integrated over the cycles of the corresponding dimension. Defining a k-cycle as a map $f : M \to X$ of a compact oriented k-dimensional manifold to our space we define

$$A(f) = \int_f A = \int_M f^* A, \tag{C.7}$$

and also refer to $A(f)$ as the value of A at cycle f.

The (multidimensional) Stokes theorem claims that if M is a manifold of dimension m with boundary ∂M, obviously of dimension $m-1$, e.g., $(M, \partial M) = (D^m, S^{m-1})$, mapped to X, via $f : M \to X$ and A is a form of rank $m-1$ on X, then

$$\int_f dA = \int_{f|_{\partial M}} A, \tag{C.8}$$

where $f|_{\partial M}$ is the restriction of f to the boundary of M, and, in particular, for a manifold without boundary, referred to as just a manifold, i.e., f is an m-cycle, e.g., $M = S^m$, the r.h.s. of Eq. (C.8) turns to zero. The standard Stokes theorem is reproduced by setting $(M, \partial M) = (D^2, S^1)$, and $X = \mathbb{R}^3$.

A form A is called closed if $dA = 0$, it is called exact if $A = dB$ for some B; obviously due to $d^2 = 0$, any exact form is closed. We say that A is cohomologically equivalent to B if $(A-B)$ is exact. The set of equivalence (cohomology) classes $[A]$ of closed k-forms A over X forms a vector space, refereed to as the k-th de Rham cohomology of X and is denoted $H^k(X)$. Obviously $H^k(X) = 0$ for $k > n = \dim(X)$ For a compact manifold all cohomology spaces are finite-dimensional vector spaces. If X is connected $H^0(X) = \mathbb{R}$, and the cohomology classes are represented by constant functions. If X is also orientable $H^n(X) = \mathbb{R}$. The correspondence $H^n(X) \to \mathbb{R}$ is obtained by integrating an n-form A over the manifold X, with the result depending on its class $[A]$ only, due to the Stokes theorem (note that any form of maximal rank is closed).

Locally, a gauge field is represented by a 1-form $A = A_j dx^j$ that takes values in the space of $n \times n$ matrices, i.e., for any j, A_j is an $n \times n$ matrix with the entries A_j^{ab}, the latter could be real

or complex numbers. A gauge transformation, associated with a matrix function $g(x)$ has a form

$$\begin{aligned} A &\mapsto g^{-1}Ag + g^{-1}dg \\ A_j &\mapsto g^{-1}A_j g + g^{-1}\frac{\partial g}{\partial x^j} \end{aligned} \tag{C.9}$$

Usually the values of $g(x)$ are restricted to special orthogonal, unitary, or special unitary matrices so that $g(x) \in G$, with $G = \mathrm{SO}(n)$, $G = \mathrm{U}(n)$, and $G = \mathrm{SU}(n)$, respectively. In Chapter 3 only $G = \mathrm{U}(1)$ and $G = \mathrm{SU}(2)$ are involved. When the gauge transformations are restricted to the aforementioned subgroups of the linear groups, the values of A_j are restricted to the corresponding Lie algebras (the latter describing infinitesimal group transformations), represented by real antisymmetric, complex anti-hermitian, and complex anti-hermitian with zero trace matrices respectively. The global construction works as follows. If $U, V \subset X$ are any two intersecting neighborhoods with the gauge field represented by forms $A|_U$ and $A|_V$, then over the intersection $U \cap V$ they are allowed to be related via a gauge transformation,naturally represented by a matrix function $g_{UV} : U \cap V \to G$. Obviously, consistency conditions should be imposed, i.e., for any three intersecting neighborhoods $U, V, W \subset X$ we should have over the intersection $U \cap V \cap W$ the consistency relation $g_{UV}g_{VW} = g_{UW}$ to be satisfied. A set $\{A_U\}$ of forms connected over intersections $U \cap V$ via gauge transformations, defined by the connecting/gluing maps g_{UV}, the latter satisfying the aforementioned consistency conditions on all triple intersections $U \cap V \cap W$, will be referred to as a global gauge field. The connecting/glueing data represented by a family $\{g_{U_\alpha U_\beta} : U_\alpha \cap U_\beta \to G\}_{\alpha,\beta \in I}$, with $\bigcup_{\alpha \in I} U_\alpha = X$, that satisfy the consistency condition, define an object, called a vector fiber bundle, in the following sense. Consider a vector-"function" on X that is locally a function, with the local functions being glued together via the connection maps. More formally, let $\Psi = \{\Psi_\alpha : U_\alpha \to \mathcal{U}\}_{\alpha \in I}$ be a family of functions with the values in a vector space $\mathcal{U}$, equipped with a Hermitian scalar product, of dimension n, referred to as a fiber, and the rank of the bundle, respectively, so that, for any $\alpha, \beta \in I$, we have $\Psi_\alpha(x) = g_{\alpha\beta}(x)\Psi_\beta(x)$ over $U_\alpha \cap U_\beta$; here we used abbreviated notation $g_{\alpha\beta}$ for $g_{U_\alpha U_\beta}$. Then Ψ is called a global section of the vector bundle, associated with the gluing data.

A globally defined gauge field can be interpreted as an object that allows derivatives of global sections to be introduced. Indeed for Ψ_α we can define its "elongated", or in other words covariant,

derivative as a 1-form $\nabla\Psi_\alpha$ with the values in V, as

$$\begin{aligned}\nabla\Psi_\alpha &= d\Psi_\alpha + A_\alpha\Psi_\alpha = (\nabla_j\Psi_\alpha)dx^j \\ \nabla_j\Psi_\alpha &= \frac{\partial\Psi_\alpha}{\partial x^j} + A_{\alpha j}\Psi_\alpha.\end{aligned} \tag{C.10}$$

It is easy to see that the local definition of covariant derivatives [Eq. (C.10)] is consistent on all $U_\alpha \cap U_\beta$ due to the transformation law, determined by gauge transformations [Eq. (C.9)], so that the covariant derivative with respect to a gauge field is defined globally. Note that in the way the material is presented here we have a notion of a gauge field and associated with the latter vector bundle. In differential geometry it is usually formulated the other way around, one starts with a notion of a vector bundle and then considers connections in a given vector bundle; with the connection being a term in differential geometry for what a physicist would call a globally defined gauge field.

The curvature F of a gauge field A is defined locally as a matrix-valued 2-form, i.e., over U_α, we have

$$\begin{aligned}F_\alpha &= dA_\alpha + \frac{1}{2}[A_\alpha, \wedge A_\alpha] = F_{\alpha,ij}dx^i \wedge dx^j \\ F_{\alpha,ij} &= \frac{1}{2}\left(\frac{\partial A_{\alpha j}}{\partial x^i} - \frac{\partial A_{\alpha i}}{\partial x^j} + [A_i, A_j]\right),\end{aligned} \tag{C.11}$$

with the following gluing data on $U_\alpha \cap U_\beta$

$$F_\alpha(x) = g^{-1}_{\alpha\beta}(x)F_\beta(x)g_{\alpha\beta}(x), \tag{C.12}$$

so that the curvature can be interpreted as a 2-form with values in another vector bundle of rank n^2, and the fiber, represented by the vector space $\mathrm{End}(\mathcal{U})$ of linear operators acting in $\mathcal{U}$, known as the endomorphism bundle, associated with the original counterpart.

Chern classes c_k, with $k = 1, 2, \ldots$ are invariants of vector bundles over X with $c_k \in H^{2k}(X)$, so that each Chern class is a cohomology class. In Chapter 3, to minimize the algebraic topology involved, we will follow the original construction of Chern, i.e., use the de Rham cohomology, defined earlier in this appendix. We start with defining a Chern class $C_k(A)$, associated with a gauge field A as a a $2k$-differential form over X that depends on A. We further show that that $C_k(A)$ is closed, which allows us to introduce the corresponding de Rham cohomology class $[C_k(A)] \in H^{2k}(X)$,

making $[C_k(A)]$ an invariant of a gauge field. We next demonstrate that the cohomology class $[C_k(A)]$ does not depend on a particular choice of the gauge field, for given gluing data, or in other words, vector bundle, so that we can define $c_k = [C_k(A)]$ as invariants of the vector bundle, rather that a gauge field, and refer to them as Chern classes.

The original Chern construction, we have adopted here, is very simple, however, it has a disadvantage: it is hard to see the integer nature of Chern classes, the latter meaning that the integral of a Chern class c_k over any $2k$-cycle, defined by Eq. (C.7) (and which does not depend on a choice of a particular representative due to Stokes theorem), is an integer. Understanding the aforementioned integer nature requires bringing in the concept of a classifying space, which, for the case of n-dimensional complex vector bundles, we are considering here, is denoted $\mathrm{BU}(n)$. The classifying space is equipped with a preferred bundle over it, called the universal bundle, and any bundle over X may be pulled back from the universal counterpart along some map $f : X \to \mathrm{BU}(n)$, so that a Chern class c_k is pull-backs [in the sense of Eq. (C.5)] of some integer-valued basis class $\bar{c}_k \in H^{2k}(\mathrm{BU}(n))$, referred to as a Chern class of the universal bundle, or simply a universal Chern class, so that $\bar{c}_k$ generate the complete cohomology of the classifying space. The cohomology of the classifying space is well known due to existence of a very simple model $\mathrm{BU}(n) = \mathrm{colim}_{N\to} G(n; N + n; \mathbb{C})$, where $G(n; M; \mathbb{C})$ is a complex Grassmanian, whose points parameterize n-dimensional vector subspaces of $\mathbb{C}^M$. We will not provide any more details on this approach, referring an interested reader to an excellent textbook [130]. Instead, in this appendix, we will demonstrate the integer nature of c_1 and c_2 for the specific and relevant for us cases, considered in section 3.3 by presenting an explicit computation. We also note that in section 3.3 we allowed minor abuse of notation, considering the Chern classes as integer numbers, rather than cohomology classes. The exact proper meaning of Eqs. (3.20) and (3.23) is that their l.h.s. represent the Chern classes c_1 and c_2, evaluated at the fundamental classes/cycles of S^2 and S^4, represented by the identical maps id_{S^2} and id_{S^4}, respectively.

Explicit expressions for for the closed forms $C_k(A)$ that represent the Chern classes are known in a form of a generating function (that generates the classes for all k), with the gauge field entering the expressions via its curvature $F(A)$. Here we present the expressions for the first and second

classes, relevant for our applications

$$C_1(A) = \frac{1}{2\pi}\mathrm{Tr}(F) = \frac{1}{2\pi}\mathrm{Tr}(F_{ij})dx^i \wedge dx^j,$$
$$C_2(A) = \frac{1}{8\pi^2}\mathrm{Tr}(F \wedge F) = \frac{1}{8\pi^2}\mathrm{Tr}(F_{ij}F_{kl})dx^i \wedge dx^j \wedge dx^k \wedge dx^l. \tag{C.13}$$

Note that Eq. (C.13) represents a local definition, i.e., strictly speaking defines the forms $C_{k,\alpha}$ over U_α. However, due to the cyclic property of the trace, the connecting/gluing maps for $C_{k,\alpha}$ turn out to be identities, so that we in fact obtain the forms C_k defined globally over the whole space X.

Verification of the closed nature of C_k, i.e., checking the conditions $dC_k = 0$ for $k = 1, 2$, is a simple and straightforward exercise that involves the properties of the exterior differential operator [Eq. (C.4)], as well as the properties of the trace and commutator. To see independence of $[C_k(A)]$ on a particular choice of a gauge field A for the same bundle (gluing data), we note that if $A' = A + a$, then a gauge transformation for a does not have the second (sometimes referred to as inhomogeneous) term in the r.h.s. of Eq. (C.9), i.e., it transforms in the exactly same way as the curvature [Eq. (C.12)], i.e., a is a globally defined 1-form with values in the endomorphism bundle. It is another straightforward exercise, which uses the same properties as the previous one, to show

$$C_1(A + a) = C_1(A) + \frac{1}{2\pi}d(\mathrm{Tr}(a)),$$
$$C_2(A + a) = C_2(A) + \frac{1}{8\pi^2}d(\mathrm{Tr}(a \wedge F)) + \mathcal{O}(a^2), \tag{C.14}$$

meaning that $C_k(A + a)$ differs from $C_k(A)$ by an exact form, i.e., the cohomology class $[C_k(A)]$ does not depend on a specific choice of a representative, so that the Chern classes c_k, for $k = 1, 2$, are finally properly defined.

We are now in a position to rationalize Eq. (3.22) and derive Eq. (3.23) from Eq. (3.22), addressing first the second task. To that end we note that if we denote $U_\pm \subset S^4$ the contractible subsets of the sphere obtained by withdrawing the north and south poles that correspond to $n_z = \pm 1$, respectively, then Eq. (3.21) defines a map $g : U_+ \cap U_- \to \mathrm{SU}(2) \cong \mathrm{Sp}(1)$ that, being viewed as a gluing data, gives rise to an SU(2)-bundle over S^4, with the non-adiabatic terms $A_\pm$, defined over $U_\pm$, respectively, representing a globally defined gauge field A in the sense explained earlier in this appendix. Therefore the l.h.s. of Eq. (3.23) represents the (integer) value of the second Chern class c_2 on the fundamental class/cycle of S^4.

We further proceed with noting that any closed form over any contractible subspace, in particular $C_2(A_\pm)$, is exact. Another straightforward exercise shows that, for $A = A_\pm$,

$$\begin{aligned} C_2(A) &= \frac{1}{8\pi^2} dB, \\ B &= \mathrm{Tr}(A \wedge dA) + \frac{1}{3}\mathrm{Tr}(A \wedge [A, \wedge A]) \\ &= \mathrm{Tr}(A \wedge F) - \frac{1}{3}\mathrm{Tr}(A \wedge A \wedge A), \end{aligned} \tag{C.15}$$

and note that B is known in quantum field theory as the Chern-Simons 3-form. Splitting the integration region S^4 in Eq. (3.23) into the north and south hemispheres, followed by applying the Stokes theorem to both integrals we obtain

$$c_2 = \frac{1}{8\pi^2} \int_{S^3} \Delta B, \quad \Delta B = (B_+ - B_-)|_{S^3}, \tag{C.16}$$

with $B_\pm = B(A_\pm)$, and the minus sign in the definition of ΔB is due to opposite orientations of the hemispheres with respect to the equator S^3. Also, we again, with a minor abuse of notation, denoted with c_2 the value $c_2(\mathrm{id}_{S^4})$ of the second Chern class on the fundamental cycle of S^4. Finally upon substitution of

$$A_+ = g^{-1} A_- g + g^{-1} dg, \tag{C.17}$$

into the second equality in Eq. (C.16) we obtain after another straightforward computation

$$\begin{aligned} \int_{S^3} \Delta B &= \frac{1}{3} \int_{S^3} \mathrm{Tr}(g^{-1}dg)^3, \\ (g^{-1}dg)^3 &= g^{-1}dg \wedge g^{-1}dg \wedge g^{-1}dg, \end{aligned} \tag{C.18}$$

which completes the derivation.

We conclude this appendix with presenting a more rigorous argument in support of the statement that the degree $\deg g$ of a map $g : S^3 \to \mathrm{SU}(2)$ is given by Eq. (3.22). It uses a much more invariant definition of the degree of a map $f : S^n \to S^n$. We first recall that the pullback operation [see Eq. (C.5)], being applied to closed forms produces a linear map $f^* : H^n(S^n) \to H^n(S^n)$ in the de Rham cohomology. Since, as noted earlier, $H^n(S^n) = \mathbb{R}$, this linear map is determined by a

number, which is called deg f. Since there are integer-valued cohomology theories, e.g., singular or bordism, that stand behind the de Rham real-valued counterpart, the degree is integer valued. We further recognize that the integrand in the r.h.s. of Eq. (C.18) is a pullback $g^*\omega$ along g of a 3-form ω over SU(2), obtained using the same expression by replacing g with the identity map $\mathrm{id}_{\mathrm{SU}(2)}$ [for the sake of completeness we note that ω is a left-invariant form on SU(2)]. This implies that Eq. (C.18) provides an integral representation for the map degree, if the normalization constant is chosen in such a way so that in case $g = \mathrm{id}_{\mathrm{SU}(2)}$ the integral in the r.h.s. of Eq. (C.18) turns to 1. Therefore, choosing

$$g(n_0, \boldsymbol{\sigma}) = \sigma_0 + i\boldsymbol{n} \cdot \boldsymbol{\sigma}, \quad n_0^2 + \boldsymbol{n}^2 = 1, \tag{C.19}$$

and performing integration explicitly, e.g., by just using a spherical coordinate system on S^3, we confirm that Eq. (3.22) has the proper normalization constant.

APPENDIX D COMPUTATION DETAILS OF ACTION AND STABILITY MATRIX FORMULATION

For the classical quadratic action with harmonic potential of path $\boldsymbol{y}(t)$

$$S^{Q}(\boldsymbol{\xi};t,t_0)=\frac{1}{2}\int_{t_0}^{t}\mathrm{d}\tau\left(g_{jk}(\boldsymbol{y}(\tau))\frac{\mathrm{d}\xi^{j}(\tau)}{\mathrm{d}\tau}\frac{\mathrm{d}\xi^{k}(\tau)}{\mathrm{d}\tau}-K_{jk}(\boldsymbol{y}(\tau))\xi^{j}(\tau)\xi^{k}(\tau)\right), \tag{D.1}$$

where $\mathrm{d}/\mathrm{d}\tau$ is used instead of $\boldsymbol{\nabla}_{\tau}$ for simplicity. By definition, the position $\boldsymbol{\xi}$ and momentum $\boldsymbol{\eta}$ are functions of time t and satisfy

$$\boldsymbol{\xi}(t)\oplus\boldsymbol{\eta}(t)=\mathrm{M}(t,t_0)\boldsymbol{\xi}(t_0)\oplus\boldsymbol{\eta}(t_0), \tag{D.2}$$

where $\mathrm{M}(t,t_0)$ is the stability matrix and for $\mathbb{R}^2$ there are for polar coordinate

$$\mathrm{M_P}(t,t_0)=\begin{pmatrix}\frac{\partial r(t)}{\partial r(t_0)} & \frac{\partial r(t)}{\partial\theta(t_0)} & \frac{\partial r(t)}{\partial p_r(t_0)} & \frac{\partial r(t)}{\partial p_\theta(t_0)}\\ \frac{\partial\theta(t)}{\partial r(t_0)} & \frac{\partial\theta(t)}{\partial\theta(t_0)} & \frac{\partial\theta(t)}{\partial p_r(t_0)} & \frac{\partial\theta(t)}{\partial p_\theta(t_0)}\\ \frac{\partial p_r(t)}{\partial r(t_0)} & \frac{\partial p_r(t)}{\partial\theta(t_0)} & \frac{\partial p_r(t)}{\partial p_r(t_0)} & \frac{\partial p_r(t)}{\partial p_\theta(t_0)}\\ \frac{\partial p_\theta(t)}{\partial r(t_0)} & \frac{\partial p_\theta(t)}{\partial\theta(t_0)} & \frac{\partial p_\theta(t)}{\partial p_r(t_0)} & \frac{\partial p_\theta(t)}{\partial p_\theta(t_0)}\end{pmatrix}=\begin{pmatrix}1 & 0 & \frac{\partial r(t)}{\partial p_r(t_0)} & 0\\ 0 & 1 & 0 & \frac{\partial\theta(t)}{\partial p_\theta(t_0)}\\ 0 & 0 & 1 & 0\\ 0 & 0 & 0 & 1\end{pmatrix} \tag{D.3}$$

and for Cartesian coordinate

$$\begin{aligned}\mathrm{M_C}(t,t_0)&=\begin{pmatrix}\frac{\partial x(t)}{\partial x(t_0)} & \frac{\partial x(t)}{\partial y(t_0)} & \frac{\partial x(t)}{\partial p_x(t_0)} & \frac{\partial x(t)}{\partial p_y(t_0)}\\ \frac{\partial y(t)}{\partial x(t_0)} & \frac{\partial y(t)}{\partial y(t_0)} & \frac{\partial y(t)}{\partial p_x(t_0)} & \frac{\partial y(t)}{\partial p_y(t_0)}\\ \frac{\partial p_x(t)}{\partial x(t_0)} & \frac{\partial p_x(t)}{\partial y(t_0)} & \frac{\partial p_x(t)}{\partial p_x(t_0)} & \frac{\partial p_x(t)}{\partial p_y(t_0)}\\ \frac{\partial p_y(t)}{\partial x(t_0)} & \frac{\partial p_y(t)}{\partial y(t_0)} & \frac{\partial p_y(t)}{\partial p_x(t_0)} & \frac{\partial p_y(t)}{\partial p_y(t_0)}\end{pmatrix}\\ &=\begin{pmatrix}1 & 0 & \frac{\partial r(t)}{\partial p_r(t_0)} & 0\\ 0 & \frac{r(t)}{r(t_0)}-r(t)p_r(t_0)\frac{\partial\theta(t)}{\partial p_\theta(t_0)} & 0 & r(t_0)r(t)\frac{\partial\theta(t)}{\partial p_\theta(t_0)}\\ 0 & 0 & 1 & 0\\ 0 & \frac{p_r(t)}{r(t_0)}-p_r(t_0)p_r(t)\frac{\partial\theta(t)}{\partial p_\theta(t_0)}-\frac{p_r(t_0)}{r(t)} & 0 & \frac{r(t_0)}{r(t)}+r(t_0)p_r(t)\frac{\partial\theta(t)}{\partial p_\theta(t_0)}\end{pmatrix}.\end{aligned} \tag{D.4}$$

These two are connected by matrices U_{t_0} and U_t^{-1} as

$$\mathrm{M_C}(t,t_0) = \mathrm{U}_t^{-1}\mathrm{M_P}(t,t_0)\mathrm{U}_{t_0}, \tag{D.5}$$

where

$$\mathrm{U}_{t_0} = \begin{pmatrix} \frac{\partial r(t_0)}{\partial x(t_0)} & \frac{\partial r(t_0)}{\partial y(t_0)} & \frac{\partial r(t_0)}{\partial p_x(t_0)} & \frac{\partial r(t_0)}{\partial p_y(t_0)} \\ \frac{\partial \theta(t_0)}{\partial x(t_0)} & \frac{\partial \theta(t_0)}{\partial y(t_0)} & \frac{\partial \theta(t_0)}{\partial p_x(t_0)} & \frac{\partial \theta(t_0)}{\partial p_y(t_0)} \\ \frac{\partial p_r(t_0)}{\partial x(t_0)} & \frac{\partial p_r(t_0)}{\partial y(t_0)} & \frac{\partial p_r(t_0)}{\partial p_x(t_0)} & \frac{\partial p_r(t_0)}{\partial p_y(t_0)} \\ \frac{\partial p_\theta(t_0)}{\partial x(t_0)} & \frac{\partial p_\theta(t_0)}{\partial y(t_0)} & \frac{\partial p_\theta(t_0)}{\partial p_x(t_0)} & \frac{\partial p_\theta(t_0)}{\partial p_y(t_0)} \end{pmatrix} = \begin{pmatrix} 1 & 0 & 0 & 0 \\ 0 & \frac{1}{r(t_0)} & 0 & 0 \\ 0 & 0 & 1 & 0 \\ 0 & -p_r(t_0) & 0 & r(t_0) \end{pmatrix}, \tag{D.6}$$

and

$$\mathrm{U}_t^{-1} = \begin{pmatrix} \frac{\partial x(t)}{\partial r(t)} & \frac{\partial x(t)}{\partial \theta(t)} & \frac{\partial x(t)}{\partial p_r(t)} & \frac{\partial x(t)}{\partial p_\theta(t)} \\ \frac{\partial y(t)}{\partial r(t)} & \frac{\partial y(t)}{\partial \theta(t)} & \frac{\partial y(t)}{\partial p_r(t)} & \frac{\partial y(t)}{\partial p_\theta(t)} \\ \frac{\partial p_x(t)}{\partial r(t)} & \frac{\partial p_x(t)}{\partial \theta(t)} & \frac{\partial p_x(t)}{\partial p_r(t)} & \frac{\partial p_x(t)}{\partial p_\theta(t)} \\ \frac{\partial p_y(t)}{\partial r(t)} & \frac{\partial p_y(t)}{\partial \theta(t)} & \frac{\partial p_y(t)}{\partial p_r(t)} & \frac{\partial p_y(t)}{\partial p_\theta(t)} \end{pmatrix} = \begin{pmatrix} 1 & 0 & 0 & 0 \\ 0 & r(t) & 0 & 0 \\ 0 & 0 & 1 & 0 \\ 0 & p_r(t) & 0 & \frac{1}{r(t)} \end{pmatrix}. \tag{D.7}$$

We denote $\mathrm{M_C}(t,t_0)$ by

$$\mathrm{M_C}(t,t_0) = \begin{pmatrix} A(t,t_0) & B(t,t_0) \\ C(t,t_0) & D(t,t_0) \end{pmatrix}, \tag{D.8}$$

then the position $\boldsymbol{\xi}$ and momentum $\boldsymbol{\eta}$ now satisfy equations

$$\begin{aligned} \xi^j(t) &= A^j{}_k(t,t_0)\xi^k(t_0) + B^{jk}(t,t_0)\eta_k(t_0), \\ \eta_j(t) &= C_{jk}(t,t_0)\xi^k(t_0) + D_j{}^k(t,t_0)\eta_k(t_0) \end{aligned} \tag{D.9}$$

and they also satisfies dynamical properties that

$$\frac{\mathrm{d}\xi^j(t)}{\mathrm{d}t} = g^{jk}(\boldsymbol{y}(t))\eta_k(t), \qquad \frac{\mathrm{d}\eta_j(t)}{\mathrm{d}t} = -K_{jk}(\boldsymbol{y}(t))\xi^k(t). \tag{D.10}$$

Use the time derivative of momentum equation, we can calculate the integral

$$\begin{aligned}\int_{t_0}^{t} \mathrm{d}\tau\,(-K_{jk}(\boldsymbol{y}(\tau))\xi^j(\tau)\xi^k(\tau)) &= \int_{t_0}^{t} \mathrm{d}\tau\,(\frac{\mathrm{d}\eta_k(\tau)}{\mathrm{d}\tau}\xi^k(\tau)) \\ &= \int_{t_0}^{t} \mathrm{d}\eta_k(\tau)\,\xi^k(\tau) \\ &= \eta_k(\tau)\xi^k(\tau)\Big|_{t_0}^{t} - \int_{t_0}^{t} \eta_k(\tau)\,\mathrm{d}\xi^k(\tau) \\ &= \eta_k(\tau)\xi^k(\tau)\Big|_{t_0}^{t} - \int_{t_0}^{t} g_{jk}(\boldsymbol{y}(\tau))\frac{\mathrm{d}\xi^j(\tau)}{\mathrm{d}\tau}\,\mathrm{d}\xi^k(\tau)\,,\end{aligned} \tag{D.11}$$

which tells us that

$$S^Q(\boldsymbol{\xi};t,t_0) = S^Q(\boldsymbol{\xi},\boldsymbol{\eta};t,t_0) = \frac{1}{2}\,\eta_k(\tau)\xi^k(\tau)\Big|_{t_0}^{t}. \tag{D.12}$$

Since $\eta_k(t_0)$ satisfies

$$\begin{aligned} B^{jl}(t,t_0)\eta_l(t_0) &= \xi^j(t) - A^j{}_l(t,t_0)\xi^l(t_0), \\ \delta_k{}^l\eta_l(t_0) &= B_{kj}(t,t_0)\xi^j(t) - B_{kj}(t,t_0)A^j{}_l(t,t_0)\xi^l(t_0), \\ \eta_k(t_0) &= B_{kj}(t,t_0)\xi^j(t) - B_{kj}(t,t_0)A^j{}_l(t,t_0)\xi^l(t_0), \end{aligned} \tag{D.13}$$

and $\eta_k(t)$ satisfies

$$\begin{aligned} D^m{}_j(t,t_0)\xi^j(t) &= D^m{}_j(t,t_0)A^j{}_l(t,t_0)\xi^l(t_0) + D^m{}_j(t,t_0)B^{jl}(t,t_0)\eta_l(t_0), \\ B^{mj}(t,t_0)\eta_j(t) &= B^{mj}(t,t_0)C_{jl}(t,t_0)\xi^l(t_0) + B^{mj}(t,t_0)D_j{}^l(t,t_0)\eta_l(t_0), \\ D^m{}_j(t,t_0)\xi^j(t) - B^{mj}(t,t_0)\eta_j(t) &= D^m{}_j(t,t_0)A^j{}_l(t,t_0)\xi^l(t_0) - B^{mj}(t,t_0)C_{jl}(t,t_0)\xi^l(t_0), \\ D^m{}_j(t,t_0)\xi^j(t) - B^{mj}(t,t_0)\eta_j(t) &= \xi^m(t_0), \\ \delta_k{}^j\eta_j(t) &= B_{km}(t,t_0)D^m{}_j(t,t_0)\xi^j(t) - B_{km}(t,t_0)\xi^m(t_0), \\ \eta_k(t) &= B_{km}(t,t_0)D^m{}_j(t,t_0)\xi^j(t) - B_{km}(t,t_0)\xi^m(t_0), \end{aligned} \tag{D.14}$$

together we have

$$\begin{aligned} S^Q(\boldsymbol{\xi};t,t_0) = B_{km}(t,t_0)D^m{}_j(t,t_0)\xi^j(t)\xi^k(t) - B_{km}(t,t_0)\xi^m(t_0)\xi^k(t) - \\ B_{kj}(t,t_0)\xi^j(t)\xi^k(t_0) + B_{kj}(t,t_0)A^j{}_l(t,t_0)\xi^l(t_0)\xi^k(t_0). \end{aligned} \tag{D.15}$$

Here we define

$$\Lambda_{jk}(t,t_0) = B_{jl}(t,t_0)D^l{}_k(t,t_0), \qquad \Theta_{jk}(t,t_0) = B_{jl}(t,t_0)A^l{}_k(t,t_0), \qquad \Xi_{jk}(t,t_0) = B_{jk}(t,t_0), \tag{D.16}$$

then the quadratic action from equation (D.1) can be written as

$$S^Q(\boldsymbol{\xi};t,t_0) = \frac{1}{2}\Big(\Lambda_{jk}(t,t_0)\xi^j(t)\xi^k(t) + \Theta_{jk}(t,t_0)\xi^j(t_0)\xi^k(t_0) - 2\Xi_{jk}(t,t_0)\xi^j(t)\xi^k(t_0)\Big). \tag{D.17}$$

To calculate the action $S_1(\boldsymbol{\xi};t_1,t_0)$ from $\boldsymbol{\xi}(t_0)$ to $\boldsymbol{\xi}(t_1)$, using the fact that $\zeta_j \ll r_1 (j=1,2)$, we have

$$S_1(\boldsymbol{\xi};t_1,t_0) = S_1(\boldsymbol{\xi}^0;t_1,t_0) + \delta S_1(\boldsymbol{\zeta}) + \mathcal{O}\big(\boldsymbol{\zeta}^3\big), \tag{D.18}$$

where $S_1(\boldsymbol{\xi}^0;t_1,t_0)$ is the action along reference trajectory from $(-r',0)$ to $(-r_1,0)$, which will also be denoted as S^0, when the path is not included in the argument of S. $\delta S_1(\boldsymbol{\zeta})$ is the difference of actual and reference trajectory up to the second order or the local coordinate $\boldsymbol{\zeta}$, which equals to

$$\begin{aligned}\delta S_1(\boldsymbol{\zeta}) &= \frac{\partial S_1(t_1,t_0)}{\partial x(t_1)}\zeta_1 + \frac{\partial S_1(t_1,t_0)}{\partial y(t_1)}\zeta_2 + \frac{\partial^2 S_1(t_1,t_0)}{\partial x(t_1)^2}\zeta_1^2 + \frac{\partial^2 S_1(t_1,t_0)}{\partial y(t_1)^2}\zeta_2^2 \\ &= p_x(t_1)\zeta_1 + \frac{1}{2}\frac{D_{11}(t_1,t_0)}{B_{11}(t_1,t_0)}\zeta_1^2 + \frac{1}{2}\frac{D_{22}(t_1,t_0)}{B_{22}(t_1,t_0)}\zeta_2^2,\end{aligned} \tag{D.19}$$

where the momentum $p_x(t_1)$ at $x=-r_1$ is mv_1

$$p_x(t_1) = mv_1 = m\sqrt{\frac{2E}{m} - \frac{2fr_1}{m}} \approx mv - \frac{fr_1}{v}, \tag{D.20}$$

while in polar coordinates the momentum $p_r(t_1)$ at r_1 is

$$p_r(t_1) = -m\sqrt{\frac{2E}{m} - \frac{2fr_1}{m}} \approx -mv + \frac{fr_1}{v}. \tag{D.21}$$

From the stability matrix we can calculate

$$\frac{D_{11}(t_1,t_0)}{B_{11}(t_1,t_0)} = \frac{m}{t_1-t_0}. \tag{D.22}$$

We conclude that

$$S_1(\boldsymbol{\xi};t_1,t_0) = S_1^0(\boldsymbol{\xi};t_1,t_0) + mv_1\zeta_1 + \frac{m}{2(t_1-t_0)}\zeta_1^2 + \frac{1}{2}\frac{D_{22}(t_1,t_0)}{B_{22}(t_1,t_0)}\zeta_2^2, \tag{D.23}$$

Using the same treatment we do with action $S_1(\boldsymbol{\xi}^0;t_1,t_0)$, we get

$$S_2(\boldsymbol{\xi};t,t_2) = S_2(\boldsymbol{\xi}^0;t,t_2) + \delta S_2(\boldsymbol{\gamma}) + \mathcal{O}(\boldsymbol{\gamma}^3), \tag{D.24}$$

with up to the second order correction

$$\begin{aligned}\delta S_2(\boldsymbol{\gamma}) &= \frac{\partial S_2(t,t_2)}{\partial x(t_2)}\gamma_1 + \frac{\partial S_2(t,t_2)}{\partial y(t_2)}\gamma_2 + \frac{\partial^2 S_2(t,t_2)}{\partial x(t_2)^2}\gamma_1^2 + \frac{\partial^2 S_2(t,t_2)}{\partial y(t_2)^2}\gamma_2^2 \\ &= -p_x(t_2)\gamma_1 - p_y(t_2)\gamma_2 + \frac{1}{2}\frac{A_{11}(t,t_2)}{B_{11}(t,t_2)}\gamma_1^2 + \frac{1}{2}\frac{A_{22}(t,t_2)}{B_{22}(t,t_2)}\gamma_2^2.\end{aligned} \tag{D.25}$$

The momentum in polar coordinate $p_r(t_2)$ at r_2 is

$$p_r(t_2) = m\sqrt{v^2 - 2\frac{f}{m}r_2} \approx mv - \frac{fr_2}{v}, \tag{D.26}$$

so the corresponding Cartesian momenta at r_2 are

$$\begin{aligned}p_x(t_2) = mv_2 &= m\cos\theta\sqrt{v^2 - 2\frac{f}{m}r_2} \approx mv - \frac{fr_2}{v}, \\ p_y(t_2) &= m\sin\theta\sqrt{v^2 - 2\frac{f}{m}r_2} \approx mv\theta - \frac{fr_2}{v}\theta.\end{aligned} \tag{D.27}$$

Also the stability matrix tells us

$$\frac{A_{11}(t,t_2)}{B_{11}(t,t_2)} = \frac{m}{t-t_2}, \tag{D.28}$$

so the action $S_2(\boldsymbol{\xi};t,t_2)$ equals to

$$S_2(\boldsymbol{\xi};t,t_2) = S_2(\boldsymbol{\xi}^0;t,t_2) - mv_2\gamma_1 - mv_2\theta\gamma_2 + \frac{m}{2(t-t_2)}\gamma_1^2 + \frac{1}{2}\frac{A_{22}(t,t_2)}{B_{22}(t,t_2)}\gamma_2^2, \tag{D.29}$$

The terms A_{22}, B_{22}, and D_{22} from the stability matrix need to be calculated for different time

intervals. For $B_{22}(t_1,t_0)$, we use the fact that $r_1 \ll r'$ and use the limit $r_1 \to 0$, we have

$$\begin{aligned} B_{22}(t_1,t_0) &= r(t_0)r(t_1)\frac{\partial\theta(t_1)}{\partial p_\theta(t_0)} \\ &= r'r_1\left(\frac{1}{\sqrt{2mE}}\left(\frac{1}{r'}-\frac{1}{r_1}\right)+\frac{f}{2E\sqrt{2mE}}\ln\left(\frac{r_1}{r'}\right)\right) \\ &= \frac{1}{\sqrt{2mE}}(r_1-r')+\frac{fr'r_1}{2E\sqrt{2mE}}\ln\left(\frac{r_1}{r'}\right) \\ &= -\frac{r'}{\sqrt{2mE}} \\ &= -\frac{r'}{mv}, \end{aligned} \tag{D.30}$$

similarly, we can get

$$\begin{aligned} B_{22}(t,t_2) &= r(t_2)r(t)\frac{\partial\theta(t)}{\partial p_\theta(t_2)} \\ &= \frac{r''}{mv}. \end{aligned} \tag{D.31}$$

For $D_{22}(t_1,t_0)$, we have

$$\begin{aligned} D_{22}(t_1,t_0) &= \frac{r(t_0)}{r(t_1)}+r(t_0)p_r(t_1)\frac{\partial\theta(t_1)}{\partial p_\theta(t_0)} \\ &= \frac{r'}{r_1}+r'\frac{p_r(t_1)}{\sqrt{2mE}}\left(\frac{1}{r'}-\frac{1}{r_1}\right)+r'\frac{p_r(t_1)f}{2E\sqrt{2mE}}\ln\left(\frac{r_1}{r'}\right) \\ &= \frac{2r'}{r_1}-1+\frac{fr_1}{mv^2}-\frac{fr'}{mv^2}-\frac{fr'}{mv^2}\ln\left(\frac{r_1}{r'}\right)+\frac{f^2r_1r'}{m^2v^4}\ln\left(\frac{r_1}{r'}\right) \\ &\approx \frac{r'f}{mv^2}\ln\left(\frac{E}{r_1f}\right), \end{aligned} \tag{D.32}$$

where we have used the facts that $E/f \sim \mathcal{O}(r')$, and since $r(t_1) \ll r(t_0)$ we have

$$\frac{r'f}{mv^2}\ln\left(\frac{E}{r'f}\right) \ll \frac{r'f}{mv^2}\ln\left(\frac{E}{r_1f}\right), \tag{D.33}$$

and

$$1 \ll \frac{r'f}{mv^2}\ln\left(\frac{E}{r_1f}\right). \tag{D.34}$$

For $A_{22}(t,t_2)$, since $r(t_2) \ll r(t)$, we have

$$\begin{aligned} A_{22}(t,t_2) &= \frac{r(t)}{r(t_2)} - r(t)p_r(t_2)\frac{\partial\theta(t)}{\partial p_\theta(t_2)} \\ &= \frac{r''}{r_2} - r''\frac{p_r(t_2)}{\sqrt{2mE}}\left(\frac{1}{r_2} - \frac{1}{r''}\right) - r''\frac{p_r(t_2)f}{2E\sqrt{2mE}}\ln\left(\frac{r''}{r_2}\right) \\ &\approx -\frac{r''f}{mv^2}\ln\left(\frac{E}{r_2 f}\right). \end{aligned} \tag{D.35}$$

So the actions $S_1(\boldsymbol{\xi};t_1,t_0)$ and $S_2(\boldsymbol{\xi};t,t_2)$ equal to

$$S_1(\boldsymbol{\xi};t_1,t_0) = S_1(\boldsymbol{\xi}^0;t_1,t_0) + mv_1\zeta_1 + \frac{m\zeta_1^2}{2(t_1-t_0)} - \frac{f\zeta_2^2}{2v}\ln\left(\frac{E}{r_1 f}\right), \tag{D.36}$$

and

$$S_2(\boldsymbol{\xi};t,t_2) = S_2(\boldsymbol{\xi}^0;t,t_2) - mv_2\gamma_1 - mv_2\theta\gamma_2 + \frac{m\gamma_1^2}{2(t-t_2)} - \frac{f\gamma_2^2}{2v}\ln\left(\frac{E}{r_2 f}\right). \tag{D.37}$$

BIBLIOGRAPHY

[1] D. R. Yarkony, "Nonadiabatic quantum chemistry - past, present, and future," *Chemical Reviews*, vol. 112, no. 1, pp. 481–498, 2012.

[2] J. C. Tully, "Perspective: Nonadiabatic dynamics theory," *The Journal of Chemical Physics*, vol. 137, no. 22, p. 22A301, 2012.

[3] H. Eyring and M. Polanyi, "Über einfache gasreaktionen," *Z Phys Chem Abt B*, vol. 12, pp. 279–311, 1931.

[4] L. D. Landau, "Zur theorie der energieubertragung. ii," *Phys. Z. Sowjetunion*, vol. 2, no. 46, pp. 1–13, 1932.

[5] C. Zener, "Non-adiabatic crossing of energy levels," *Proc. R. Soc. Lond. A*, vol. 137, no. 833, pp. 696–702, 1932.

[6] A. Nitzan, *Chemical dynamics in condensed phases: relaxation, transfer and reactions in condensed molecular systems*. Oxford university press, 2006.

[7] H. Köppel, L. S. Cederbaum, W. Domcke, and S. S. Shaik, "Symmetry Breaking and Non-Born-Oppenheimer Effects in Radical Cations," *Angewandte Chemie International Edition in English*, vol. 22, no. 3, pp. 210–224, 1983.

[8] M. Abe, Y. Ohtsuki, Y. Fujimura, Z. Lan, and W. Domcke, "Geometric phase effects in the coherent control of the branching ratio of photodissociation products of phenol," *The Journal of Chemical Physics*, vol. 124, no. 22, p. 224316, 2006.

[9] M. H. Kim, L. Shen, H. Tao, T. J. Martínez, and A. G. Suits, "Conformationally controlled chemistry: Excited-state dynamics dictate ground-state reaction," *Science*, vol. 315, no. 5818, pp. 1561–1565, 2007.

[10] L. Seidner and W. Domcke, "Microscopic modelling of photoisomerization and internal-conversion dynamics," *Chemical Physics*, vol. 186, no. 1, pp. 27–40, 1994.

[11] B. G. Levine and T. J. Martínez, "Isomerization through conical intersections," *Annual Review of Physical Chemistry*, vol. 58, no. 1, pp. 613–634, 2007.

[12] W. Domcke, D. R. Yarkony, and H. Köppel, *Conical intersections: electronic structure, dynamics & spectroscopy*, vol. 15. World Scientific, 2004.

[13] S. Matsika and P. Krause, "Nonadiabatic Events and Conical Intersections," *Annual Review of Physical Chemistry*, vol. 62, no. 1, pp. 621–643, 2011.

[14] W. Domcke and D. R. Yarkony, "Role of conical intersections in molecular spectroscopy and photoinduced chemical dynamics," *Annual Review of Physical Chemistry*, vol. 63, no. 1, pp. 325–352, 2012.

[15] S. G. Krantz and H. R. Parks, *The implicit function theorem: history, theory, and applications*. Springer Science & Business Media, 2012.

[16] D. R. Yarkony, "Diabolical conical intersections," *Rev. Mod. Phys.*, vol. 68, pp. 985–1013, 1996.

[17] O. P. J. Vieuxmaire, Z. Lan, A. L. Sobolewski, and W. Domcke, "Ab initio characterization of the conical intersections involved in the photochemistry of phenol," *The Journal of Chemical Physics*, vol. 129, no. 22, p. 224307, 2008.

[18] S. Perun, A. L. Sobolewski, and W. Domcke, "Conical intersections in thymine," *The Journal of Physical Chemistry A*, vol. 110, no. 49, pp. 13238–13244, 2006.

[19] F. Sicilia, L. Blancafort, M. J. Bearpark, and M. A. Robb, "New algorithms for optimizing and linking conical intersection points," *Journal of Chemical Theory and Computation*, vol. 4, no. 2, pp. 257–266, 2008.

[20] I. N. Ragazos, M. A. Robb, F. Bernardi, and M. Olivucci, "Optimization and characterization of the lowest energy point on a conical intersection using an MC-SCF lagrangian," *Chemical Physics Letters*, vol. 197, no. 3, pp. 217–223, 1992.

[21] S. Matsika and D. R. Yarkony, "Conical Intersections of Three Electronic States Affect the Ground State of Radical Species with Little or No Symmetry: Pyrazolyl," *Journal of the American Chemical Society*, vol. 125, no. 41, pp. 12428–12429, 2003.

[22] B. G. Levine, J. D. Coe, and T. J. Martínez, "Optimizing Conical Intersections without Derivative Coupling Vectors: Application to Multistate Multireference Second-Order Perturbation Theory (MS-CASPT2)," *The Journal of Physical Chemistry B*, vol. 112, no. 2, pp. 405–413, 2008.

[23] M. Z. Zgierski, S. Patchkovskii, T. Fujiwara, and E. C. Lim, "On the origin of the ultrafast internal conversion of electronically excited pyrimidine bases," *The Journal of Physical Chemistry A*, vol. 109, no. 42, pp. 9384–9387, 2005.

[24] N. Ismail, L. Blancafort, M. Olivucci, B. Kohler, and M. A. Robb, "Ultrafast decay of electronically excited singlet cytosine via a π,π^* to n_0,π^* state switch," *Journal of the American Chemical Society*, vol. 124, no. 24, pp. 6818–6819, 2002.

[25] T. Horio, T. Fuji, Y.-I. Suzuki, and T. Suzuki, "Probing ultrafast internal conversion through conical intersection via time-energy map of photoelectron angular anisotropy," *Journal of the American Chemical Society*, vol. 131, no. 30, pp. 10392–10393, 2009.

[26] S. Matsika, "Radiationless decay of excited states of uracil through conical intersections," *The Journal of Physical Chemistry A*, vol. 108, no. 37, pp. 7584–7590, 2004.

[27] R. Szabla, R. W. Gora, and J. Sponer, "Ultrafast excited-state dynamics of isocytosine," *Phys. Chem. Chem. Phys.*, vol. 18, pp. 20208–20218, 2016.

[28] P. W. Kim, J. Pan, N. C. Rockwell, C.-W. Chang, K. C. Taylor, J. C. Lagarias, and D. S. Larsen, "Ultrafast e to z photoisomerization dynamics of the cph1 phytochrome," *Chemical Physics Letters*, vol. 549, pp. 86–92, 2012.

[29] C.-W. Jiang, R.-H. Xie, F.-L. Li, and R. E. Allen, "Ultrafast cis-to-trans photoisomerization of a bridged azobenzene through $n\pi^*$ excitation: Rotational pathway is not restricted," *Chemical Physics Letters*, vol. 521, pp. 107–112, 2012.

[30] S. Hahn and G. Stock, "Femtosecond secondary emission arising from the nonadiabatic photoisomerization in rhodopsin," *Chemical Physics*, vol. 259, no. 2, pp. 297–312, 2000.

[31] R. Schoenlein, L. Peteanu, R. Mathies, and C. Shank, "The first step in vision: femtosecond isomerization of rhodopsin," *Science*, vol. 254, no. 5030, pp. 412–415, 1991.

[32] M. Abe, Y. Ohtsuki, Y. Fujimura, and W. Domcke, "Optimal control of ultrafast cis-trans photoisomerization of retinal in rhodopsin via a conical intersection," *The Journal of Chemical Physics*, vol. 123, no. 14, p. 144508, 2005.

[33] L. Seidner, G. Stock, A. L. Sobolewski, and W. Domcke, "Ab initio characterization of the $S_1 - S_2$ conical intersection in pyrazine and calculation of spectra," *The Journal of Chemical Physics*, vol. 96, no. 7, pp. 5298–5309, 1992.

[34] W. Domcke, D. R. Yarkony, and H. Köppel, *Conical intersections: theory, computation and experiment*, vol. 17. World Scientific, 2011.

[35] V. Vallet, Z. Lan, S. Mahapatra, A. L. Sobolewski, and W. Domcke, "Photochemistry of pyrrole: Time-dependent quantum wave-packet description of the dynamics at the $^1\pi\sigma^* - S_0$ conical intersections," *The Journal of Chemical Physics*, vol. 123, no. 14, p. 144307, 2005.

[36] B. Nikoobakht and H. Köppel, "Quantum dynamics study of singlet-triplet transitions in s-trans-1,3-butadiene," *Chemical Physics Letters*, vol. 651, pp. 221–232, 2016.

[37] M. C. E. Galbraith, S. Scheit, N. V. Golubev, G. Reitsma, N. Zhavoronkov, V. Despré, F. Lépine, A. I. Kuleff, M. J. J. Vrakking, O. Kornilov, H. Köppel, and J. Mikosch, "Few-femtosecond passage of conical intersections in the benzene cation," *Nature Communications*, vol. 8, no. 1, p. 1018, 2017.

[38] Y. Tanimura and S. Mukamel, "Multistate quantum Fokker-Planck approach to nonadiabatic wave packet dynamics in pump–probe spectroscopy," *The Journal of Chemical Physics*, vol. 101, no. 4, pp. 3049–3061, 1994.

[39] A. Kühl and W. Domcke, "Multilevel redfield description of the dissipative dynamics at conical intersections," *The Journal of Chemical Physics*, vol. 116, no. 1, pp. 263–274, 2002.

[40] L. Chen, M. F. Gelin, V. Y. Chernyak, W. Domcke, and Y. Zhao, "Dissipative dynamics at conical intersections: simulations with the hierarchy equations of motion method," *Faraday Discuss.*, vol. 194, pp. 61–80, 2016.

[41] M. Thoss and H. Wang, "Quantum dynamical simulation of ultrafast molecular processes in the condensed phase," *Chemical Physics*, vol. 322, no. 1, pp. 210–222, 2006.

[42] S. Fernandez-Alberti, D. V. Makhov, S. Tretiak, and D. V. Shalashilin, "Non-adiabatic excited state molecular dynamics of phenylene ethynylene dendrimer using a multiconfigurational ehrenfest approach," *Phys. Chem. Chem. Phys.*, vol. 18, pp. 10028–10040, 2016.

[43] H. Beck, A. Jäckle, G. Worth, and H.-D. Meyer, "The multiconfiguration time-dependent Hartree (MCTDH) method: a highly efficient algorithm for propagating wavepackets," *Physics Reports*, vol. 324, no. 1, pp. 1–105, 2000.

[44] T. J. Martínez, "Insights for light-driven molecular devices from ab initio multiple spawning excited-state dynamics of organic and biological chromophores," *Accounts of Chemical Research*, vol. 39, no. 2, pp. 119–126, 2006.

[45] M. Ben-Nun, J. Quenneville, and T. J. Martínez, "Ab initio multiple spawning: Photochemistry from first principles quantum molecular dynamics," *The Journal of Physical Chemistry A*, vol. 104, no. 22, pp. 5161–5175, 2000.

[46] L. S. Schulman, *Techniques and applications of path integration*. Courier Corporation, 2012.

[47] M. C. Gutzwiller, *Chaos in classical and quantum mechanics*, vol. 1. Springer Science & Business Media, 2013.

[48] M. F. Herman and E. Kluk, "A semiclasical justification for the use of non-spreading wavepackets in dynamics calculations," *Chemical Physics*, vol. 91, no. 1, pp. 27–34, 1984.

[49] E. Kluk, M. F. Herman, and H. L. Davis, "Comparison of the propagation of semiclassical frozen gaussian wave functions with quantum propagation for a highly excited anharmonic oscillator," *The Journal of Chemical Physics*, vol. 84, no. 1, pp. 326–334, 1986.

[50] L. D. Landau and E. M. Lifshitz, *Quantum mechanics: non-relativistic theory*, vol. 3. Elsevier, 2013.

[51] J. C. Tully, "Nonadiabatic molecular dynamics," *International Journal of Quantum Chemistry*, vol. 40, no. S25, pp. 299–309, 1991.

[52] J. C. Tully, "Molecular dynamics with electronic transitions," *The Journal of Chemical Physics*, vol. 93, no. 2, pp. 1061–1071, 1990.

[53] M. Barbatti, "Nonadiabatic dynamics with trajectory surface hopping method," *Wiley Interdisciplinary Reviews: Computational Molecular Science*, vol. 1, no. 4, pp. 620–633, 2011.

[54] J. E. Subotnik and N. Shenvi, "A new approach to decoherence and momentum rescaling in the surface hopping algorithm," *The Journal of Chemical Physics*, vol. 134, no. 2, p. 024105, 2011.

[55] T. Nelson, S. Fernandez-Alberti, V. Chernyak, A. E. Roitberg, and S. Tretiak, "Nonadiabatic excited-state molecular dynamics modeling of photoinduced dynamics in conjugated molecules," *The Journal of Physical Chemistry B*, vol. 115, no. 18, pp. 5402–5414, 2011.

[56] B. Heggen, Z. Lan, and W. Thiel, "Nonadiabatic decay dynamics of 9H-guanine in aqueous solution," *Phys. Chem. Chem. Phys.*, vol. 14, pp. 8137–8146, 2012.

[57] H. Nieber and N. L. Doltsinis, "Elucidating ultrafast nonradiative decay of photoexcited uracil in aqueous solution by ab initio molecular dynamics," *Chemical Physics*, vol. 347, no. 1, pp. 405–412, 2008.

[58] V. N. Gorshkov, S. Tretiak, and D. Mozyrsky, "Semiclassical monte-carlo approach for modelling non-adiabatic dynamics in extended molecules," *Nature Communications*, vol. 4, p. 2144, 2013.

[59] A. J. White, V. N. Gorshkov, R. Wang, S. Tretiak, and D. Mozyrsky, "Semiclassical monte carlo: A first principles approach to non-adiabatic molecular dynamics," *The Journal of Chemical Physics*, vol. 141, no. 18, p. 184101, 2014.

[60] P. Pechukas, "Time-Dependent Semiclassical Scattering Theory. I. Potential Scattering," *Phys. Rev.*, vol. 181, pp. 166–174, 1969.

[61] P. Pechukas, "Time-Dependent Semiclassical Scattering Theory. II. Atomic Collisions," *Phys. Rev.*, vol. 181, pp. 174–185, 1969.

[62] C. J. Cramer, *Essentials of computational chemistry: theories and models*. John Wiley & Sons, 2013.

[63] A. Szabo and N. S. Ostlund, *Modern quantum chemistry: introduction to advanced electronic structure theory*. Courier Corporation, 2012.

[64] M. Iannuzzi, *Ab Initio Molecular Dynamics*, ch. 6, pp. 93–120. John Wiley & Sons, Ltd, 2009.

[65] C. A. Ullrich, *Time-dependent density-functional theory: concepts and applications*. OUP Oxford, 2011.

[66] G. C. Schatz and M. A. Ratner, *Quantum mechanics in chemistry*. Courier Corporation, 2002.

[67] C. J. Smallwood, W. B. Bosma, R. E. Larsen, and B. J. Schwartz, "The role of electronic symmetry in charge-transfer-to-solvent reactions: Quantum nonadiabatic computer simulation of photoexcited sodium anions," *The Journal of Chemical Physics*, vol. 119, no. 21, pp. 11263–11277, 2003.

[68] G. Cui and W. Fang, "Ab initio based surface-hopping dynamics study on ultrafast internal conversion in cyclopropanone," *The Journal of Physical Chemistry A*, vol. 115, no. 9, pp. 1547–1555, 2011. PMID: 21322652.

[69] J. M. Hostettler, A. Bach, and P. Chen, "Adiabatic and nonadiabatic dissociation of ethyl radical," *The Journal of Chemical Physics*, vol. 130, no. 3, p. 034303, 2009.

[70] A. Matsugi, "Roaming dissociation of ethyl radicals," *The Journal of Physical Chemistry Letters*, vol. 4, no. 24, pp. 4237–4240, 2013. PMID: 26296171.

[71] J. Clark, T. Nelson, S. Tretiak, G. Cirmi, and G. Lanzani, "Femtosecond torsional relaxation," *Nature Physics*, vol. 8, no. 3, p. 225, 2012.

[72] A. J. Neukirch, L. C. Shamberger, E. Abad, B. J. Haycock, H. Wang, J. Ortega, O. V. Prezhdo, and J. P. Lewis, "Nonadiabatic ensemble simulations of cis-stilbene and cis-azobenzene photoisomerization," *Journal of Chemical Theory and Computation*, vol. 10, no. 1, pp. 14–23, 2014. PMID: 26579888.

[73] A. Kazaryan, Z. Lan, L. V. Schäfer, W. Thiel, and M. Filatov, "Surface Hopping Excited-State Dynamics Study of the Photoisomerization of a Light-Driven Fluorene Molecular Rotary Motor," *Journal of Chemical Theory and Computation*, vol. 7, no. 7, pp. 2189–2199, 2011.

[74] R. Mathies, C. Brito Cruz, W. Pollard, and C. Shank, "Direct observation of the femtosecond excited-state cis-trans isomerization in bacteriorhodopsin," *Science*, vol. 240, no. 4853, pp. 777–779, 1988.

[75] R. A. Marcus, "On the theory of oxidation—reduction reactions involving electron transfer. v. comparison and properties of electrochemical and chemical rate constants1," *The Journal of Physical Chemistry*, vol. 67, no. 4, pp. 853–857, 1963.

[76] P. F. Barbara, T. J. Meyer, and M. A. Ratner, "Contemporary issues in electron transfer research," *The Journal of Physical Chemistry*, vol. 100, no. 31, pp. 13148–13168, 1996.

[77] P. Peumans, S. Uchida, and S. R. Forrest, "Efficient bulk heterojunction photovoltaic cells using small-molecular-weight organic thin films," in *Materials for Sustainable Energy: A Collection of Peer-Reviewed Research and Review Articles from Nature Publishing Group*, pp. 94–98, World Scientific, 2011.

[78] S. M. Falke, C. A. Rozzi, D. Brida, M. Maiuri, M. Amato, E. Sommer, A. De Sio, A. Rubio, G. Cerullo, E. Molinari, and C. Lienau, "Coherent ultrafast charge transfer in an organic photovoltaic blend," *Science*, vol. 344, no. 6187, pp. 1001–1005, 2014.

[79] T. G. Goodson, "Optical excitations in organic dendrimers investigated by time-resolved and nonlinear optical spectroscopy," *Accounts of Chemical Research*, vol. 38, no. 2, pp. 99–107, 2005. PMID: 15709729.

[80] E. Collini and G. D. Scholes, "Coherent intrachain energy migration in a conjugated polymer at room temperature," *Science*, vol. 323, no. 5912, pp. 369–373, 2009.

[81] H. Lee, Y.-C. Cheng, and G. R. Fleming, "Coherence dynamics in photosynthesis: Protein protection of excitonic coherence," *Science*, vol. 316, no. 5830, pp. 1462–1465, 2007.

[82] M. Reufer, M. J. Walter, P. G. Lagoudakis, A. B. Hummel, J. S. Kolb, H. G. Roskos, U. Scherf, and J. M. Lupton, "Spin-conserving carrier recombination in conjugated polymers," *Nature materials*, vol. 4, no. 4, p. 340, 2005.

[83] S. Mai, P. Marquetand, and L. González, "Non-adiabatic and intersystem crossing dynamics in SO_2. ii. the role of triplet states in the bound state dynamics studied by surface-hopping simulations," *The Journal of Chemical Physics*, vol. 140, no. 20, p. 204302, 2014.

[84] A. Cannizzo, A. M. Blanco-Rodríguez, A. El Nahhas, J. Šebera, S. Záliš, A. Vlček, and M. Chergui, "Femtosecond fluorescence and intersystem crossing in rhenium(i) carbonyl-bipyridine complexes," *Journal of the American Chemical Society*, vol. 130, no. 28, pp. 8967–8974, 2008. PMID: 18570416.

[85] R. S. Becker, A. P. Pelliccioli, A. Romani, and G. Favaro, "Vibronic quantum effects in fluorescence and photochemistry. competition between vibrational relaxation and photochemistry and consequences for photochemical control," *Journal of the American Chemical Society*, vol. 121, no. 10, pp. 2104–2109, 1999.

[86] S. V. Kilina, D. S. Kilin, and O. V. Prezhdo, "Breaking the phonon bottleneck in pbse and cdse quantum dots: Time-domain density functional theory of charge carrier relaxation," *ACS Nano*, vol. 3, no. 1, pp. 93–99, 2009. PMID: 19206254.

[87] L. Wang, D. Trivedi, and O. V. Prezhdo, "Global flux surface hopping approach for mixed quantum-classical dynamics," *Journal of Chemical Theory and Computation*, vol. 10, no. 9, pp. 3598–3605, 2014. PMID: 26588504.

[88] W. H. Miller, *Classical-Limit Quantum Mechanics and the Theory of Molecular Collisions*, pp. 69–177. John Wiley & Sons, Ltd, 2007.

[89] N. Makri, "Time-dependent quantum methods for large systems," *Annual Review of Physical Chemistry*, vol. 50, no. 1, pp. 167–191, 1999. PMID: 15012410.

[90] K. Drukker, "Basics of surface hopping in mixed quantum/classical simulations," *Journal of Computational Physics*, vol. 153, no. 2, pp. 225 – 272, 1999.

[91] R. Kapral, "Progress in the theory of mixed quantum-classical dynamics," *Annual Review of Physical Chemistry*, vol. 57, no. 1, pp. 129–157, 2006. PMID: 16599807.

[92] R. Car and M. Parrinello, "Unified approach for molecular dynamics and density-functional theory," *Phys. Rev. Lett.*, vol. 55, pp. 2471–2474, Nov 1985.

[93] H.-D. Meyera and W. H. Miller, "A classical analog for electronic degrees of freedom in nonadiabatic collision processes," *The Journal of Chemical Physics*, vol. 70, no. 7, pp. 3214–3223, 1979.

[94] S.-I. Sawada, A. Nitzan, and H. Metiu, "Mean-trajectory approximation for charge- and energy-transfer processes at surfaces," *Phys. Rev. B*, vol. 32, pp. 851–867, Jul 1985.

[95] M. Barbatti, M. Ruckenbauer, F. Plasser, J. Pittner, G. Granucci, M. Persico, and H. Lischka, "Newton-x: a surface-hopping program for nonadiabatic molecular dynamics," *Wiley Interdisciplinary Reviews: Computational Molecular Science*, vol. 4, no. 1, pp. 26–33, 2014.

[96] A. V. Akimov and O. V. Prezhdo, "The pyxaid program for non-adiabatic molecular dynamics in condensed matter systems," *Journal of Chemical Theory and Computation*, vol. 9, no. 11, pp. 4959–4972, 2013. PMID: 26583414.

[97] A. V. Akimov and O. V. Prezhdo, "Nonadiabatic dynamics of charge transfer and singlet fission at the pentacene/c60 interface," *Journal of the American Chemical Society*, vol. 136, no. 4, pp. 1599–1608, 2014. PMID: 24397723.

[98] I. Schapiro, M. N. Ryazantsev, L. M. Frutos, N. Ferré, R. Lindh, and M. Olivucci, "The ultrafast photoisomerizations of rhodopsin and bathorhodopsin are modulated by bond length alternation and hoop driven electronic effects," *Journal of the American Chemical Society*, vol. 133, no. 10, pp. 3354–3364, 2011. PMID: 21341699.

[99] E. Tapavicza, I. Tavernelli, and U. Rothlisberger, "Trajectory surface hopping within linear response time-dependent density-functional theory," *Phys. Rev. Lett.*, vol. 98, p. 023001, Jan 2007.

[100] C. F. Craig, W. R. Duncan, and O. V. Prezhdo, "Trajectory surface hopping in the time-dependent kohn-sham approach for electron-nuclear dynamics," *Phys. Rev. Lett.*, vol. 95, p. 163001, Oct 2005.

[101] E. R. Bittner and P. J. Rossky, "Quantum decoherence in mixed quantum-classical systems: Nonadiabatic processes," *The Journal of Chemical Physics*, vol. 103, no. 18, pp. 8130–8143, 1995.

[102] J. E. Subotnik and N. Shenvi, "Decoherence and surface hopping: When can averaging over initial conditions help capture the effects of wave packet separation?," *The Journal of Chemical Physics*, vol. 134, no. 24, p. 244114, 2011.

[103] J. E. Subotnik, "Fewest-switches surface hopping and decoherence in multiple dimensions," *The Journal of Physical Chemistry A*, vol. 115, no. 44, pp. 12083–12096, 2011. PMID: 21995423.

[104] H. M. Jaeger, S. Fischer, and O. V. Prezhdo, "Decoherence-induced surface hopping," *The Journal of Chemical Physics*, vol. 137, no. 22, p. 22A545, 2012.

[105] J.-Y. Fang and S. Hammes-Schiffer, "Improvement of the internal consistency in trajectory surface hopping," *The Journal of Physical Chemistry A*, vol. 103, no. 47, pp. 9399–9407, 1999.

[106] O. V. Prezhdo and P. J. Rossky, "Relationship between quantum decoherence times and solvation dynamics in condensed phase chemical systems," *Phys. Rev. Lett.*, vol. 81, pp. 5294–5297, Dec 1998.

[107] B. J. Schwartz, E. R. Bittner, O. V. Prezhdo, and P. J. Rossky, "Quantum decoherence and the isotope effect in condensed phase nonadiabatic molecular dynamics simulations," *The Journal of Chemical Physics*, vol. 104, no. 15, pp. 5942–5955, 1996.

[108] F. Webster, E. T. Wang, P. J. Rossky, and R. A. Friesner, "Stationary phase surface hopping for nonadiabatic dynamics: Two-state systems," *The Journal of Chemical Physics*, vol. 100, no. 7, pp. 4835–4847, 1994.

[109] M. J. Bedard-Hearn, R. E. Larsen, and B. J. Schwartz, "Mean-field dynamics with stochastic decoherence (mf-sd): A new algorithm for nonadiabatic mixed quantum/classical molecular-dynamics simulations with nuclear-induced decoherence," *The Journal of Chemical Physics*, vol. 123, no. 23, p. 234106, 2005.

[110] Y. L. Volobuev, M. D. Hack, M. S. Topaler, and D. G. Truhlar, "Continuous surface switching: An improved time-dependent self-consistent-field method for nonadiabatic dynamics," *The Journal of Chemical Physics*, vol. 112, no. 22, pp. 9716–9726, 2000.

[111] M. D. Hack and D. G. Truhlar, "Electronically nonadiabatic trajectories: Continuous surface switching ii," *The Journal of Chemical Physics*, vol. 114, no. 7, pp. 2894–2902, 2001.

[112] C. Zhu, A. W. Jasper, and D. G. Truhlar, "Non-born–oppenheimer trajectories with self-consistent decay of mixing," *The Journal of Chemical Physics*, vol. 120, no. 12, pp. 5543–5557, 2004.

[113] C. Zhu, S. Nangia, A. W. Jasper, and D. G. Truhlar, "Coherent switching with decay of mixing: An improved treatment of electronic coherence for non-born–oppenheimer trajectories," *The Journal of Chemical Physics*, vol. 121, no. 16, pp. 7658–7670, 2004.

[114] N. Shenvi, J. E. Subotnik, and W. Yang, "Simultaneous-trajectory surface hopping: A parameter-free algorithm for implementing decoherence in nonadiabatic dynamics," *The Journal of Chemical Physics*, vol. 134, no. 14, p. 144102, 2011.

[115] J. E. Subotnik, "Augmented ehrenfest dynamics yields a rate for surface hopping," *The Journal of Chemical Physics*, vol. 132, no. 13, p. 134112, 2010.

[116] N. Shenvi and W. Yang, "Achieving partial decoherence in surface hopping through phase correction," *The Journal of Chemical Physics*, vol. 137, no. 22, p. 22A528, 2012.

[117] R. Kapral and G. Ciccotti, "Mixed quantum-classical dynamics," *The Journal of Chemical Physics*, vol. 110, no. 18, pp. 8919–8929, 1999.

[118] S. Nielsen, R. Kapral, and G. Ciccotti, "Mixed quantum-classical surface hopping dynamics," *The Journal of Chemical Physics*, vol. 112, no. 15, pp. 6543–6553, 2000.

[119] C.-Y. Hsieh and R. Kapral, "Nonadiabatic dynamics in open quantum-classical systems: Forward-backward trajectory solution," *The Journal of Chemical Physics*, vol. 137, no. 22, p. 22A507, 2012.

[120] D. Mac Kernan, G. Ciccotti, and R. Kapral, "Trotter-based simulation of quantum-classical dynamics," *The Journal of Physical Chemistry B*, vol. 112, no. 2, pp. 424–432, 2008. PMID: 18154283.

[121] W. Boucher and J. Traschen, "Semiclassical physics and quantum fluctuations," *Phys. Rev. D*, vol. 37, pp. 3522–3532, Jun 1988.

[122] O. V. Prezhdo and V. V. Kisil, "Mixing quantum and classical mechanics," *Phys. Rev. A*, vol. 56, pp. 162–175, Jul 1997.

[123] C. C. Martens and J.-Y. Fang, "Semiclassical-limit molecular dynamics on multiple electronic surfaces," *The Journal of Chemical Physics*, vol. 106, no. 12, pp. 4918–4930, 1997.

[124] H.-D. Meyer and W. H. Miller, "Analysis and extension of some recently proposed classical models for electronic degrees of freedom," *The Journal of Chemical Physics*, vol. 72, no. 4, pp. 2272–2281, 1980.

[125] G. Stock and M. Thoss, "Semiclassical description of nonadiabatic quantum dynamics," *Phys. Rev. Lett.*, vol. 78, pp. 578–581, 1997.

[126] A. Piryatinski, M. Stepanov, S. Tretiak, and V. Chernyak, "Semiclassical scattering on conical intersections," *Phys. Rev. Lett.*, vol. 95, p. 223001, 2005.

[127] T. Pacher, L. S. Cederbaum, and H. Köppel, *Adiabatic and Quasidiabatic States in a Gauge Theoretical Framework*, pp. 293–391. John Wiley & Sons, Ltd, 2007.

[128] W. Dittrich and M. Reuter, *Classical and quantum dynamics*, vol. 20. Springer, 1994.

[129] H. A. Bethe and E. E. Salpeter, *Quantum mechanics of one-and two-electron atoms*. Springer Science & Business Media, 2012.

[130] J. Milnor and J. D. Stasheff, *Characteristic Classes.(AM-76)*, vol. 76. Princeton university press, 2016.

[131] T. Pacher, C. A. Mead, L. S. Cederbaum, and H. Köppel, "Gauge theory and quasidiabatic states in molecular physics," *The Journal of Chemical Physics*, vol. 91, no. 11, pp. 7057–7062, 1989.

[132] C. A. Mead, "The "noncrossing" rule for electronic potential energy surfaces: The role of time-reversal invariance," *The Journal of Chemical Physics*, vol. 70, no. 5, pp. 2276–2283, 1979.

[133] C. A. Mead, "Molecular kramers degeneracy and non-abelian adiabatic phase factors," *Phys. Rev. Lett.*, vol. 59, pp. 161–164, 1987.

[134] S. Matsika and D. R. Yarkony, "On the effects of spin-orbit coupling on conical intersection seams in molecules with an odd number of electrons. I. Locating the seam," *The Journal of Chemical Physics*, vol. 115, no. 5, pp. 2038–2050, 2001.

[135] S. Matsika and D. R. Yarkony, "On the effects of spin-orbit coupling on conical intersection seams in molecules with an odd number of electrons. II. Characterizing the local topography of the seam," *The Journal of Chemical Physics*, vol. 115, no. 11, pp. 5066–5075, 2001.

[136] S. Matsika and D. R. Yarkony, "Spin-orbit coupling and conical intersections in molecules with an odd number of electrons. III. A perturbative determination of the electronic energies, derivative couplings and a rigorous diabatic representation near a conical intersection," *The Journal of Chemical Physics*, vol. 116, no. 7, pp. 2825–2835, 2002.

[137] S. Matsika and D. R. Yarkony, "Spin-Orbit Coupling and Conical Intersections. IV. A Perturbative Determination of the Electronic Energies, Derivative Couplings, and a Rigorous Diabatic Representation near a Conical Intersection. The General Case†," *The Journal of Physical Chemistry B*, vol. 106, no. 33, pp. 8108–8116, 2002.

[138] B. M. Broderick, Y. Lee, M. B. Doyle, O. S. Vasyutinskii, and A. G. Suits, "Velocity distribution of hydrogen atom spin polarization," *The Journal of Physical Chemistry Letters*, vol. 4, no. 20, pp. 3489–3493, 2013.

[139] D. Picconi and S. Y. Grebenshchikov, "Photodissociation dynamics in the first absorption band of pyrrole. I. Molecular Hamiltonian and the Herzberg-Teller absorption spectrum for the $^1A_2(\pi\sigma^*) \leftarrow \tilde{X}^1A_1(\pi\pi)$ transition," *The Journal of Chemical Physics*, vol. 148, no. 10, p. 104103, 2018.

[140] D. Picconi and S. Y. Grebenshchikov, "Photodissociation dynamics in the first absorption band of pyrrole. II. Photofragment distributions for the $^1A_2(\pi\sigma^*) \leftarrow \tilde{X}^1A_1(\pi\pi)$ transition," *The Journal of Chemical Physics*, vol. 148, no. 10, p. 104104, 2018.

[141] S. Matsika and D. R. Yarkony, "Beyond Two-State Conical Intersections. Three-State Conical Intersections in Low Symmetry Molecules: the Allyl Radical," *Journal of the American Chemical Society*, vol. 125, no. 35, pp. 10672–10676, 2003.

[142] R. P. Krawczyk, A. Viel, U. Manthe, and W. Domcke, "Photoinduced dynamics of the valence states of ethene: A six-dimensional potential-energy surface of three electronic states with several conical intersections," *The Journal of Chemical Physics*, vol. 119, no. 3, pp. 1397–1411, 2003.

[143] J. D. Coe and T. J. Martínez, "Competitive decay at two- and three-state conical intersections in excited-state intramolecular proton transfer," *Journal of the American Chemical Society*, vol. 127, no. 13, pp. 4560–4561, 2005. PMID: 15796506.

[144] M. Kowalewski, K. Bennett, and S. Mukamel, "Monitoring nonadiabatic avoided crossing dynamics in molecules by ultrafast x-ray diffraction," *Structural Dynamics*, vol. 4, no. 5, p. 054101, 2017.

[145] M. Kowalewski, B. P. Fingerhut, K. E. Dorfman, K. Bennett, and S. Mukamel, "Simulating coherent multidimensional spectroscopy of nonadiabatic molecular processes: From the infrared to the x-ray regime," *Chemical Reviews*, vol. 117, no. 19, pp. 12165–12226, 2017.

[146] M. Baer, *Beyond Born-Oppenheimer: electronic nonadiabatic coupling terms and conical intersections*. John Wiley & Sons, 2006.

[147] M. Baer, "Introduction to the theory of electronic non-adiabatic coupling terms in molecular systems," *Physics Reports*, vol. 358, no. 2, pp. 75 – 142, 2002.

[148] M. F. Herman, "Nonadiabatic semiclassical scattering. i. analysis of generalized surface hopping procedures," *The Journal of Chemical Physics*, vol. 81, no. 2, pp. 754–763, 1984.

[149] B. R. Landry and J. E. Subotnik, "Communication: Standard surface hopping predicts incorrect scaling for marcus' golden-rule rate: The decoherence problem cannot be ignored," *The Journal of Chemical Physics*, vol. 135, no. 19, p. 191101, 2011.

[150] E. J. Heller, "Time-dependent approach to semiclassical dynamics," *The Journal of Chemical Physics*, vol. 62, no. 4, pp. 1544–1555, 1975.

[151] N. Makri and W. H. Miller, "Monte carlo integration with oscillatory integrands: implications for feynman path integration in real time," *Chemical Physics Letters*, vol. 139, no. 1, pp. 10 – 14, 1987.

[152] J. Doll, D. Freeman, and M. Gillan, "Stationary phase monte carlo methods: An exact formulation," *Chemical Physics Letters*, vol. 143, no. 3, pp. 277 – 283, 1988.

[153] T. Nelson, S. Fernandez-Alberti, V. Chernyak, A. E. Roitberg, and S. Tretiak, "Nonadiabatic excited-state molecular dynamics: Numerical tests of convergence and parameters," *The Journal of Chemical Physics*, vol. 136, no. 5, p. 054108, 2012.

[154] A. A. Kirillov, *Elements of the Theory of Representations*, vol. 220. Springer Science & Business Media, 2012.

[155] M. Spivak, *Calculus on manifolds: a modern approach to classical theorems of advanced calculus*. CRC Press, 2018.

[156] R. Bott and L. W. Tu, *Differential forms in algebraic topology*, vol. 82. Springer Science & Business Media, 2013.

ABSTRACT

NONADIABATIC DYNAMICS: GENERAL THEORY AND SEMICLASSICAL APPROACH

by

RUIXI WANG

December 2019

Advisor: Dr. Vladimir Y. Chernyak

Major: Chemistry (Physical)

Degree: Doctor of Philosophy

Nonadiabatic dynamics has been an essential part of quantum chemistry since the 1930's. Nonadiabatic effects play a crucial role in photo-physical and photo-chemical reactions for both small and large molecules in both gas and condensed phases. Modeling dynamics of photoinduced reactions has been a new frontier of chemistry. Many dynamical phenomena, such as intersystem crossing, non-radiative relaxation, and charge energy transfer, require a nonadiabatic description which incorporates transitions between electronic states.

In Chapter 2, the property of scattering region in the semiclassical limit is investigated. We suggest that a nuclear wavepacket close enough to the conical intersection will propagate ballistically in a straight line through the scattering region with distance λ_+, the impact parameter, away from the conical intersection. Upon taking the semiclassical limit, we have proven that in a certain neighborhood of the conical intersection, the adiabatic propagation and ballistic propagation are both valid. The resulted complete propagator is governed by the semiclassical propagation along the reference path which connects the initial and final points, and an integration over the impact parameter, hence only depends on the initial and final classical states of the system.

In Chapter 3, we identify the main differences between the effects of Kramers symmetry on the systems with even and odd number of electrons, the ways how the aforementioned symmetry affects the structure of the Conical Seams (CSs), and how it shows up in semiclassical propagation of nuclear wavepackets, crossing the CSs. We identify the topological invariants, associated with CSs,

in three cases: even and odd number of electrons with time-reversal symmetry, as well as absence of the latter. We obtain asymptotically exact semiclassical analytical solutions for wavepackets scattered on a CS for all three cases, identify topological features in a non-trivial shape of the scattered wavepacket, and connect them to the topological invariants, associated with CSs. We argue that, due to robustness of topology, the non-trivial wavepacket structure is a topologically protected evidence of a wavepacket having passed through a CS, rather than a feature of a semiclassical approximation.

In Chapter 4, we present, in detail, an algorithm based on Monte-Carlo sampling of the semiclassical time-dependent wavefunction, that involves running simple surface hopping dynamics, followed by a post-processing step which adds little cost. The method requires only a few quantities from quantum chemistry calculations, can systematically be improved, and provides excellent agreement with exact quantum mechanical results. Here we show excellent agreement with exact solutions for scattering results of standard test problems. Additionally, we find that convergence of the wavefunction is controlled by complex valued phase factors, the size of the nonadiabatic coupling region, and the choice of sampling function. These results help in determining the range of applicability of the method, and provide a starting point for further improvement.

AUTOBIOGRAPHICAL STATEMENT

RUIXI WANG

Education

12/2019	Ph.D., Chemistry (Physical), Wayne State University.
05/2012	B.S., Chemistry (with honor), New Mexico State University.
01/2010	Chemistry, Sichuan University.

Publications

- White, Alexander J.; Gorshkov, Vyacheslav N.; Wang, Ruixi; Tretiak, Sergei; Mozyrsky, Dmitry. *Semiclassical Monte Carlo: A first principles approach to non-adiabatic molecular dynamics*, J. Chem. Phys., **141**, 184101 (2014).

- Wang, Ruixi; Chernyak, Vladimir Y.; *Dynamical Consequences of Time-Reversal Symmetry for Systems with Odd Number of Electrons: Conical Intersections, Semiclassical Dynamics, and Topology*, Chem. Phys., **515**, 3-20 (2018).

Experience

- Graduate Teaching Assistant, Wayne State University. Physical Chemistry and Laboratory, General Chemistry and Laboratory, September 2012 - May 2014, September 2014 - August 2017.

- Graduate Student Assistant, Wayne State University. Chemicals Barcoding. September 2017 - May 2018.

- Summer Graduate Student, Los Alamos National Laboratory. June 2014 - August 2014.